

**ESTIMATION OF NET GROUNDWATER USE IN IRRIGATED  
RIVER BASINS USING GEO-INFORMATION TECHNIQUES**

**A CASE STUDY IN RECHNA DOAB, PAKISTAN**

Promotor: Prof. dr. ir. R.A. Feddes  
Professor of Soil Physics, Agrohydrology and Groundwater  
Management, Wageningen University, Wageningen

Co-promotor: Prof. dr. W.G.M. Bastiaanssen  
Visiting Professor in Application of Remote Sensing in Water  
Resources Management, ITC, Enschede

Members Examination committee:

Prof. dr. ir. P. A. A. Troch, Wageningen University

Dr. ir. P.J.M. de Laat, IHE, Delft

Dr. ir. M.G. Bos, Alterra-ILRI, Wageningen University and Research  
Centre

Dr. C.J. Perry, IWMI, Colombo

**ESTIMATION OF NET GROUNDWATER USE IN IRRIGATED  
RIVER BASINS USING GEO-INFORMATION TECHNIQUES**

**A CASE STUDY IN RECHNA DOAB, PAKISTAN**

Mobin-ud-Din Ahmad

Thesis  
to fulfil the requirements for the degree of doctor  
on the authority of the rector magnificus  
of Wageningen University,  
Prof. dr. ir. L. Speelman,  
to be publicly defended on Wednesday 18<sup>th</sup> December 2002  
at 15:00 hours in the auditorium of ITC, Enschede

ISBN 90-5808-761-1  
ITC Dissertation number 94

Mobin-ud-Din Ahmad, 2002

Estimation of net groundwater use in irrigated river basins using geo-information techniques: A case study in Rechna Doab, Pakistan/ Ahmad, M.D.  
Ph.D. Thesis, Wageningen University – with references – with summaries in English and Dutch.

*To my Parents*



## CONTENTS

<b>ACKNOWLEDGEMENTS</b>	<b>ix</b>
<b>LIST OF FREQUENTLY USED SYMBOLS</b>	<b>xi</b>
<b>ABSTRACT</b>	<b>xv</b>
<b>1 INTRODUCTION</b>	<b>1</b>
1.1 Groundwater for irrigation	1
1.2 Available techniques for recharge and groundwater use estimation	5
1.3 Research objective	7
1.4 Outline of the thesis	7
<b>2 DESCRIPTION OF THE STUDY AREA</b>	<b>9</b>
2.1 Geographical settings	9
2.2 Irrigation system	11
2.3 Data collection	13
2.3.1 Field scale	13
2.3.2 Regional scale	14
<b>3 WATER FLOW IN THE CONTEXT OF CONJUNCTIVE USE</b>	<b>17</b>
3.1 Water flow in porous media	17
3.2 Soil water balance	19
3.3 Net recharge and net groundwater use	23
3.4 Summary and conclusions	25
<b>4 SUSTAINABLE USE OF GROUNDWATER FOR IRRIGATION: A NUMERICAL ANALYSIS OF THE SUBSOIL WATER FLUXES</b>	<b>27</b>
4.1 Introduction	27
4.2 Materials and methods	30
4.3 Results	34
4.4 Conclusions	43
<b>5 SATELLITE SURVEILLANCE OF EVAPORATIVE DEPLETION ACROSS THE INDUS BASIN</b>	<b>45</b>
5.1 Introduction	45
5.2 Study area and climate	46
5.3 Theoretical background	47
5.4 Results	51
5.5 Validation	55
5.6 Evaporative depletion in the Indus Basin	58
5.7 Conclusions	61

<b>6</b>	<b>RETRIEVING SOIL MOISTURE STORAGE IN THE UNSATURATED ZONE FROM SATELLITE IMAGERY AND BI-ANNUAL PHREATIC SURFACE FLUCTUATIONS</b>	<b>63</b>
6.1	Introduction	63
6.2	Soil moisture	64
6.3	Study area	66
6.4	Field scale results	66
6.5	Outline of a new simple parameterisation of matric pressure head distribution	68
6.6	Application of new parameterisation at regional scale	72
6.7	Summary and conclusions	78
<b>7</b>	<b>ESTIMATION OF DISAGGREGATED CANAL WATER DELIVERIES IN PAKISTAN USING GEOMATICS</b>	<b>79</b>
7.1	Introduction	79
7.2	Materials and methods	81
	7.2.1 Data collection	81
	7.2.3 Water distribution models	84
7.3	Results and discussion	89
7.4	Conclusions	96
<b>8</b>	<b>NET GROUNDWATER USE IN RECHNA DOAB FOR SUSTAINABLE POLICY AND DECISION MAKING</b>	<b>97</b>
8.1	Concept and basic equations for net groundwater use	97
8.2	Conventional techniques	98
8.3	Geo-information techniques for unsaturated zone water balance	100
8.4	Comparison between conventional and geo-information techniques	107
8.5	Summary and conclusion	110
<b>9</b>	<b>SUMMARY AND CONCLUSIONS</b>	<b>111</b>
	<b>SAMENVATTING EN CONCLUSIES</b>	<b>117</b>
	<b>REFERENCES</b>	<b>123</b>
	<b>ITC DISSERTATION LIST</b>	<b>137</b>
	<b>CURRICULUM VITAE</b>	<b>143</b>



## ACKNOWLEDGEMENTS

This study would never have materialized without the contribution of many individuals and organizations to whom I have the pleasure of expressing my appreciation and gratitude.

First of all, I gratefully acknowledge the persistent support and encouragement from my former supervisors at the International Water Management Institute (IWMI), Prof. G.V. Skogerboe, Dr. S.A. Prathapar and Dr. P. Strosser. They helped me to pursue my Ph.D. studies at ITC, The Netherlands by facilitating a sandwich programme between ITC and IWMI.

My deepest and foremost gratefulness is due to my advisors: Prof. W.G.M. Bastiaanssen and Prof. R.A. Feddes. Their intellectual inspiration, guidance, encouragement and regular lengthy stimulating discussions have been invaluable to me. They made me determined to continue, to revise, and strive for improvement. Their continual willingness to listen, discuss and render critical judgments helped me to produce this dissertation in its present shape. I also had the honour to work with Prof. A. Stein for a part of my research. I am indebted for his expert advices and the time he spared me. I extend my profound gratitude to Dr. A.S.M. Gieske and Prof. A.M.J. Meijerink for taking keen interest in my research and our valuable scientific discussions.

The fieldwork for this study was conducted at the experimental plots of Ayub Agricultural Research Institute (AARI), Faisalabad and Soil Salinity Research Institute (SSRI), Pindi Bhattian, Pakistan. I appreciate the help and support provided by these institutes. As a part of this study, secondary information was collected from various government agencies in Pakistan, including the Pakistan Meteorological Department (PMD), the Punjab Irrigation Research Institute, the SCARP Monitoring Organization (SMO) and the federal Water and Power Development Authority (WAPDA). I highly acknowledge their positive attitude towards sharing their valuable databases – free of cost – for my research purposes.

IWMI funded part of the fieldwork through their Conjunctive Water Management Project. I am thankful to the team members of this project, and especially Dr. W.A. Jehangir, Dr. S. Ejaz, Mr. H. M. Nafeez, and Mr. K. Ullah, for their help and kind cooperation. Also my particular thanks to Mr. A. Iqbal and Mr. M. Arshad for their assistance during the field data collection. Special thanks goes to Mr. A. Rauf for helping me in the installation of Bowen Ratio Towers. Further more, I am grateful to Dr. M. Aslam, Dr. A. Sarwar and Mr. I. Masih for sharing a part of their dataset, which was used in Chapter 7 of this thesis. I would like to thank the IWMI Pakistan RS/GIS Group, and particularly Mr. S. Asif, Ms. S. Ali, Mr. Y. Chemin and Mr. A. Hussain, for both their help and providing me a harmonious working environment.

I extend my deepest gratitude to a number of ITC staff: Where the administrative and financial arrangements are concerned, I want to express my gratitude to Ms. L. Colenbrander, Ms. G.M.J. Allessie and Ms. B. Geerdink from student affairs. I sincerely

appreciate the help and positive attitude of the ITC Library staff, in particular Ms. C. Gerritsen, for timely arranging research articles from other libraries. I would also like to express my sincere appreciation for the technical and logistical support I received from the Mr. J.P.G. Bakx Remote Sensing Laboratory, computer cluster managers Mr. G.J. Polman and Mr. J.A. Mulder and secretaries Ms. R. Hummel, Ms. T.B. Boogaard, Ms. J. Walet and Ms. H. Al-Malih. I am grateful to Mr. A. Mennings who helped me to finalize the cover of this thesis.

I have been fortunate in having a number of IWMI colleagues here in the Netherlands. I am thankful to all of them in particular to Paul-William Vehmeyer for his hospitality and care throughout our stay in the Netherlands. I am thankful to Mr. R. Waters for quickly and carefully editing the English in my thesis. During my stay at ITC-Enschede, I also received considerable support and friendship from my colleagues Dr. M. Bakr, Dr. H. Farah, Mr. M. Kheirhah, Mr. L. Chandrapala, Mr. O. Obakeng, Mr. P. Debba, Mr. J. Pillai and the Pakistani student community.

I express my deepest appreciation to my parents and other family members. This research would not have been possible without their prayers, encouragements and good wishes. Lastly, I express my gratefulness to my wife Sadia and daughter Manaal for their support and care during the period of my studies.

*Mobin-ud-Din Ahmad*  
December 2002.

## LIST OF FREQUENTLY USED SYMBOLS

Symbol	Representation	Dimensions
$A$	Area	$L^2$
$dh$	Change in depth of phreatic surface	$L$
$E$	Actual soil evaporation rate	$LT^{-1}$
$e$	Vapour pressure	$L^{-1}MT^{-2}$
$ET_a$	Actual evapotranspiration rate	$LT^{-1}$
$ET_o$	Reference crop evapotranspiration rate	$LT^{-1}$
$ET_p$	Potential crop evapotranspiration rate	$LT^{-1}$
$G_0$	Soil heat flux density	$MT^{-3}$
$H$	Sensible heat flux density	$MT^{-3}$
$h_m$	Soil matric pressure head: matric head	$L$
$I_{cw}$	Irrigation rate with canal water	$LT^{-1}$
$I_{ngw}$	Net groundwater use rate: $I_{ngw} = I_{tw} + q_{(h_m=0)}^{\uparrow} - q_{(h_m=0)}^{\downarrow}$	$LT^{-1}$
$I_{rr}$	Irrigation rate	$LT^{-1}$
$I_{tw}$	Irrigation rate with groundwater withdrawal by tubewells	$LT^{-1}$
$K^{\downarrow}$	Global radiation at the surface	$MT^{-3}$
$P$	Precipitation rate, Perimeter (in Chapter 7)	$LT^{-1}, L$
$P_n$	Net precipitation rate i.e., the fraction of precipitation which actually infiltrates	$LT^{-1}$
$q^{\uparrow}$	Upward soil water flux density	$LT^{-1}$
$q^{\downarrow}$	Downward soil water flux density	$LT^{-1}$
$q_{(h_m=0)}^{\uparrow}$	Upward soil water flux density at the phreatic surface: i.e. capillary rise	$LT^{-1}$
$q_{(h_m=0)}^{\downarrow}$	Downward soil water flux density at the phreatic surface: i.e. recharge rate	$LT^{-1}$
$q_{bot}$	Lower boundary flux density at the bottom of the SWAP-column	$LT^{-1}$
$Q_{cw}$	Canal discharge rate	$L^3T^{-1}$

Symbol	Representation	Dimensions
$Q_{in}$	Lateral groundwater inflow	$L^3T^{-1}$
$q_{nr}$	Net recharge rate: $q_{nr} = q_{(h_m=0)}^{\downarrow} - q_{(h_m=0)}^{\uparrow}$	$LT^{-1}$
$Q_{out}$	Lateral groundwater outflow	$L^3T^{-1}$
$r_0$	Surface albedo	-
$r_{ah}$	Near-surface aerodynamic resistance	$L^{-1}T$
$R_n$	Net-radiation flux density: $R_n = G_0 + H + \lambda E$	$MT^{-3}$
$S$	Sink term for root water uptake	$L^3L^{-3}T^{-1}$
$S_r$	Specific retention	$L^3L^{-3}$
$S_y$	Specific yield	-
$T$	Actual crop transpiration rate	$LT^{-1}$
$t$	Time	T
$T_0$	Surface temperature	$\Theta$
$T_{air}$	Air temperature	$\Theta$
$u$	Wind velocity	$LT^{-1}$
$u_*$	Friction velocity	$LT^{-1}$
$W$	Soil moisture storage	L
$W_{rz}$	Root zone soil moisture storage	L
$W_u$	Unsaturated zone soil moisture storage	L
$z$	Gravitational head	L
$z$	Vertical coordinate (positive upward)	L
$z^*$	Height above phreatic surface	L
$\mu$	Storage coefficient: $\mu = dW/dh$ (see Figure 3.2)	-
$\theta$	Volumetric soil moisture content	$L^3L^{-3}$
$\theta_{res}$	Residual volumetric soil moisture content	$L^3L^{-3}$
$\theta_{sat}$	Saturated volumetric soil moisture content	$L^3L^{-3}$
$\lambda E$	Latent heat flux density	$MT^{-3}$
$\xi$	Groundwater resource ratio: $\xi = I_{tw} / (I_{cw} + I_{tw} + P_n)$	-
$\beta$	Bowen ratio: $\beta = \frac{H}{\lambda E}$	-

Symbol	Representation	Dimensions
$\lambda$	Evaporative fraction: $= \frac{\lambda E}{R_n - G_0} = \frac{\lambda E}{\lambda E + H} = \frac{1}{1 + \beta}$	-
$\eta$	Compactness index: $\eta = 4\pi \frac{A}{(P)^2}$ (in Chapter 7)	-
$\rho_{\text{air}}$	Moist air density	$L^{-3}M$
$\Psi_h$	Stability correction for heat transport	-
$\Psi_m$	Stability correction for momentum transport	-
$\gamma$	Psychrometric coefficient	$L^{-1}MT^{-2}\Theta^{-1}$
$\rho_w$	Density of water	$L^{-3}M$



## ABSTRACT

Ahmad, M.D. 2002. *Estimation of net groundwater use in irrigated river basins using geo-information techniques: A case study in Rechna Doab, Pakistan*. Ph.D. Thesis, Wageningen University, the Netherlands.

Over-exploitation of groundwater resources threatens the future of irrigated agriculture, especially in the arid and semi-arid regions of the world. In order to reverse this trend and to ensure future food security, the achievement of sustainable groundwater use has become a global issue. To address the challenges of aquifer mining and sustainable management, a quantitative analysis of recharge and groundwater use is essential. Spatio-temporally distributed information on *net groundwater use* – i.e. the difference between tubewell withdrawals for irrigation and net recharge – is often unknown at the river basin scale. Conventionally, groundwater managers and policy makers look at either groundwater withdrawal by tubewells or phreatic surface fluctuations (if available). However, these methods are ineffective for describing the vertical water fluxes occurring between the unsaturated and saturated zones. Even in detailed groundwater modelling, these vertical water fluxes are difficult to assess.

This endeavour aspires to develop a methodology for computing the various water balance components of the unsaturated zone by using geo-information techniques. These water balance components are then used to compute the net groundwater use. With this approach, groundwater recharge will not be quantified explicitly, but is a part of net groundwater use. Records of routine climatic data, canal discharges at major oftakes, phreatic surface depth, and coarse information on soil textural properties are required as input data. The Rechna Doab region (approximately 2.97 million ha), located in the Indus basin irrigation system of Pakistan, has been used for this case study.

In order to better understand the interaction and dynamics of sub-soil water fluxes, field studies were conducted in rice-wheat and cotton-wheat areas representing shallow (2 m), as well as deep (10 m), phreatic surface conditions. A detailed physically based transient agro-hydrological model (SWAP) has been used to compute sub-soil water fluxes including recharge, and capillary rise. The SWAP model was calibrated using *in situ* measurements of soil moisture content and actual evapotranspiration. The results of the field modelling were used to develop and test a new, simple method for computing soil moisture storage changes in the unsaturated zone, using root zone soil moisture content and depth to the phreatic surface. This method can also be applied in combination with remote sensing and GIS data to compute soil moisture storage changes across vast areas.

Regional scale actual evapotranspiration and soil moisture maps were derived using the remote sensing algorithm termed SEBAL (Surface Energy Balance Algorithm for Land). New geomatic approaches were developed and tested that estimate the disaggregated canal water distribution in an irrigated basin, using discharge measurements at main canal oftakes and satellite imagery. The accuracy of the computed canal water distribution was highest when Landsat image (with a resolution of 30 m) was used to identify the shape of the irrigated areas. This implies that high-resolution satellite images can be used to discern canal water use from groundwater use.

Net groundwater use was computed for the entire Rechna Doab using the derived maps of spatially distributed water balance components. On an annual basis, an average net groundwater use of 82 mm yr<sup>-1</sup> was estimated, which coincides with groundwater inflows of 53 mm yr<sup>-1</sup> that conserve the water balance of the saturated zone. Using the technique presented in this thesis, the computed net groundwater use, based on an unsaturated zone water balance, deviates from classical method estimates, using specific yield and fluctuation of the phreatic surface, by 65%. The deviation from estimates using tubewell withdrawal related data is even higher (several hundred percent).

**Keywords:** remote sensing, GIS, water balance, groundwater, net groundwater use, recharge, water management, Rechna Doab, Pakistan.





# 1 INTRODUCTION

## 1.1 Groundwater for irrigation

Irrigation sector has expanded enormously over the past five decades enhancing agricultural production to meet world food and fibre demand. Today, irrigation is practiced worldwide on about 260 million ha. Four countries—India, China, the United States, and Pakistan—account for just over half of the world's irrigated land (Figure 1.1). Many nations, including Pakistan, rely on irrigated land for more than half of their domestic food production. On irrigated farms, two or three crops per year can be grown and yields are high; therefore, the spread of irrigation has been the key to this century's rise in food production. Globally, irrigated agriculture produces about 40% of agricultural outputs and 60% of grain production.

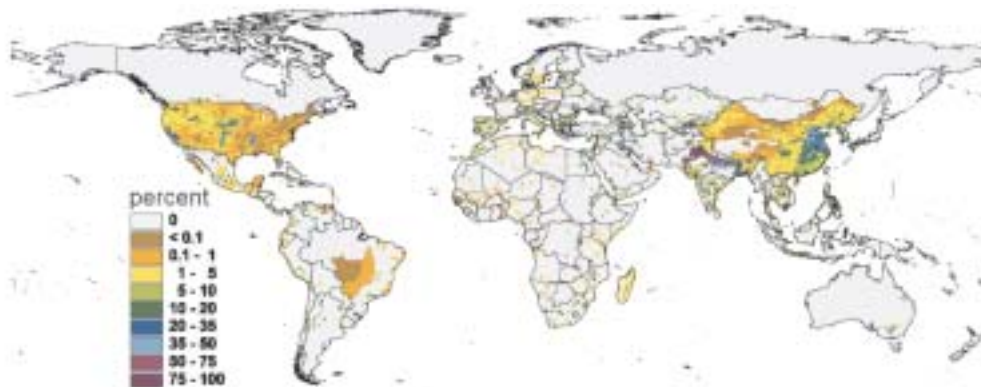


**Figure 1.1** The global extent of irrigated areas in 1995 (Source: Döll and Siebert, 1999).

The other side of the story is that two thirds of the world's fresh water is used for irrigation, with an appreciable contribution coming from groundwater resources. Most of the 750-800 billion  $\text{m}^3 \text{yr}^{-1}$  of global groundwater withdrawals are used for agriculture (Shah *et al.*, 2000). During the last 10 to 20 years, there has been a significant increase in the *utilization of groundwater* resources for agricultural irrigation, because of their widespread distribution and low development cost (Clarke *et al.*, 1996). This has not been restricted to semi-arid regions, but also occurred in more humid areas, in order to provide a greater intensity as well as more reliable supplies for existing cultivated areas. Groundwater has been the heart of the green revolution in agriculture across many Asian nations, and has permitted cultivation of high value crops in various arid to semi-arid regions. Today, the United States, China, India, and Pakistan are the biggest consumers of groundwater and its use is still increasing (Postel, 1999).

At the same time, global water scarcity forms a major constraint on sustaining and enhancing agricultural productivity. Between 1900 and 1995, the demand for freshwater increased six fold, twice the rate of the population growth (Gleick, 1988). Just two decades ago, most serious water supply problems were confined to manageable pockets of the world. Today, they exist on every continent and are spreading rapidly. It is estimated that by the year 2025, two-thirds of the world population will be living in areas facing water-stressed conditions. In Bangladesh, groundwater already represents 35% of total annual water withdrawals, in India it is 32%, Pakistan 30%, and China 11%. In some of the most populous and poverty-stricken regions of the world, particularly in south Asia, groundwater use has emerged at the centre of the food-agriculture economy. For example, in India 60% of the irrigated food grain production depends on irrigation from groundwater wells (Janakarajan, 2000). Across vast areas, farmers are pumping groundwater faster than nature is replenishing it, causing a continuous drop in phreatic surface. As a consequence, the situation is deteriorating; as the demand for water increases, its availability is dwindling.

Groundwater can be obtained either by extraction from aquifers or by means of capillary flow from the phreatic surface. A description of the hydrological cycle elucidates the interactions between water in irrigation canals, in the root zone, and in the groundwater system. When groundwater irrigation is considered, it refers to groundwater withdrawals by tubewells. Generally, groundwater is used to irrigate fields that surround the pump, and hence, is a localized activity. Therefore, comprehensive statistics on the use of groundwater for irrigation are not available (Foster *et al.*, 2000). This is a classical problem of present-day groundwater management planning.

Groundwater management has two contradictory aspects: 1) rise of the phreatic surface and 2) depletion of fresh water aquifers due to overdraft. One source for the rising phreatic surfaces is water loss from irrigation canals and irrigated fields. This lost water increases the soil moisture storage; and after a certain saturation point, it percolates down to the phreatic surface. If this imbalance continues, the phreatic surface will steadily rise and reach into the root zone. Sometimes, it causes secondary salinization by transporting salts from the lower layers up to the root zone. As a consequence, crop growth is hampered because of the non-suitable environment for plants.

On the contrary, in fresh groundwater areas, depletion of the aquifer and a fall of the phreatic surface are caused by unplanned over-utilization of groundwater. In many irrigation systems, this leads to deterioration of groundwater quality due to saltwater intrusion from saline zones. Persistent reliance on such groundwater in irrigated areas has results in the transport of salts from deep aquifers into the root zone and results in secondary salinity and sodicity.

These opposite effects are both a consequence of the spatial imbalances between water supply and water demand. In the past, human settlements formed around abundant water bodies; but this is no longer the case, at least with regard to groundwater (Shah *et al.*, 2000). For example, nearly two thirds of Mexico's territory,

where most of the big cities, industries and irrigated lands are located, possess only one-third of its water resources (Wester *et al.*, 1999). Even though groundwater extractions represent only 38% of the total aquifer recharge at national level, aquifer over-exploitation is becoming critical in the arid and semi-arid areas of the center, north and northwest of Mexico (CAN/World Bank, 1999).

The situation in China is not much different from Mexico. South China has 54% of the population, contributes 68% of China's total groundwater recharge, but includes only 36% of the nation's farmlands, and therefore, is able to use only a small fraction of its groundwater resources. In contrast, North China has 46% of the population, only 31% of China's groundwater, but 64% of the farmlands and therefore, is facing serious groundwater over-use problems (Kramer and Zhu, 1988; Lunzhang, 1994).

Similarly, the Ganga-Meghna-Brahmaputra river basin in south Asia, home to 500 million of the world's poorest people, faces acute waterlogging and flood-tendency problems, despite the addition of over 3 million irrigation tubewells over the past 50 years. In much of this basin, pre-monsoon phreatic surface levels are unlikely to fall by more than 1.5–2 m, even if the number of irrigation wells was doubled. In addition, 20–25 km<sup>3</sup> of the 1,400 km<sup>3</sup> Ganga-Brahmaputra river flood discharge were stored to augment the Ganga's low-flows. If anything, increased irrigation with groundwater would alleviate the endemic waterlogging and flood-tendency that impose enormous costs on the people of the region (Centre for Science and Environment, 1991; Shah *et al.*, 2000). But, peninsular India and western India, which include India's breadbaskets the Punjab and Haryana, have massive problems from groundwater over-development. Phreatic surfaces in these regions have dropped beyond the reach of the muscle-driven water lifts used by farmers for centuries for protective irrigation. Barely 30 years ago in North Gujarat, bullock-bailers could lift groundwater for irrigation, because water levels in the wells were 10–15 m: Today, tubewells reach down 400–450 m to obtain economic discharge. The 26–56 kilo watt (35–75-hp) pumps needed for lifting water from such depths are so expensive that farmers have involved the tubewell companies in the costs and risks of these irrigation investments (Shah and Bhattacharya, 1993).

#### *The Indus river basin irrigation system of Pakistan*

The Indus basin irrigation system of Pakistan is another typical case: some parts are waterlogged, while others show overdraft. Before the introduction of the earthen gravity irrigation system, the phreatic surface was 20 to 30 m deep, and a natural water balance was established. But with the construction of large gravity irrigation systems, this balance has been disturbed and the phreatic surfaces have risen with increased recharge, which is a result of water losses from the earthen conveyance systems and from irrigated fields (Wolter and Bhutta, 1997). Approximately 13% of the water is being recharged to saline groundwater areas. This has adversely affected the environment by causing secondary salinization.

To control the problems of waterlogging and soil salinity, the Government of Pakistan has installed deep public tubewells and, through tax incentives and subsidies, has encouraged the installation of private tubewells (Haq, 2000). This has resulted in rapid

and uneven growth in the number of private tubewells in Pakistan, particularly in the Punjab province (Figure 1.2). Now, the greatest proportion of groundwater supplies comes from private tubewells, which was minimal in the initial stages of the development of this resource. The rapid development of tubewells is a clear indication of the current level of farmer's reliance on groundwater for irrigation.

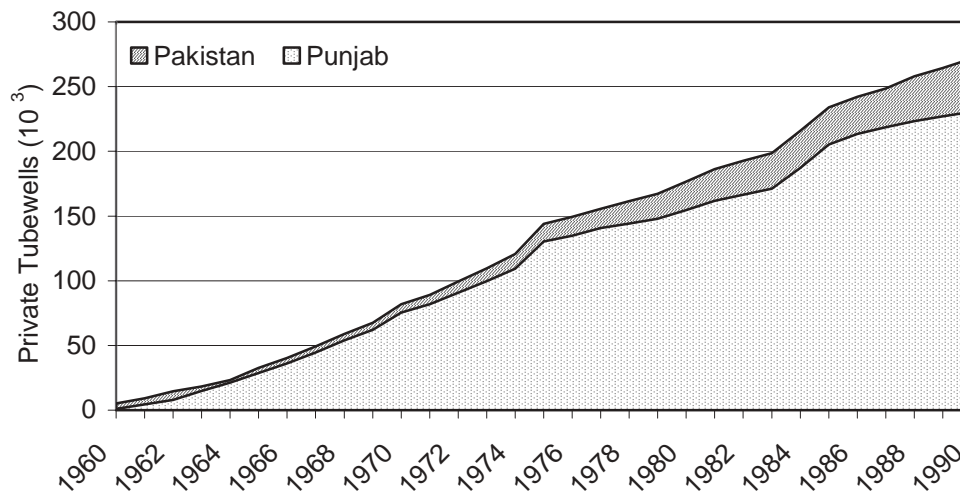


**Figure 1.2** Growth of private tubewells in the Punjab and Pakistan (After Hussan and Bhutta, 1996)

According to a recent estimate, over 500,000 tubewells exist in Pakistan (Ahmad *et al.*, 2000), which contribute 35% of the total water available for agriculture. This has resulted in uneven changes in phreatic surface across the Indus basin (Figure 1.3). This uneven distribution of tubewells is the result of spatial variations in groundwater quality across the Indus basin. In some of the canal commands, the phreatic surface is still increasing while others show declining trends. Groundwater use reached a maximum level of 61 billion m<sup>3</sup> during 1996-97 and started decreasing afterwards. In 1998, 48 billion m<sup>3</sup> of water was pumped (GOP, 1998). There is mounting evidence that this has increased the groundwater flow from highly saline and sodic areas into fresh groundwater zones. Despite these major remedial efforts, salinity continues to present a threat to the sustainability of irrigated agriculture due to the recycling of large quantities of poor quality irrigation groundwater (e.g. Kijne and Kuper, 1995).

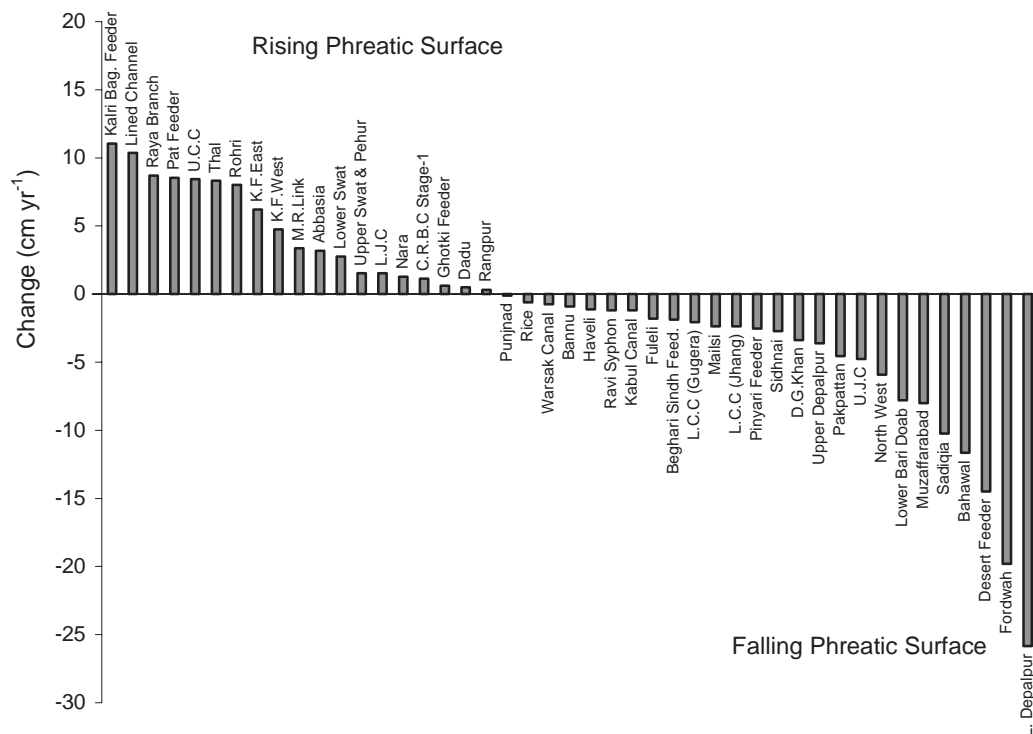


**Figure 1.3** Average annual change in the depth of phreatic surfaces in different canal commands of the Indus Basin Irrigation System Pakistan during 1990 to 1996 (Data source: SCARP Monitoring Organization SMO, 1996).

Groundwater can be a primary buffer against drought, since groundwater systems tend to respond more slowly than surface water systems to short-term variability in climate. The mismanagement of this buffering system has direct and serious impacts on the environment and, ultimately, on food security.

## 1.2 Available techniques for recharge and groundwater use estimation

The problems related to groundwater management are clear, but the solutions are not. An increasing emphasis is placed on how to manage groundwater (and surface water) in a sustainable manner (Downing, 1998; Sophocleous, 1998). A major impediment to finding solutions is the lack of quantitative understanding of the interaction between soil moisture and groundwater. Even though these interactions control the behaviour of groundwater flow systems, recharges to the groundwater aquifer and subsequent man-induced groundwater extractions are uncertainties, which are reflected in the quantitative description of interaction between surface and groundwater systems

(Townley, 1998). Solving this question requires a complete understanding of the hydrological processes at the land surface in relation to the aquifers.

Significant research efforts have addressed the *estimation of groundwater recharge*. In these investigations, several approaches, such as physical, chemical, and numerical modelling techniques, have been developed (Simmers, 1988; Cook *et al.*, 1990; Gieske, 1992). These can be grouped into five categories: empirical methods, direct measurements, tracer techniques, Darcian approaches, and water balance methods (Lerner *et al.*, 1990).

*Empirical methods* are often used in a data scarce environment. Recharge is then correlated with other variables, such as precipitation, canal flows, soil type and land use. Some of these relationships are site specific and are only used for forecasts, while others can have wider applications. Empirical methods cannot estimate recharge rates under non-conventional conditions; hence, physical approaches for recharge estimation are generally preferred.

*Direct measurements* with lysimeters containing undisturbed soil profiles are potentially the most accurate method for estimating recharge, but are difficult, time consuming and expensive to set-up (Gee and Hillel, 1988). Their results represent point scale information, and their application is limited to experimental studies. They are more suitable for humid climates than for arid to semi-arid climates. Because the recharge process is quick in humid regions, data collected over a short time period are sufficient to get complete insight into the recharge process.

*Tracer techniques* are amongst the most widely used methods for recharge estimation in arid and semi-arid regions. They too, only provide point or field scale information. A significant disadvantage of tracer techniques is that they do not directly measure recharge and therefore, lead to inaccurate estimates (Lerner *et al.*, 1990).

*The Darcian approach* analyzes the water fluxes in the unsaturated zone. The information from this method is valid only for field scale studies (Cook *et al.*, 1990), although it is often used for climate studies (e.g. Sellers *et al.*, 1996). The principal advantage of this method is the attempt to identify the actual physical processes of water flow in the unsaturated zone. Using numerical models, transient flow and storage change can be taken into account. To extend these models to a region, the area is generally classified into homogenous sub-regions, and these models are used for recharge estimations for each sub-region (Beekma *et al.*, 1997).

*Water balance methods* are applicable for both point and basin scale estimates. They have three categories: soil water balance, river channel water balance and groundwater (saturated zone) balance. The major advantage of water balance methods is that they use readily available data, can be applied rapidly, and account for all water entering and leaving the system. But, the major disadvantage of these methods is that *recharge is the residual term*, so their accuracy depends upon the accuracy of all the other water balance terms. If these groundwater balance methods include some spatial averaging, the degree of averaging is usually unclear and depends upon the density of observation points. Their application is limited to data scarce environments in semi-arid regions.

The choice and application of methods depend on many factors. It is often reported that in arid and semi-arid regions, groundwater recharge is heterogeneous in both time and space (Hendrickx and Walker, 1997). Simmers (1988) reported that “*no single comprehensive estimation technique can yet be identified from the spectrum of methods available; all are reported to give suspect results*”. Therefore, for reliable quantification and prediction of spatially distributed recharge, it is recommended to use more than one method. This is a tedious task for most the arid and semi-arid regions because of wide spatial and temporal variations and scarce hydro-geological information.

*Groundwater use* estimates in large irrigated schemes are often based on the number of tubewells, their discharge capacity, and their operational hours (NESPAC-SGI, 1991; Maupin, 1999). The operational hours are calculated from electricity/fuel usage or through surveys in that irrigation scheme. Such estimates only provide a range of groundwater extraction values and do not account for groundwater recycling.

Recent advances in remote sensing techniques make it possible to estimate various hydrological parameters with increasing accuracy, especially in the fields of irrigated area and actual evapotranspiration mapping (Bos *et al.*, 2001). Remotely sensed information on these parameters enhances our understanding of the hydrologic cycle (Lerner *et al.*, 1990, Cook *et al.*, 1992, Van Dijk *et al.*, 1996). An innovative avenue is to integrate Remote Sensing (RS), Geographical Information System (GIS), geo-statistics, and selective ground truth data collection. This geo-information can help in describing the spatial variation in hydrological processes, notably the water fluxes at the land-atmosphere interface, groundwater use and recharge in a data scarce environment.

### **1.3 Research objective**

The main objective of this study is:

*To determine spatial and temporal variations in net groundwater use in irrigated river basins, using water balance components obtained from remote sensing data and geo-statistical procedures.*

### **1.4 Outline of the thesis**

A brief description of Rechna Doab, a sub-basin of the Indus basin irrigation system, and the field data collection campaign is presented in Chapter 2.

Chapter 3 describes the basic concepts of soil moisture movement, groundwater flow, and water balance. The different terms in the context of groundwater management are defined in this section: recharge, net recharge, and net groundwater use. The potential of geo-information techniques for unsaturated zone water balance analysis of large areas is also explained.

Chapter 4 deals with quantification of water flow in soils at the field level. Two locations, representing the different cropping cycles, soils, and depth to phreatic surface in Rechna Doab, have been investigated. A one-dimensional physically based Soil-Water-Atmosphere-Plant (SWAP) model (Van Dam *et al.*, 1997) will be calibrated against soil moisture profiles in the root-zone and *in situ* evapotranspiration measurements from Bowen ratio towers. The rate of net recharge and net groundwater use is estimated.

Chapter 5 describes the application of the Surface Energy Balance Algorithm for Land (SEBAL) for the computation of annual actual evapotranspiration across the Indus Basin. These values will be validated against the results of two independent field and regional level studies in Rechna Doab.

Chapter 6 deals with the verification of empirical relationships between the evaporative fraction of the surface energy balance and root zone soil moisture at field scale. A method is developed to compute soil moisture storage values in the complete unsaturated zone from 1) root zone soil moisture content derived from satellite imagery and 2) depth to phreatic surface information measured bi-annually with piezometers. Later these established relationships will be used for the estimation of spatio-temporal variability of soil moisture storage under irrigated crops in Rechna Doab.

Chapter 7 deals with alternative approaches for disaggregating canal water deliveries in Rechna Doab using Geomatics. Six models to compute canal water deliveries will be developed and tested using information from discharge measurements at the main inlet of the irrigation system and from satellite imagery.

Chapter 8 demonstrates the new approach for net groundwater use estimation, based on water balance components, in different canal command areas of Rechna Doab obtained in chapters 5 through 7. The results will be compared against more conventional techniques.

Finally, Chapter 9 summarizes and concludes the findings of this study.



## 2 DESCRIPTION OF THE STUDY AREA

### 2.1 Geographical settings

With more than 16 million ha of irrigable land and 128 billion m<sup>3</sup> of annual canal diversions, the Indus river basin is one of the largest contiguous irrigation systems in the world. Its massive dimension and the lack of existing information makes this basin a prime region for exploring potential of geo-information techniques to estimate water balance and effects of groundwater on irrigation systems. This Ph.D. investigation was conducted in Rechna Doab (Figure 2.1), which is located in the heart of the Indus river basin irrigation system.

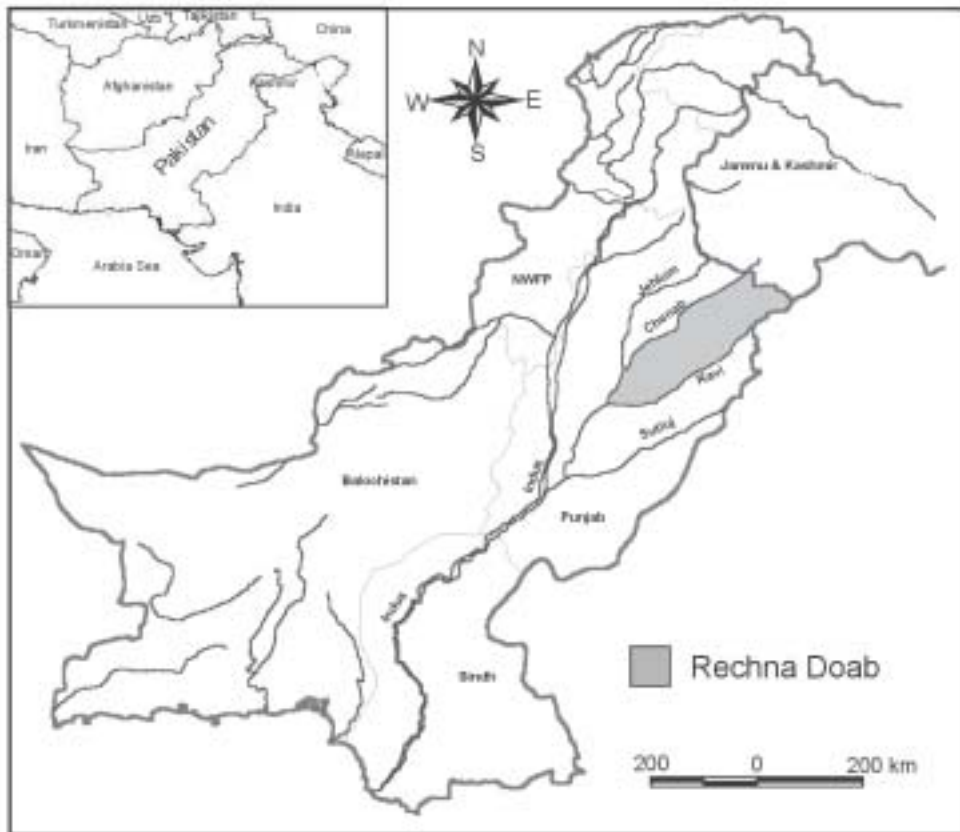


**Figure 2.1** Location of Rechna Doab in Punjab, Pakistan.

Rechna Doab is the interfluvial area between the Chenab and Ravi Rivers. It lies between longitude 71°48' E to 75°20' E and latitude 30°31'N to 32°51' N. The gross

area of this Doab is approximately 2.97 million ha, with a maximum length of 403 km and maximum width of 113 km, including 2.3 million hectares of cultivated land. It is one of the oldest and most intensively developed irrigated areas of the Punjab, Pakistan. The area falls in the rice-wheat and sugarcane agro-ecological zones of the Punjab province. Rice, cotton, and forage crops dominate the summer season (*khariif*). Wheat and forage are the major crops in the winter season (*rabi*). In some parts, sugarcane is also cultivated, which is an annual crop.

The climate is characterized by large seasonal fluctuations of air temperatures and rainfall. The summer is long and hot, lasting from April through September, with maximum air temperature ranging from 21°C to 49°C. Winter lasts from December through February, with maximum air temperature ranging from 25°C to 27°C during the day and sometimes falling below zero at night. The spring and fall months are generally limited to March and October. Annual precipitation is about 400 mm. The monsoon elapses from June to September and accounts for about 75% of annual rainfall. The climate records of Faisalabad along with the general crop calendar are shown in Figure 2.2.

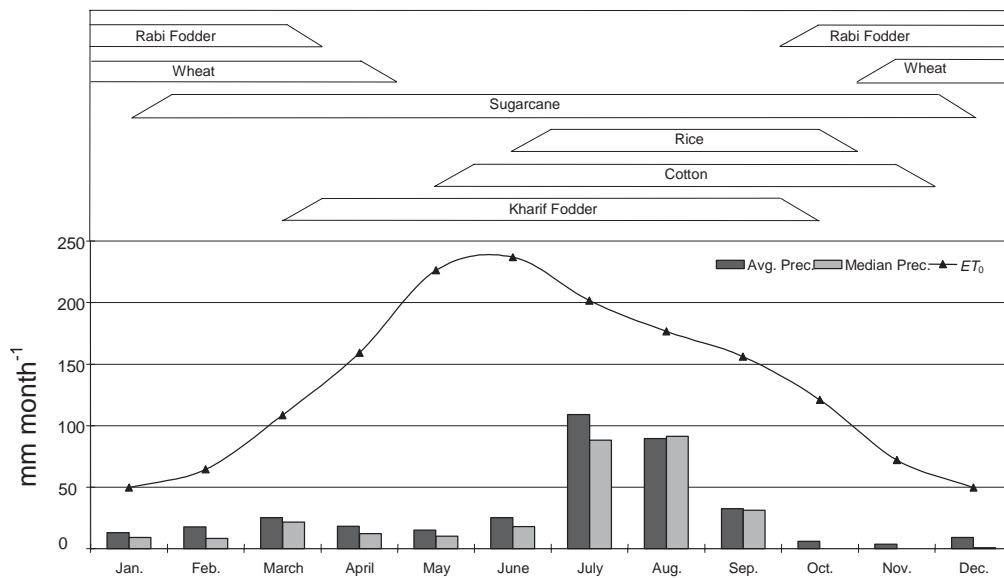


**Figure 2.2** Cropping calendar, monthly precipitation rate and reference crop evapotranspiration rate  $ET_0$  computed according to Penman-Monteith for Faisalabad.

The Rechna Doab soils consist of alluvial deposits transported by the Indus river and its tributaries. The soils textures are predominantly medium to moderately coarse (Figure 2.3), with favourable permeability characteristics and show a similarity throughout the area. The soils are generally low in organic matter and are generally

basic, with a pH in the range of 8 to 8.5. The Rechna Doab soils are adaptable to wide variety of crops.

The topography of Rechna Doab is relatively flat, with a land surface gradient ranging from about  $0.25 \text{ m km}^{-1}$  in the north and northeast to less than  $0.2 \text{ m km}^{-1}$  to the south and southwest. The hydraulic gradient in the upper half of Rechna Doab is steeper than the land surface gradient, but flattens out markedly in the doab's lower reaches (Vander Velde and Kijne, 1992). The aquifer depth varies from 300 to 500 m (Mundorf *et al.*, 1976).

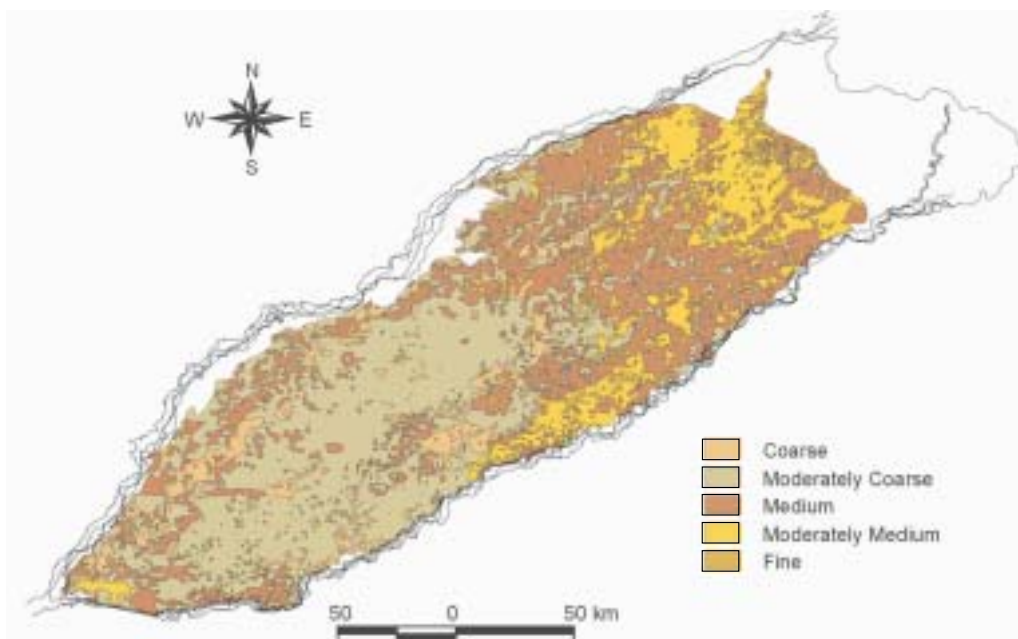


**Figure 2.3** Soil texture map of Rechna Doab (Source: WAPDA, 1981).

## 2.2 Irrigation system

Due to scanty and erratic rainfall, successful agriculture is only possible in Rechna Doab through irrigation. The canal irrigation system (Figure 2.4) was introduced in 1892 with the construction of the Lower Chenab Canal (LCC). Presently, almost  $\frac{2}{3}$  of Rechna Doab is fed by a perennial canal system; i.e., the water flows constantly into a secondary (distributary) and tertiary (watercourse) canal system as long as there is need for water and sufficient flow in the rivers. A normal flow period per year is about 340 days. Non-perennial irrigation systems receive water during the *kharif*, which are restricted to the upper Chenab Canal (UCC) and Marala-Ravi Link (MR Link) canal. The outlets (*moghas*) from the distributaries are not gated and are designed to deliver a fixed quantity of water when the canals are flowing at full capacity.

The design flows in the distributaries are based on the historical size of the command area. This system was designed to spread a limited amount of canal water over the entire area, to support a cropping intensity of approximately 65%. The original design objective of the irrigation development was to protect against crop failure and prevent famine. However, the cropping intensities have increased up to 150% in the last two to three decades, enabled by additional supplies from groundwater extraction. On a weekly or 10-day rotation period (locally called "*warabandi*"), each farmer is allotted a fixed quantity of canal water proportional to his land holdings. To ameliorate the impact of crop water deficits, public and private tubewells were installed on a large scale. Canal and ground water are now commonly used in conjunction.

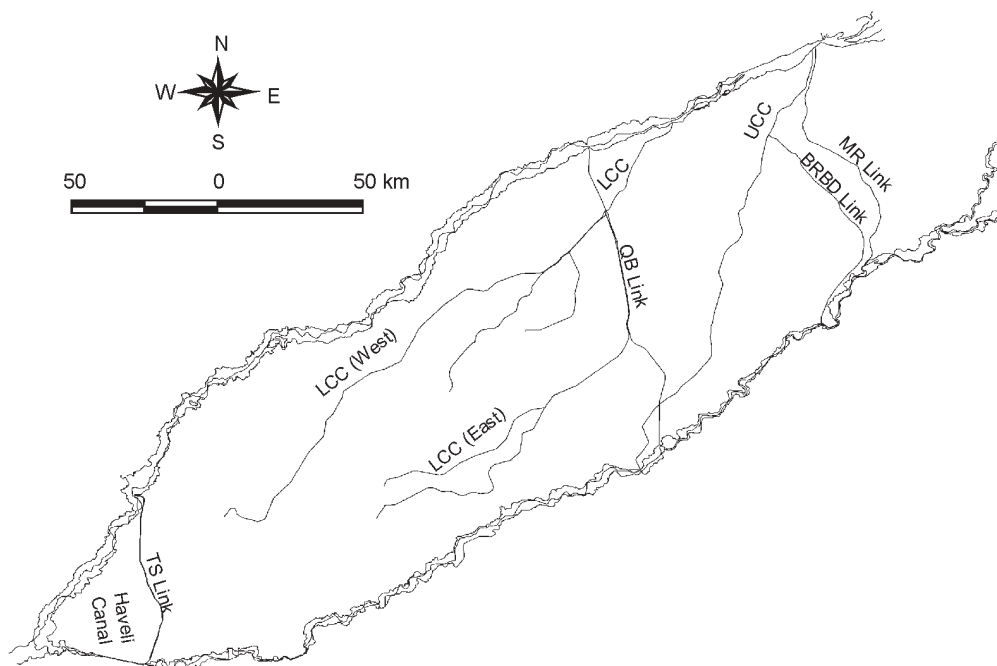


**Figure 2.4** Irrigation network in Rechna Doab, Pakistan. Upper Chenab Canal (UCC), Bamnawala-Ravi-Bedian-Depalpur (BRBD), Marala-Ravi (MR) Link, Qadirabad-Balluki (QB) Link, Lower Chenab Canal (LCC), Trimu-Sadhnai (TS) Link and Haveli canal.

The sustainability of irrigated agriculture is threatened with environmental hazards such as waterlogging and salinization. Before the establishment of the irrigation system, the phreatic surface was 20 to 30 meter below the ground surface (Wolters and Bhutta, 1997). Over the years, persistent distribution and conveyance losses from this huge gravity flow system have altered the natural hydrological balance and caused waterlogging problems. The phreatic surface surveys of 1959-64 reveal that,

in Rechna Doab, 10.9% of the area had a phreatic surface within 1.5 m from the soil surface, 39.3% between 1.5 and 3 m, and the remaining 49.8% at more than 3 m. By 1980, the major SCARP (Salinity Control and Reclamation Project) tubewells within Rechna Doab caused lowering of the phreatic surface. The evaluation of data from a network of 981 piezometers for 1980-96 revealed that instances of high water levels were insignificant. Much of the area has phreatic surfaces at least 1.5 m below the soil surface and predominantly more than 3 m, thereby indicating no perceivable threats to the drainage of the root zone (Rehman *et al.*, 1997). In parts of Rechna Doab, mining of groundwater resources became now a threat to irrigated agriculture.

Salinity hazards in Rechna Doab can be categorized into two types: *Primary (i.e. fossil) salinity* and *secondary salinity*. Fossil salinity is related to inherent salts present during the soil formation (Smedema, 2000). Secondary salinization is a complex problem. In some areas, secondary salinization is linked to a shallow phreatic surface, whereas in other parts, it is a consequence of irrigating with brackish groundwater.

## 2.3 Data collection

### 2.3.1 Field scale

For detailed analysis and understanding of the different hydrological processes at the field scale, and for calibration of GIS and remote sensing models, *two experimental sites near Pindi Bhattian and Faisalabad were selected* (see Figure 2.4).

The site at *Pindi Bhattian* is an experimental field of 0.42 ha (72 m long and 58 m wide) at the Soil Salinity Research Institute (SSRI), which is located on the north-western border of Rechna Doab (co-ordinates: 73°20'50.2" E. 31°52'34.2" N.). The site is flat and situated at an altitude of 212 m above mean sea level. The average precipitation is approximately 500 mm yr<sup>-1</sup>. Two thirds of the precipitation occurs during the monsoon period from July to September. A double crop system is practised with rice sown in the summer season (*kharif*) and wheat in the winter season (*rabi*). The phreatic surface is approximately 2 m below the soil surface. Surface irrigation with borders is practised, and a conjunctive use of canal water and groundwater is applied.

The second site at *Faisalabad* is the experimental field of 0.21 ha (51 m long and 42 m wide) at the Cotton Research Institute of the Ayub Agricultural Research Institute (AARI), which is situated in the centre of Rechna Doab (co-ordinates: 73°2'49.8" E. 31°23'26.2" N.). This flat area lies at an altitude of 130 m above mean sea level. The climate, drier than in Pindi Bhattian, includes an average annual precipitation of 360 mm yr<sup>-1</sup>, with a large fraction falling during the monsoon period. Cotton was sown in *kharif* and wheat in *rabi*. The phreatic surface is fairly deep, approximately 10 m below the surface. There is conjunctive use of canal and groundwater resources.

The amount of daily canal water deliveries to two selected distributaries, Gajiana and Ghour Dour of the Upper Gugera branch of LCC, during *kharif* 2001 were obtained

from the Irrigation Department and the International Water Management Institute (IWMI). For the same period, daily watercourse head discharges for three sample watercourses (one on the Gajiana and two on the Ghour Dour distributary) were also obtained from IWMI. The distributary and watercourse discharges were computed from water level gauge readings using the calibrated relationship between water level and discharge obtained with a cut-throat flume and/or a current meter (Qureshi *et al.*, 2001).

### 2.3.2 Regional scale

Most of the regional scale information used in this study is summarized in Table 2.2. This information was collected from a number of secondary sources. Daily climatic records for seven stations, Faisalabad, Saikot, Jehlum, Sargodha, Multan, Bahwal Nagar and Lahore, were collected from the Pakistan Meteorological Department. SCRAP Monitoring Organization (SMO) of WAPDA installed a nodal network of piezometers across the Indus basin irrigation system. About 981 piezometers are located in Rechna Doab, where SMO is responsible for monitoring the phreatic surface twice a year, in pre- and post-monsoon conditions. The number of actually surveyed piezometers varies from year to year because of the lack of funds at SMO. Despite this limitation, the information available for the period 1980-2000 was collected for this study. The seasonal and temporal changes in phreatic surface behaviour are presented in Figure 2.5. The figure shows that, due to monsoon precipitation, the phreatic surface rises during the *kharif* in large areas across Rechna Doab. However, there are small pockets where it falls due to groundwater extraction during the *kharif*. The temporal analysis shows a significant lowering of phreatic surface in Rechna Doab, which is the result of groundwater extraction for irrigation and installation of sub-surface drainage systems in the lower parts of the doab.

**Table 2.2** Regional scale data collection by the Pakistan Meteorological Department (PMD), Salinity Control and Reclamation Program (SCRAP) Monitoring Organization (SMO), Water and Power Development Authority (WAPDA), Provincial Irrigation Department (PID) and International Water Management Institute (IWMI).

Parameter	Source	Frequency	Time Period
Climatic Data	PMD	Daily	1980-2000
Piezometric Level/Phreatic Surface	SMO, WAPDA	Bi-annual	1980-2000
Canal Discharges			
Main Canal	WAPDA	10-Daily	1990-2000
Distributaries (selected)	PID, IWMI	Daily	<i>kharif</i> 2001
Watercourses (selected)	IWMI	Daily	<i>kharif</i> 2001

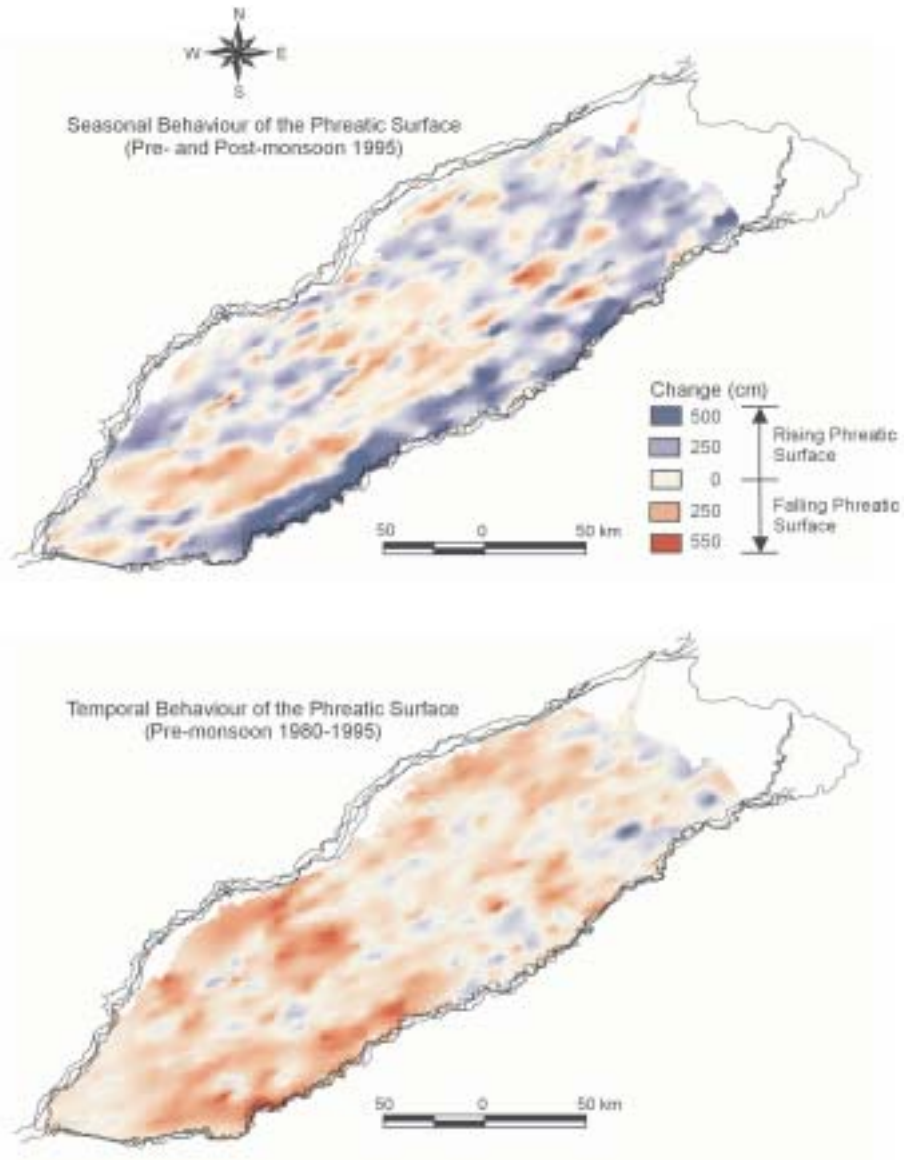


**Figure 2.5** Seasonal (pre- and post-monsoon, 1995) and temporal changes (pre-monsoon, 1980-1995).

The water diversions to main canals in Rechna Doab were collected on a 10-daily time interval since 1990-2000 from WAPDA. The monthly canal deliveries used for irrigation in the year 1999-00 are presented in Figure 2.6. The figure clearly indicates that almost 2/3 of the canal water in Rechna Doab flows through the Lower Chenab Canal (LCC).

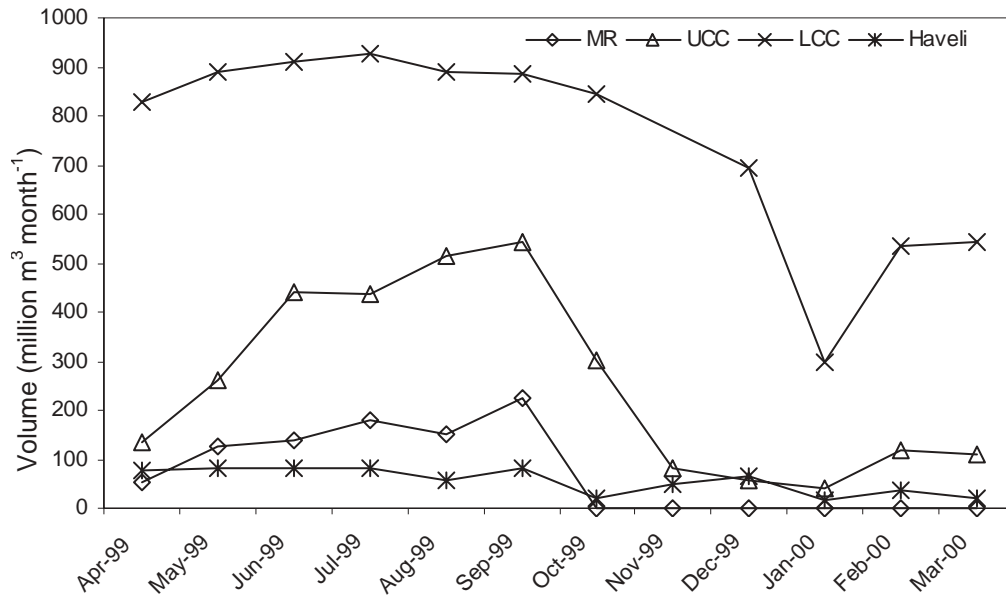


**Figure 2.6** Monthly canal water supplies to Lower Chenab Canal (LCC), Upper Chenab Canal UCC, Marala-Ravi MR Link, and Haveli in Rechna Doab (Water Resources Management Directorate, WAPDA 2000).



### 3 WATER FLOW IN THE CONTEXT OF CONJUNCTIVE USE

#### 3.1 Water flow in porous media

##### *Water flow in the unsaturated zone*

Water beneath the land surface occurs in two principal zones; the unsaturated zone and the saturated zone. The description of the interaction between soil moisture in the unsaturated zone and groundwater in the saturated zone requires all water fluxes to be known. According to Darcy's law, the soil water flow rate  $q$  ( $\text{LT}^{-1}$ ) is proportional to the hydraulic head loss  $\partial H/\partial z$  ( $\text{LL}^{-1}$ ) over a given length of the flow path and its hydraulic conductivity  $K$  ( $\text{LT}^{-1}$ ):

$$q = -K \frac{\partial H}{\partial z} \quad (3.1)$$

where  $z$  (L) is the vertical coordinate (upwards is positive). The total head  $H$  (L) is given by (Feddes *et al.*, 1988):

$$H = h_m + z \quad (3.2)$$

where  $h_m$  (L) is the soil matric pressure head, and  $z$  is the elevation head. Generally, the influence of the osmotic pressure head  $h_{\text{osm}}$  is low, because both solutes and water are moving together. This condition implies that the soil water potential is defined with respect to free water of similar chemical composition as the soil moisture located at reference level. For one-dimensional flow in the unsaturated zone, Darcy's law takes the form:

$$q = -K(h_m) \frac{\partial(h_m + z)}{\partial z} \quad (3.3)$$

*Under transient conditions*, when soil moisture content changes with time, conservation of matter is accounted for by the continuity equation:

$$\frac{\partial \theta}{\partial t} = -\frac{\partial q}{\partial z} - S(z) \quad (3.4)$$

where  $\theta$  ( $\text{L}^3\text{L}^{-3}$ ) is the volumetric soil moisture content,  $t$  (T) is the time, and  $S$  ( $\text{L}^3\text{L}^{-3}\text{T}^{-1}$ ) is the actual soil water extraction rate by plant roots. Combining Eqs. 3.3 and 3.4 results in the well-known Richards' equation:

$$\frac{\partial \theta}{\partial t} = C(h_m) \frac{\partial h_m}{\partial t} = \frac{\partial \left( K(h_m) \frac{\partial h_m}{\partial z} + 1 \right)}{\partial z} - S(z) \quad (3.5)$$

where  $C$  ( $L^{-1}$ ) is the differential water capacity ( $d\theta/dh_m$ ), which is the inverse of the slope of the soil moisture characteristic curve. Richards' equation has a clear physical basis at a scale where the soil can be considered to be a continuum of soil, air and water. Most of the computer codes for calculating one-dimensional flow in the unsaturated zone are based on the numerical solution of Richards' equation (Eq. 3.5). To solve this equation two hydraulic properties are required:  $\theta(h_m)$  and  $K(h_m)$ .

For determining hydraulic properties, direct measurement methods and many indirect estimation procedures result in discontinuous water retention and hydraulic conductivity data. Therefore, algebraic functions using measured or statistically determined data points have been suggested to solve Richards' equation (Brooks and Corey, 1964; Mualem, 1976; and Van Genuchten, 1980). These functions are useful for a number of reasons. Particularly, they facilitate interpolation within the range of measurements, and, if necessary, systematic extrapolation of retention and conductivity curves. Also, in case of hysteresis, scanning curves can be derived by some modification of the analytical function. Also scaling, which is used to describe the spatial variability of  $\theta(h_m)$  and  $K(\theta)$ , requires an analytical expression of the reference curve (Miller and Miller, 1956).

Brooks and Corey (1964) proposed an analytical  $\theta(h_m)$  function, which has been used for a number of years. Mualem (1976) derived a predictive model of the  $K(\theta)$  relation based on their retention function. Van Genuchten (1980) proposed a more flexible  $\theta(h_m)$  function than the Brooks and Corey relation and combined it with Mualem's predictive model to derive  $K(\theta)$ . The van Genuchten-Mualem model forms the basis of several national and international data-banks (e.g. Carsel and Parrish, 1988; Yates *et al.*, 1992; and Wösten *et al.*, 1998). The analytical  $\theta(h_m)$  function proposed by Van Genuchten (1980) reads:

$$\theta(h_m) = \theta_{res} + \frac{\theta_{sat} - \theta_{res}}{\left[ 1 + |\alpha h_m|^n \right]^{\frac{n-1}{n}}} \quad (3.6)$$

where  $\theta_{sat}$  ( $L^3 L^{-3}$ ) is the saturated soil moisture content,  $\theta_{res}$  ( $L^3 L^{-3}$ ) is the residual soil moisture content in the very dry range, and  $\alpha$  ( $L^{-1}$ ) and  $n$  (-) are empirical shape factors. Using Eq. 3.6, Van Genuchten (1980) derived the following continuous  $K(\theta)$  function for all values of  $h_m$ :

$$K(\theta) = K_{\text{sat}} \left( \frac{\theta - \theta_{\text{res}}}{\theta_{\text{sat}} - \theta_{\text{res}}} \right)^{\lambda} \left[ 1 - \left( \frac{\theta - \theta_{\text{res}}}{\theta_{\text{sat}} - \theta_{\text{res}}} \right)^{\frac{n}{n-1}} \right]^{\frac{n-1}{n}} \quad (3.7)$$

### Water flow in the saturated zone

Flow in the saturated zone along principal coordinate axes may consequently be described as (e.g. Kashef, 1976; and Reeve, 1957):

$$q_x = -K_x \frac{\partial H}{\partial x}, \quad q_y = -K_y \frac{\partial H}{\partial y}, \quad q_z = -K_z \frac{\partial H}{\partial z} \quad (3.8)$$

where  $K_x$ ,  $K_y$  and  $K_z$  are the space components of the saturated hydraulic conductivity  $K_{\text{sat}}$  ( $\text{LT}^{-1}$ ). In the saturated zone,  $h_m$  approaches zero and  $K_{\text{sat}}$  is constant. For an isotropic homogeneous aquifer, groundwater flow under steady state conditions can be expressed with the Laplace equation.

## 3.2 Soil water balance

Under conditions of irrigation with canal water  $I_{\text{cw}}$ , as well as tubewells pumping groundwater,  $I_{\text{tw}}$ , the water balance components of the unsaturated-saturated zone system can be given as shown in Figure 3.1.

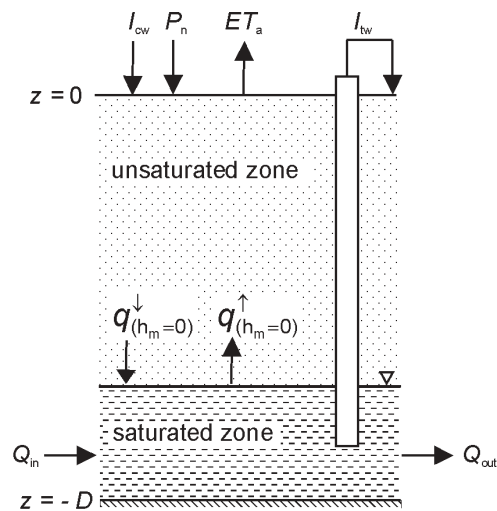


**Figure 3.1** Schematic diagram of the different water balance components in both the unsaturated and saturated zone under steady state conditions.

The phreatic surface, where soil matric pressure head  $h_m=0$ , represents the interface between the saturated and unsaturated zone. The schematisation of Figure 3.1 assumes the water fluxes to be vertical within the unsaturated zone and allows for horizontal/lateral inflow  $Q_{in}$  and outflow  $Q_{out}$  ( $L^3T^{-1}$ ) in the saturated zone.

Under *steady state conditions* where the change in soil moisture storage  $dW=0$ , the water balance for the *unsaturated zone* can be expressed as “In – Out” = 0 i.e.

$$P_n + I_{cw} + I_{tw} - ET_a + q_{(h_m=0)}^{\uparrow} - q_{(h_m=0)}^{\downarrow} = 0 \quad (3.9)$$

where  $I_{cw}$  ( $LT^{-1}$ ) is the irrigation rate with canal water (i.e. water imported from an external source),  $I_{tw}$  ( $LT^{-1}$ ) is the irrigation rate with groundwater ( i.e. saturated zone) withdrawals by tubewell,  $P_n$  ( $LT^{-1}$ ) is the net precipitation rate (i.e. fraction of precipitation which actually infiltrates in to the soil),  $ET_a$  ( $LT^{-1}$ ) is the actual evapotranspiration rate,  $q_{(h_m=0)}^{\downarrow}$  ( $LT^{-1}$ ) is the recharge rate to the groundwater, and  $q_{(h_m=0)}^{\uparrow}$  ( $LT^{-1}$ ) is the rate of capillary rise from the groundwater.

Similarly, the steady state water balance for the *saturated zone* for an area  $A$  ( $L^2$ ) can be expressed as:

$$q_{(h_m=0)}^{\downarrow} - q_{(h_m=0)}^{\uparrow} - I_{tw} + \frac{Q_{in} - Q_{out}}{A} = 0 \quad (3.10)$$

Note that  $q_{(h_m=0)}^{\downarrow}$ ,  $q_{(h_m=0)}^{\uparrow}$  and  $I_{tw}$  describe the sources and sinks towards the groundwater system. The  $Q_{out}$  and  $Q_{in}$  terms relate to the groundwater fluxes  $q_x$ ,  $q_y$  and  $q_z$  of Eq. 3.8.

Unsaturated and saturated zones are connected with each other and sometimes it is more feasible to consider the overall water balance of the *unsaturated-saturated zone system*. Combining Eqs. 3.9 and 3.10 yields the *integrated water balance* of the complete *unsaturated–saturated zone* without changes in state:

$$P_n + I_{cw} - ET_a + \frac{Q_{in} - Q_{out}}{A} = 0 \quad (3.11)$$

In the integrated water balance, the terms  $q_{(h_m=0)}^{\downarrow}$ ,  $q_{(h_m=0)}^{\uparrow}$  and  $I_{tw}$ , which describe the vertical exchange of fluxes between the unsaturated and saturated zone, disappear. The terms  $q_{(h_m=0)}^{\downarrow}$  and  $q_{(h_m=0)}^{\uparrow}$  represent the exchanges at the phreatic surface due to the gradient in  $H$  (Eq. 3.2), where as  $I_{tw}$  represents the man-induced outflow from the saturated zone which infiltrates into the unsaturated zone at the soil surface.

In irrigated fields, however, steady-state conditions mostly do not exist. In practice, the water flow in the saturated and unsaturated zone is under transient conditions, and lateral flows  $Q$  and soil moisture storage  $W$  (L) change over time  $t$  (T):  $dW / dt$ . The *transient water balance of the combined unsaturated-saturated zone* for any irrigated area can thus be expressed as:

$$P_n + I_{cw} - ET_a + \frac{Q_{in} - Q_{out}}{A} = \frac{dW}{dt} \quad (3.12)$$

where

$$\frac{dW}{dt} = \int_{z=-D}^{z=0} [\theta(z, t_2) - \theta(z, t_1)] dz \quad (3.13)$$

where  $\theta$  ( $L^3 L^{-3}$ ) is volumetric moisture content and  $D$  (L) is the depth from ground surface to the base of the aquifer or the impermeable layer (Fig 3.2).

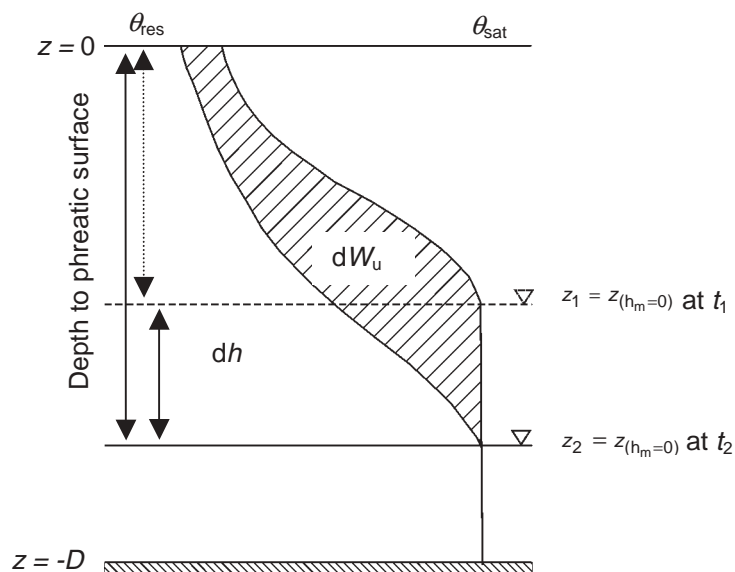


**Figure 3.2** Schematisation of change of soil moisture storage,  $dW$ , with change (i.e. decrease) in height of the phreatic surface,  $dh$ , in unconfined aquifers.

*Under shallow phreatic surface conditions* the changes in the depth of the phreatic surface with time have immediate impact on the soil moisture storage  $W$  of the entire soil profile. In land drainage studies,  $dW / dt$  is often computed from changes in depth

of phreatic surface  $dh / dt$  using the concept of storage coefficient  $\mu$  ( $\mu = \frac{dW}{dh}$ ) (Smedema and Rycroft, 1983) as follows:

$$\frac{dW}{dt} = \frac{dW}{dh} \frac{dh}{dt} = \mu \frac{dh}{dt} \quad (3.14)$$

The storage coefficient  $\mu$  is generally calculated either by simultaneously measuring the phreatic surface change and the drain discharge over a certain time period or alternatively, can be found from the water retention characteristics of the soil profile (Braun and Kruijne, 1994).

Therefore, for *shallow phreatic surface conditions*, the transient water balance of the combined saturated-unsaturated zone system can be written by combining Eqs. 3.12 and 3.14 into:

$$P_n + I_{cw} - ET_a + \frac{Q_{in} - Q_{out}}{A} = \mu \frac{dh}{dt} \quad (3.15)$$

For *deep phreatic surfaces* however, changes in the phreatic surface has minimal effect on the soil moisture storage of the entire soil profile, particularly for small time intervals, and hence, the concept of storage coefficient  $\mu$  cannot be applied. The transient water balance of the saturated zone is then dealt with by using the concept termed specific yield  $S_y$ : “The specific yield of a rock or soil, with respect to water, is the ratio of the volume of water which, after being saturated, it will yield by gravity, to its own volume” (Meinzer, 1923). The transient water balance of the saturated zone is thus expressed as:

$$q_{(h_m=0)}^{\downarrow} - q_{(h_m=0)}^{\uparrow} - I_{tw} + \frac{Q_{in} - Q_{out}}{A} = S_y \frac{dh}{dt} \quad (3.16)$$

where

$$S_y = \theta_{sat} - S_r \quad (3.17)$$

where  $S_r$  ( $L^3L^{-3}$ ) is the specific retention (the volume of water retained by soil per unit of soil). Specific yield  $S_y$  can be measured in the laboratory (Eq. 3.17) or estimated through pumping tests conducted in the field over a period of hours or days (Remson and Lang, 1995). The accuracy of the  $S_y$  measurement usually depends on the depth of the phreatic surface and the amount of time allowed for the test.

### 3.3 Net recharge and net groundwater use

For groundwater management, quantitative information on water exchange between the unsaturated and the saturated zone is essential, i.e.  $q_{(h_m=0)}^\downarrow$ ,  $q_{(h_m=0)}^\uparrow$  and  $I_{tw}$  (See Figure 3.1). The *percolation* rate reaching the saturated zone  $q_{(h_m=0)}^\downarrow$  is defined as *recharge*. Throughout this thesis, the  $q_{(h_m=0)}^\uparrow$  flux is referred to as *capillary rise*. Then *net recharge rate*  $q_{nr}$  to the saturated zone is defined as:

$$q_{nr} = q_{(h_m=0)}^\downarrow - q_{(h_m=0)}^\uparrow \quad (3.18)$$

which describes the net amount of water conveyed to the phreatic surface through the unsaturated zone.

In this thesis, the difference between  $I_{tw}$  and  $q_{nr}$  is defined as *net groundwater use*  $I_{ngw}$ , being mathematically expressed as:

$$I_{ngw} = I_{tw} - q_{nr} \quad (3.19)$$

The practical application of Eqs. 3.18 and 3.19 is generally confined to field scale hydrological studies, as is described in Chapter 4.

Irrigation managers are usually interested net groundwater use  $I_{ngw}$  of the *whole area under service*, i.e. *vast river basin systems*. Net groundwater use  $I_{ngw}$  can, alternatively to Eq. 3.19, be estimated for large areas from the *transient water balance* of the **saturated zone** which reads as:

$$I_{ngw} = \frac{Q_{in} - Q_{out}}{A} - S_y \frac{dh}{dt} \quad (3.20)$$

The net groundwater use  $I_{ngw}$  calculation from Eq. 3.20 requires data on the phreatic surface fluctuation  $dh$ , specific yield  $S_y$  and lateral groundwater flows  $Q_{in}$  and  $Q_{out}$ . Therefore, in addition to measurements of the phreatic surface depth, an estimate of specific yield is required. In groundwater modelling studies lateral flows can be determined from measurements of the height of phreatic surface above a certain reference level by piezometers, when the transmissivity of the aquifer is known (Boonstra and Bhutta, 1995). Phreatic surface measurements are not generally available for small time intervals. Conventionally, over larger time intervals (i.e., a year or more),  $Q_{in}$  and  $Q_{out}$  are assumed to be equal; and then, the rise or fall of phreatic surface is only attributed to  $-S_y \frac{dh}{dt}$ , i.e. net groundwater use. This method is therefore known as the  $S_y$ -method. This approach uses a gross simplification of a very

complex phenomenon, namely, movement of water to and from the phreatic surface. Therefore, the accuracy and validity of the results are based on the reliability and number of the observation points (often less than desired) and on the assumption that lateral groundwater flows can be ignored.

For extensive river basins, however, a different theoretical approach must be followed, because it is difficult to obtain the required information with sufficient accuracy at the required scale, and also, because lateral flows can generally not be ignored in areas using groundwater withdrawals for irrigation. Then, net groundwater use  $I_{ngw}$  must be determined as a residual term from water balance analysis of the *unsaturated zone* over a specific time period  $dt$ , which is expressed as:

$$P_n + I_{cw} + I_{tw} - ET_a + q_{(h_m=0)}^{\uparrow} - q_{(h_m=0)}^{\downarrow} = \frac{dW_u}{dt} \quad (3.21)$$

where

$$\frac{dW_u}{dt} = \int_{z=-z_2}^{z=0} \theta_{(z,t_2)} dz - \int_{z=-z_1}^{z=0} \theta_{(z,t_1)} dz \quad (3.22)$$

where  $dW_u$  represent the change in the *unsaturated zone storage*.

Combining Eqs. 3.18, 3.19 and 3.21, yields a new expression to compute net groundwater use  $I_{ngw}$  as a function of field surface parameters, which can now be obtained through satellite imagery with limited additional field information and which excludes the need to explicitly solve lateral in-flows and out-flows:

$$I_{ngw} = ET_a - P_n - I_{cw} + \frac{dW_u}{dt} \quad (3.23)$$

$ET_a$  can be calculated using satellite imagery techniques and routine meteorological data (Chapter 5),  $P_n$  can be interpolated from precipitation gauge readings,  $\frac{dW_u}{dt}$  can

be estimated from satellite imagery using bi-annual measurements of phreatic surface depth and Van Genuchten-Mualem parameters (Chapter 6), and  $I_{cw}$  can be obtained from satellite imagery and field discharge at major canal diversions (Chapter 7). Eq. 3.23 will thus not quantify net recharge  $q_{nr}$ . That becomes feasible only if information on  $I_{tw}$  is available and  $q_{nr}$  can be calculated from Eq. 3.19.

In irrigation schemes where information about  $S_y$  and  $dh$  is available, the  $I_{ngw}$  values obtained from Eq. 3.23 can further be used in the estimation of lateral groundwater flow,  $\frac{Q_{in} - Q_{out}}{A}$ , by re-writing Eq. 3.20 to:



$$\frac{Q_{in} - Q_{out}}{A} = I_{ngw} + S_y \frac{dh}{dt} \quad (3.24)$$

From a groundwater management point of view, such information is very useful, as it precisely explains whether the rise or fall of phreatic surface at a particular location is the result of localized irrigation activity ( $I_{tw}$ ,  $q_{nr}$ ) or is due to regional groundwater flow.

### 3.4 Summary and conclusions

This section recapitulates the main methods and equations presented in Chapter 3 which have been used to estimate net groundwater use at different scales (Box. 3.1).

Recharge  $q_{(h_m=0)}^{\downarrow}$  and net recharge  $q_{nr}$  can only be solved at the *field scale* by the use of a physically-based soil hydrodynamic simulation model like Soil-Water-Atmosphere-Plant (SWAP) (Van Dam *et al.*, 1997). Such models require field data about irrigation rate (both  $I_{cw}$  and  $I_{tw}$ ), cropping calendar, soil hydraulic properties, meteorological data, and depth and changes in the phreatic surface depth.

*At the basin scale*, it is not possible to calculate  $q_{nr}$  without having distributed information about  $I_{tw}$ . However, net groundwater use  $I_{ngw}$  can be calculated, which is most important for groundwater management. This calculation is possible using either the saturated zone water balance Eq. 3.20 (*conventional method*) or the unsaturated zone water balance Eq. 3.23 (*using distributed input from geo-information techniques*). The chief advantage of Eq. 3.23 is that it estimates  $I_{ngw}$  without explicitly solving for groundwater lateral flows. Therefore, if the change in phreatic surface depth  $dh$  and specific yield  $S_y$  information is available, then  $I_{ngw}$  from Eq. 3.23 can be used to calculate lateral groundwater flows as an offshoot of the saturated zone water balance.

**Box 3.1** Summary of the main governing equations for the estimation of Net Recharge and Net Groundwater Use at different scales.

**Net Recharge  $q_{nr}$**

Is the rate of net amount of water conveyed to the phreatic surface through the soil matrix.

$$q_{nr} = q_{(h_m=0)}^{\downarrow} - q_{(h_m=0)}^{\uparrow} \quad (3.18)$$

**Net Groundwater Use  $I_{ngw}$**

Is the difference between groundwater withdrawal by tubewells for irrigation  $I_{tw}$  and net recharge  $q_{nr}$ .

At the *field scale*, it can be estimated as:

$$I_{ngw} = I_{tw} - q_{nr} \quad (3.19)$$

At the *regional or basin scale*, it can be estimated either by the *saturated zone water balance*:

$$I_{ngw} = \frac{Q_{in} - Q_{out}}{A} - S_y \frac{dh}{dt} \quad (3.20)$$

or by the *unsaturated zone water balance*:

$$I_{ngw} = ET_a - P_n - I_{cw} + \frac{dW_u}{dt} \quad (3.23)$$

## 4 SUSTAINABLE USE OF GROUNDWATER FOR IRRIGATION: A NUMERICAL ANALYSIS OF THE SUBSOIL WATER FLUXES\*

### 4.1 Introduction

Groundwater plays a vital role in sustaining agricultural productivity in many irrigated areas of the world. In most of these regions, aquifer exploitation has reached its maximum sustainable potential or has already exceeded it. Further increase in groundwater use will cause a lowering of the phreatic surface, below which extraction will no longer be economically viable and will harm the environment. Furthermore, if the present groundwater extraction patterns continue, it will soon result in saltwater intrusion. Irrigation with saline groundwater will increase the risk of secondary salinity and sodicity by importing salts from the deep aquifer into the root zone. But also, the opposite condition of a rising phreatic surface is being witnessed. The immediate effect of these conditions is that the required increase in food production needed to feed the rapidly growing population cannot be attained in arid and semi-arid zones. To avoid these undesirable scenarios, groundwater withdrawals should be balanced with the rate of replenishment (De Vries, 1984).

Groundwater conditions are classically described by means of phreatic surface fluctuations. This provides direct information on the rate of change of the groundwater levels. There is, however, one major drawback in studying phreatic surface data: how can rise or fall of the phreatic surface be arrested? To answer this question, the cycle between tubewell extractions and recharge needs to be known. Also, the groundwater contribution to crop evapotranspiration through capillary rise needs to be quantified, because this can be of paramount importance in areas with a shallow phreatic surface and in areas prone to waterlogging. This paper deals with a methodology that describes the subsoil water fluxes and address the need for greater information in managing this type of irrigation configurations. In particular, the fluxes at the interface between the unsaturated and saturated zones need to be quantified. The difference between groundwater removal through tubewell and capillary rise vs. recharge is not straightforward to determine, even on a field scale. To understand these complex transient recharge and groundwater use processes, a complete understanding of soil water fluxes in the unsaturated zone is essential (e.g. Hendrickx and Walker, 1997).

The Indus basin irrigation system of Pakistan is one of the largest contiguous surface irrigation systems in the world. A fixed quantity of canal water proportional to land holding is supplied on a weekly or 10-day rotation period locally called *warabandi*. The losses from the earthen canal network and irrigated fields have resulted in a rise of the phreatic surface in several places. The problem of rising phreatic surface has sometimes resulted in waterlogging and salinization in the Indus Plain (Smedema,

---

\* Adapted from Ahmad, M.D., W.G.M. Bastiaanssen and R.A. Feddes, 2002. Sustainable use of groundwater for irrigation: A numerical analysis of the subsoil water fluxes. *Irrigation and Drainage* 51(3): 227-241.

2000). The first symptoms of the problem appeared in the first half the 20<sup>th</sup> century, but the problem reached alarming proportions between 1950-1960.

To combat this problem, the government of Pakistan took several measures, including encouraging the farming community, through tax reduction and other subsidies, to install private tubewells to pump groundwater for irrigation. This additional and timely water supply from groundwater resulted in a rapid increase in cropped area and yield. As a result, in the non-saline groundwater area, the number of tubewells increased drastically and there was a considerable increase in the area under cultivation. Presently, groundwater withdrawal has reached its maximum potential. Further unplanned increases in groundwater withdrawal may ruin aquifers. As not all irrigation water is consumed by the crops, a recharge from irrigated plots to the aquifer is expected. The question is: how much recharge?

The unsaturated zone, through which important processes such as evapotranspiration and recharge take place, is heterogeneous and complex. A transient soil moisture transport model can provide a proper indication of how moisture in the unsaturated zone and the saturated phreatic aquifer interact. Investigation of the processes of recharge and net groundwater use with physically based models has two great advantages over other approaches. First, models can be used to understand processes that are difficult to measure *in situ*. Second, models can be used to forecast hydrologic processes under changing boundary conditions, such as changes in groundwater extraction and artificial recharge (Allison *et al.*, 1994). This is highly useful for the modelling of different groundwater application scenarios.

The rate and volume of recharge and groundwater use largely depends upon irrigation and agronomic practices, and upon the physical characteristics of the soil, such as infiltration rate, water retention capacity, and unsaturated hydraulic conductivity. Under gravity irrigation, net groundwater use can be significantly less than expected, because a large fraction of irrigation water returns to the aquifer. Hence, management and policy making of groundwater issues are feasible, provided that the flow to and from the irrigated fields is understood. The main objectives of this research work are:

- To calibrate a numerical model that predicts the soil water fluxes at the interface between the unsaturated and saturated zone;
- To understand the soil moisture dynamics in the unsaturated zone of crops irrigated with groundwater in the Rechna Doab, Pakistan;
- To estimate groundwater over-exploitation in areas with deep and shallow phreatic surfaces.

#### *Definitions*

To understand and quantify the recharge mechanisms and groundwater contribution to irrigated agriculture in phreatic aquifer systems, different soil water fluxes in a one-dimensional vertical soil column are presented in Figure 4.1. The water balance of the unsaturated zone reads as:

$$P_n + I_{cw} + I_{tw} - ET_a + q_{(h_m=0)}^{\uparrow} - q_{(h_m=0)}^{\downarrow} = \frac{dW_u}{dt} \quad (3.21)$$

where  $P_n$  is the net precipitation rate (gross precipitation rate minus rate of interception losses  $P_i$  and rate of surface runoff,  $dW_u$  is the change in the unsaturated zone storage over a period of time  $dt$ ,  $I_{cw}$  is irrigation rate with canal water,  $I_{tw}$  is irrigation rate with groundwater (tubewell water),  $ET_a$  is the rate of actual evapotranspiration, and  $q$  is the lower boundary flux of the unsaturated zone. Recharge  $q_{(h_m=0)}^{\downarrow}$  is the percolation or soil water flux that reaches the phreatic surface, i.e. the location where matric head is zero ( $h_m = 0$ ). Similarly, we have defined the capillary rise as  $q_{(h_m=0)}^{\uparrow}$ , hence, it is the upward flux from phreatic surface to unsaturated zone. The capillary flux does not necessarily convey moisture to the root zone. That depends on the distance between the phreatic water surface and the root zone, among many other factors. Net recharge  $q_{nr}$  (Eq. 3.18) is the rate of water conveyed to the phreatic surface through the soil matrix. Net groundwater use  $I_{ngw}$  (Eq. 3.19) is defined as the difference between groundwater withdrawals by tubewell for irrigation  $I_{tw}$  and net recharge  $q_{nr}$ .

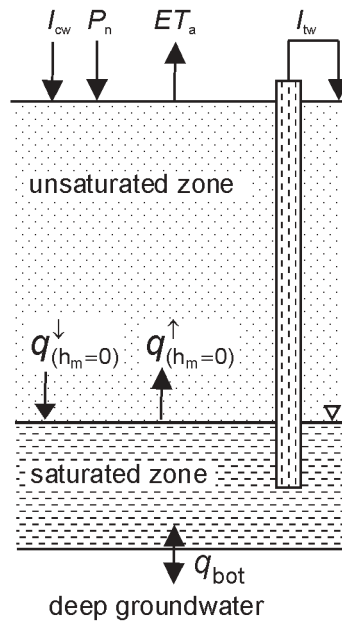


**Figure 4.1** Schematisation of different soil water fluxes in a phreatic aquifer ( $I_{cw}$  is canal water irrigation,  $P_n$  is net precipitation,  $ET_a$  is actual evapotranspiration,  $I_{tw}$  is tubewell irrigation,  $q_{(h_m=0)}^{\downarrow}$  is recharge,  $q_{(h_m=0)}^{\uparrow}$  is capillary rise, and  $q_{bot}$  is bottom flux).

Water supply to the cropped area can be from three different sources:  $I_{cw}$ ,  $I_{tw}$  and  $P_n$ . For sustainable groundwater management, it is important to estimate the reliance of agriculture on groundwater resources. The groundwater resource ratio  $\xi$  can be estimated by the ratio of irrigation with groundwater  $I_{tw}$  to the total inflow from all resources ( $\xi = I_{tw} / (I_{cw} + I_{tw} + P_n)$ ).

## 4.2 Materials and methods

### *Description of SWAP model*

Water flow in the unsaturated zone is predominantly vertical, and can generally be simulated as one-dimensional flow (Romano *et al.*, 1998). Earlier versions of the one-dimensional physically based Soil-Water-Atmosphere-Plant (SWAP) model were developed by Feddes *et al.*, (1978), Belmans *et al.*, (1983), and Kabat *et al.*, (1992). It has been tested for a number of hydrological studies under a wide range of climate and agricultural systems (e.g. Feddes *et al.*, 1988). SWAP has previously been applied and validated for the irrigation conditions in Pakistan, Iran and India (Bastiaanssen *et al.*, 1996; Van Dam and Feddes, 1996; Smets *et al.*, 1997; Beekma *et al.*, 1997, Sarwar *et al.*, 2000 and Droogers *et al.* 2001). In the present study, particular emphasis has been given to changes of the vertical soil water fluxes with depth.

The SWAP model is based on the Richard's equation, which combines Darcy's law and the continuity equation, for moisture transfer and the advection-dispersion equation for solute transfer (Van Dam *et al.*, 1997; Van Dam and Feddes, 2000). SWAP predicts the dynamic interaction between soil, water, atmosphere, and plants on a daily time step. In order to solve these equations, the program uses a finite difference scheme with explicit linearization. In order to apply this finite difference scheme, the soil profile is divided into thin layers and soil horizons of similar hydraulic properties. SWAP may simulate up to three rotating crops in a year and contains three crop growth routines. In this study, a simple crop development model available in SWAP is used which only requires information about the leaf area index (or soil cover fraction), crop height, and rooting depth, all as a function of crop development stage.

### *Study area*

This research work was carried out in the Rechna Doab area of the Indus basin irrigation system. For a detailed analysis and understanding of the different components at the field scale, two experimental sites *Pindi Bhattian* and *Faisalabad*, were selected (Figure 2.4). These sites represent shallow and deep phreatic surface conditions and have rice-wheat and cotton-wheat cropping systems, respectively. The detailed description of these sites is presented in section 2.3.1.

### Field data collection

Field data on various agronomic aspects required for SWAP simple crop growth model and water balance components were collected for two growing season, *kharif* 2000 and *rabi* 2001. Bowen ratio towers for measuring the actual evapotranspiration rates ( $ET_a$ ) were installed and operated between June 21 (2000) and March 21 (2001), in parallel, at both experimental plots. Air temperature and humidity were measured at different heights: above the canopy, at 2 meters and at 4 meters from the ground surface. Wind speed was measured at 4 meters above natural ground level, along with precipitation ( $P$ ) and incoming solar radiation. For missing days, climatic data from the nearest meteorological stations were collected. The irrigation application rates ( $I_{cw}$ ,  $I_{tw}$ ) were monitored using cut-throat flumes or a current meter. Daily fluctuations in phreatic surfaces were recorded manually at both sites using a piezometer with sounding device and an automatic water level recorder (*Diver*). The recorder measures absolute pressure (water pressure + atmospheric pressure) expressed in schematised of water column. To obtain accurate changes in water level, one needs to compensate for atmospheric pressure. Soil moisture changes in the root zone at a depth of 35, 70, and 100 cm were monitored in the field using a *theta probe* based on the frequency domain technique. The theta probe measures the volumetric moisture contents through the variability of the dielectric constant. The frequently measured parameters for input and calibration of the SWAP model are summarized in Table 4.1.

**Table 4.1** Field Data collection for SWAP Model.

Parameter	Collection Method/Instrument	Frequency
Air Temperature	Thermocouple	5 min
Relative Humidity	Thermocouple	5 min
Shortwave Radiation	Pyranometer	5 min
Precipitation	Tipping bucket	30 min
Wind speed	Anemometer	5 min
Phreatic Surface	Piezometric level (using sounding device and <i>Diver</i> )	Daily
Soil moisture content	Frequency domain technique	Weekly
Irrigation	Cut-throat flume & current meter	Event wise
Agronomic Data	Field surveys	Continuous

Crop growth in SWAP is computed using the Leaf Area Index (LAI), crop height and rooting depth. The crop height needs to be specified for the calculation of the crops'

aerodynamic resistance. LAI is necessary for the computation of potential transpiration from crop reference evapotranspiration. The root depth determines from which depth water is withdrawn from the soil into the plant. There are more sophisticated model options related to carbon assimilation and the simulation of crop growth, but these options were not explored. The interception  $P_i$  is a function of the gross precipitation  $P$ , LAI, and the maximum storage of a thin water layer on the canopy.

The extensive field data collection program assumed that all terms except  $q$  could be measured. As the moisture profiles and  $dW_u$  are applicable to the first 1 m of soil only, it follows from the formulation in Eq. 3.21, that  $q$  applies to the flux through the soil profile at 1 m depth. This may not be regarded as the deep percolation flux. As the subsoil water fluxes cannot be measured, a transient moisture flow model such as SWAP is required. The input parameter for SWAP consists of  $P$ ,  $l_{tw}$  and  $l_{cw}$ , and they are taken directly from the field data collection program. In addition, potential evapotranspiration  $ET_p$  needs to be specified. The SWAP outputs consist of  $ET_a$ , soil moisture storage in simulated profile  $dW_u$ , and the flux at any depth  $q(z)$ . The data of  $ET_a$  and  $dW_u$  can be used for calibration of the model. The data series of  $q(z)$  cannot be verified with *in situ* measurements.

#### *Input parameters*

The upper boundary condition of SWAP consists of daily inputs of climatic data for the computation of  $ET_p$  and for irrigation applications. Fixed irrigation depths were actual measurements in the field. Following the experiences of Sarwar *et al.*, (2000), potential evapotranspiration  $ET_p$  was calculated using the Priestly and Taylor (1972) equation. During certain days of the hot season prior to the monsoon, the actual evapotranspiration  $ET_a$  measurement from the Bowen ratio system was higher than the predicted  $ET_p$  from the Priestley and Taylor equation. The  $ET_a$  resulting from the Bowen ratio surface energy balance method enabled us to adjust the value of empirical coefficient for local advective conditions. The value of  $\alpha=1.4$ , for both *kharif* and *rabi*, was found to be more realistic for the environmental conditions of Pakistan than the standard  $\alpha=1.26$  (see also Choudhury *et al.*, 1994). For the calculation of net radiation  $R_n$ , surface albedo  $r_0$  of 0.14, 0.15, 0.18 and 0.21 were used for rice, cotton, wheat and fallow land, respectively.

Water stress in SWAP is described by the sink term and a matric potential based root water uptake function as proposed by Feddes *et al.*, (1978). Crops react differently to soil water limitations, and their sensitivity to matric potential needs to be specified. In the present study, the in-situ Bowen ratio provided us with the unique opportunity to calibrate the SWAP model against the measured  $ET_a$ . *This is the first study in Pakistan to calibrate a hydrological model with measured  $ET_a$ .* Initially, the root water uptake sink-term values of Haryana state, India (Bastiaanssen *et al.*, 1996) were used in this study. Then, these sink-term values ( $h_1$  to  $h_4$ , see Table 4.2) were adjusted to get good agreement between  $ET_a$  estimates from SWAP and the Bowen ratio technique. Sink-term values describe the water uptake response of a certain crop at different pressure heads in the soil matrix, i.e. a potential-driven water uptake function. The crop parameters used in this study are summarized in Table 4.2.



**Table 4.2** Crop input parameters used for the SWAP model.

Input parameter	Faisalabad		Pindi Bhattian					
	Cotton	Wheat	Rice	wheat				
Length of crop cycle (days)	192	127	122	139				
Maximum rooting depth (cm)	160	110	55	110				
Limiting pressure heads (cm) for the root water uptake function of Feddes <i>et al.</i> , (1978)	$h_1 =$	-10.0	$h_1 =$	-10.0	$h_1 =$	-0.1	$h_1 =$	-0.1
	$h_2 =$	-30.0	$h_2 =$	-30.0	$h_2 =$	-30.0	$h_2 =$	-30.0
	$h_3^h =$	-300.0	$h_3^h =$	-400.0	$h_3^h =$	-100.0	$h_3^h =$	-300.0
	$h_3^l =$	-1500.0	$h_3^l =$	-1200.0	$h_3^l =$	-200.0	$h_3^l =$	-1500.0
	$h_4 =$	-16000.0	$h_4 =$	-8500.0	$h_4 =$	-16000.0	$h_4 =$	-16000.0

$h_1$  relates to the air entry potential. The water uptake by roots is maximal between  $h_2$  and  $h_3$ .  $h_4$  relates to the potential at wilting point.

The SWAP model offers a broad range of bottom boundary conditions. The option of using daily fluctuations of the phreatic surface (because they had been measured) was chosen as the bottom boundary condition. The bottom flux  $q_{bot}$  through the saturated soil column is the residual and is the result of all the errors in simulation and measurements of  $P$ ,  $I_{tw}$  and  $I_{cw}$ . As  $q_{bot}$  applies to the bottom of the 1D-column only,  $q_{bot}$  does not express percolation fluxes, but merely describes the regional connection between the fields investigated and their neighbouring fields. A positive bottom soil water flux is related to an upward soil water flux.

#### Soil hydraulic properties

The finite difference scheme has a vertical grid with a total length of 1125 cm and 300 cm for the Faisalabad and Pindi Bhattian areas, respectively. The schematised soil columns for the sites represent the deep and shallow phreatic surface conditions. For both sites, the soil profile was divided into forty numerical compartments and grouped into four soil horizons with different hydraulic properties. Soil hydraulic functions need to be specified for each layer. The soil hydraulic functions, expressing the relationship between soil moisture content  $\theta$ , soil matric head  $h_m$ , and hydraulic conductivity  $K$  are described by the Van Genuchten-Mualem parameters (VGM), (Van Genuchten, 1987; Wösten and Van Genuchten, 1988). Beekma *et al.*, (1993) have determined the VGM parameters; residual moisture content  $\theta_{res}$ , saturated moisture content  $\theta_{sat}$ , saturated hydraulic conductivity  $K_{sat}$ , and shape parameters  $n$  and  $\lambda$  using a series of field measurements and laboratory techniques in Rechna Doab. These values have been adjusted to match the *in situ* measurements of soil moisture content (Table 4.3). By minimizing the difference between *in situ* and modelled soil moisture content and evaporative fluxes, the flux  $q$  at a depth of one meter is accurately known.

**Table 4.3** Calibrated Van Genuchten-Mualem (VGM) parameters used to describe soil hydraulic properties in the SWAP model.

Soil type	Faisalabad				Pindi Bhattian			
	0-40 cm	40-85 cm	85-155 cm	More than 155 cm	0-10 cm	10-60 cm	60-150 cm	More than 150 cm
	Loam	Loam	Silt Loam	Loamy Sand	Sandy Loam	Sandy Clay Loam	Loam	Silt Loam
Parameters								
$\theta_{res}$ (cm <sup>3</sup> cm <sup>-3</sup> )	0.044	0.035	0.100	0.028	0.000	0.000	0.000	0.000
$\theta_{sat}$ (cm <sup>3</sup> cm <sup>-3</sup> )	0.340	0.354	0.250	0.400	0.424	0.380	0.440	0.400
$K_{sat}$ (cm d <sup>-1</sup> )	145.000	180.000	180.000	180.000	20.000	35.000	45.000	45.000
(cm <sup>-1</sup> )	0.018	0.018	0.012	0.011	0.064	0.0243	0.030	0.0124
$\lambda$ (-)	2.500	2.500	2.500	2.679	-1.382	1.850	1.700	2.750
$n$ (-)	1.260	1.260	1.130	2.680	1.399	1.250	1.200	1.200

## 4.3 Results

### *Soil moisture content*

The simulated moisture in the root zone is compared with measurements of soil moisture content at three different depths in the top 100 cm of subsoil for both fields at Faisalabad and Pindi Bhattian (see Figure 4.2). The simulated soil moisture content agrees very well with the measured values at both sites throughout the simulation period. The model reproduced temporal variations in the soil moisture content for heterogeneous soils under cotton-wheat and rice-wheat crop rotations. The effect of irrigation  $I_{rr}$  on soil moisture content was most evident at 35 cm depth, for both cases. The reason for less frequent measurements of soil moisture content in the *kharif* for Pindi Bhattian was the ponding of water in the rice fields. Measurements were taken during the last few weeks when there was no standing water left. The high soil moisture content during the entire rice-growing season is clearly shown in Figure 4.2. The overall root mean square error after calibrating the Van Genuchten–Mualem parameters was found to be 0.022 cm<sup>3</sup> cm<sup>-3</sup> and 0.027 cm<sup>3</sup> cm<sup>-3</sup> for Faisalabad and Pindi Bhattian, respectively. These calibration results indicate that estimates of general crop and soil parameters, such as those specified in Tables 4.2 and 4.3, are sufficient to simulate the water fluxes in the first 1-meter of the soil profile.

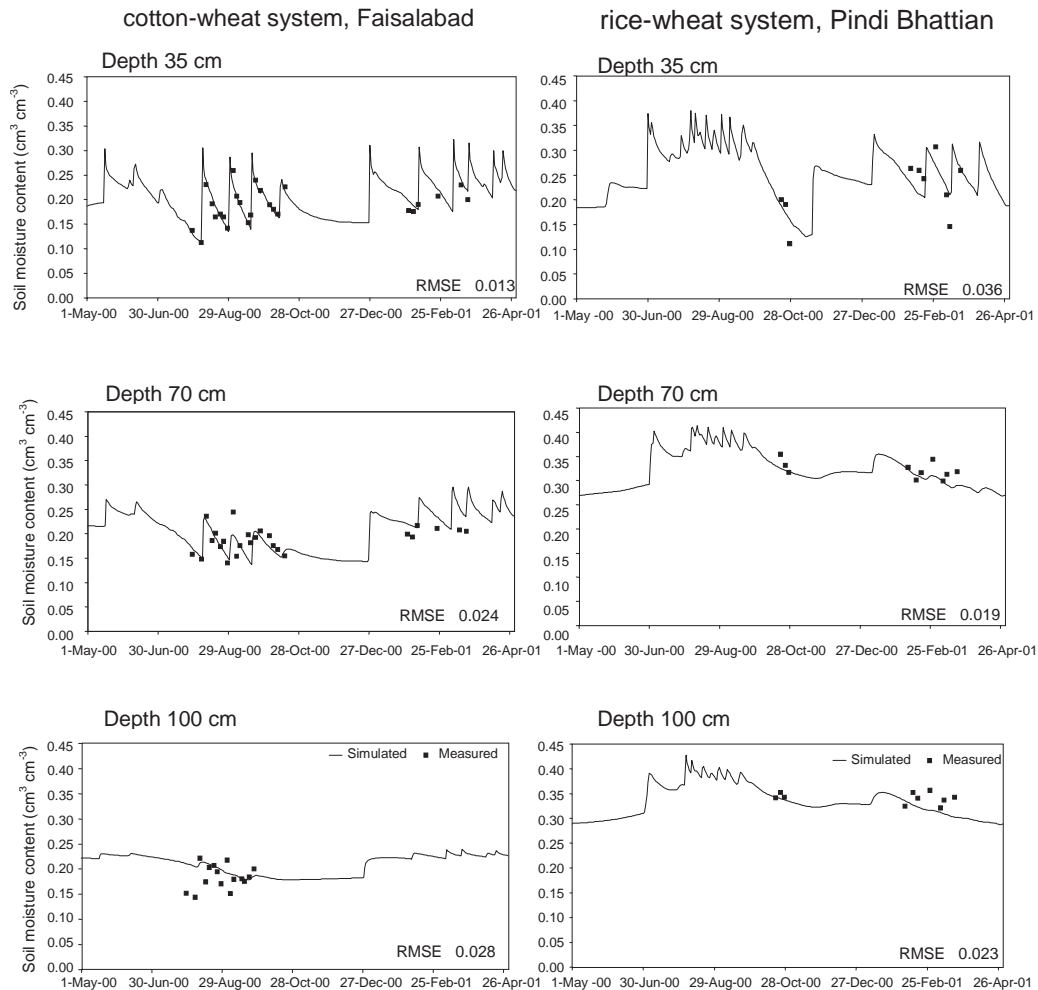
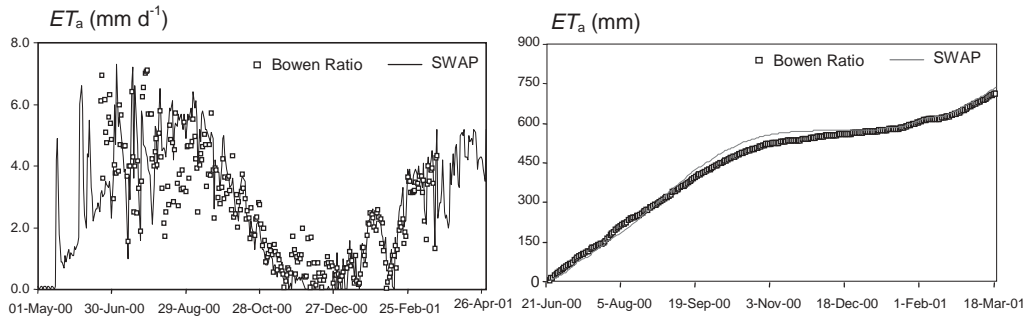


**Figure 4.2** Comparison of measured and simulated soil moisture content at different depths for a cotton-wheat system (Faisalabad) and a rice-wheat system (Pindi Bhattian).

#### Actual Evapotranspiration

Actual evapotranspiration  $ET_a$  computed with the SWAP model was compared with the measurement of  $ET_a$  from the Bowen ratio towers (Figure 4.3). The temporal variation in  $ET_a$  for both sites under different cropping rotations, soil types and irrigation systems could be simulated satisfactorily. A difference of 20.8 mm (2.9%) for accumulated evapotranspiration with a RMS error of 1.1 mm d<sup>-1</sup> was observed for the wheat-cotton rotation from June 21 (2000) to April 21 (2001). Similarly, for the rice-wheat rotation, a minor difference in the accumulated values of 10.7 mm (1.4%) with an RMS error of 0.9 mm d<sup>-1</sup> was observed over the period of June 21 to April 21.

cotton-wheat system, Faisalabad



rice-wheat system, Pindi Bhattian

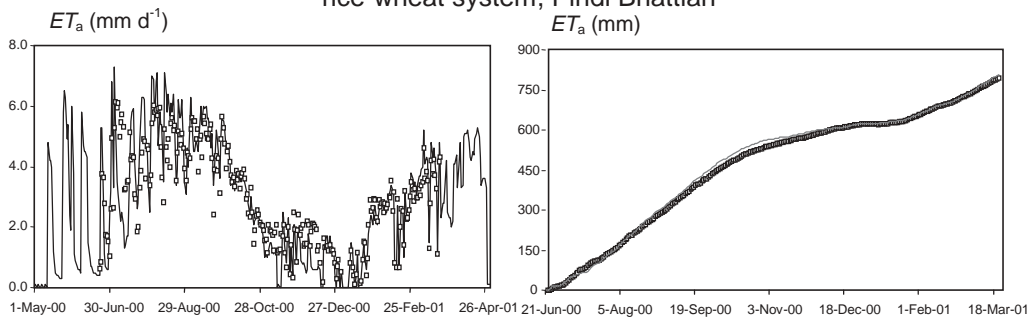


**Figure 4.3** Comparison of daily and cumulative actual evapotranspiration ( $ET_a$ ) estimated from SWAP and the Bowen ratio system for cotton-wheat system, (Faisalabad) and the rice-wheat system (Pindi Bhattian).

*Seasonal and annual water balance*

Daily values of precipitation  $P$ , irrigation  $I_{rr}$  from both canal and groundwater, and potential evapotranspiration  $ET_p$  were specified as model input. The rest of the water balance terms were computed from SWAP, such as interception losses  $P_i$ , actual crop transpiration  $T$ , actual soil evaporation  $E$ , change in soil moisture storage  $dW$  at any depth, and the Darcian flux at any depth. There was no noticeable surface runoff during the study period. The results of the complete water balance for cotton-wheat areas of Faisalabad and rice-wheat areas of Pindi Bhattian are presented in the Tables 4.4 and 4.5 respectively.

**Table 4.4** Seasonal and annual water balance for cotton-wheat system, Faisalabad. Gross rainfall  $P$ , interception losses  $P_i$ , irrigation  $I_{rr}$  from both canal and groundwater, actual crop transpiration  $T$ , actual soil evaporation  $E$ , change in storage  $dW$ , and bottom flux  $q_{bot}$  (positive upward).

Period	Crop	measured		simulated				
		$P$ (cm)	$I_{rr}$ (cm)	$q_{bot}$ (cm)	$P_i$ (cm)	$T$ (cm)	$E$ (cm)	$dW$ (cm)
May 1-May 24, 2000	Fallow	0.00	7.60	-1.11	0.00	0.00	1.78	4.71
May 25-Dec. 5, 2000	Cotton	19.70	33.20	-10.60	0.66	53.19	11.60	-23.15
Dec. 6-Dec. 22, 2000	Fallow	0.00	0.00	-0.56	0.00	0.00	0.03	-0.59
Dec. 23-Apr. 30, 2001	Wheat	9.32	43.60	-7.44	0.39	28.83	3.79	12.47
May 1, 2000-April 30, 2001		29.02	84.40	-19.71	1.05	82.02	17.20	-6.56

**Table 4.5** Seasonal and annual water balance for rice-wheat system, Pindi Bhattian. Gross rainfall  $P$ , interception losses  $P_i$ , irrigation  $I_{rr}$  from both canal and groundwater, actual crop transpiration  $T$ , actual soil evaporation  $E$ , change in storage  $dW$  and bottom flux  $q_{bot}$  (positive upward).

Period	Crop	measured		simulated				
		$P$ (cm)	$I_{rr}$ (cm)	$q_{bot}$ (cm)	$P_i$ (cm)	$T$ (cm)	$E$ (cm)	$dW$ (cm)
May 1-June 29, 2000	Fallow	13.75	0.00	5.24	0.00	0.00	11.62	7.37
June 30-Oct. 31, 2000	Rice	18.65	64.98	-30.74	0.44	27.15	27.24	-1.94
Nov. 1-Nov. 8, 2000	Fallow	0.63	8.09	0.41	0.00	1.21	3.15	4.77
Nov. 9- Apr. 28, 2001	Wheat	3.42	26.24	-4.27	0.64	31.36	3.22	-9.83
Apr. 29-Apr. 30, 2001	Fallow	0.00	0.00	-0.02	0.00	0.00	0.03	-0.05
May 1, 2000-April 30, 2001		36.45	99.31	-29.38	1.08	59.72	45.26	0.32

The total inflow (i.e.  $I_{rr}$  and  $P_n$  at the cotton-wheat area of Faisalabad) was 52.2 cm during the complete growing cycle of the cotton crop, and the actual evapotranspiration (sum of  $E$  and  $T$ ) was 64.8 cm (higher than the total water inflow to the field). This implies that 23.2 cm of water was depleted from the soil profile. In contrast, the amount of irrigation in the *rabi* was higher than the actual evapotranspiration. This resulted in a considerable recovery of soil moisture storage during the cool winter period. However on the annual cycle, there was a negative change in storage for the cotton-wheat area of Faisalabad. The decrease in soil moisture storage of 6.6 cm was mainly the result of a negative bottom flux of 19.7 cm occurring during the irrigation season due to deeper groundwater extractions in the neighbouring areas. During the fallow period outside of the cropping seasons, the bottom flux was negligibly small, indicating that groundwater extractions in the region did not occur.

In the rice-wheat growing area of Pindi Bhattian, there was a 7.4 cm increase in storage during the fallow period before the rice transplantation, which is typically related to land preparation. During the *kharif*, there was a high application of irrigation (65 cm), mainly from groundwater resources. The significant groundwater extraction used to irrigate the rice crop results in the downward bottom flux ( $q_{bot}=-30.7$  cm). On

an annual basis, there is only a slight increase in the soil moisture storage ( $dW=0.3$  cm), which implies that the system, for this year of study at least, was in equilibrium. Another remarkable discovery is the very high soil evaporation of rice crops during land preparation and before closure of the canopy; the actual transpiration and evaporation rates are similar.

#### *Subsoil water fluxes*

One of the main objectives of this study was to quantify the soil water fluxes. Figure 4.4 presents the time-depth domain of the water fluxes, which synthesize all the moisture movements in one graph. The vertical coordinate of this graph represents the depth below ground surface, the x-axis represents the time. In this way, specific days of the season with a high percolation flux can be detected, and also, the variation of water flux with depth can be noticed. The soil water flux is represented by different colour intensities. A negative value of soil water flux represents the downward flow of water, while a positive flux represent upward flow. In both cases, it is obvious that whenever there is irrigation or precipitation, there is infiltration followed by a downward soil water movement. The effect of infiltration is clearly pronounced at shallow depths (up to 50-70 cm from the ground surface). The redistribution of water in the unsaturated zone is governed by the gradient in soil moisture potential. After irrigation, the soil water flux is downward. During periods of zero infiltration and a high evaporative demand, the gradient reverses and the direction of the water flux changes to an upward orientation towards the evaporating surface. As a consequence, a zero flux plane is present. This process is typical for intensively irrigated soils, and Figure 4.4 basically the sub-soil as a black box.

In the rice-growing area, the downward soil water flux reaches the phreatic surface. This process is rapid because of a higher frequency of irrigation combined with shallow phreatic surface conditions and hence less travel time. In the cotton-wheat area with a deep phreatic surface, a continuous flow process was not observed; the soil water fluxes in the zone between 3 and 8 m were essentially nil. However, the groundwater extraction induces downward soil water fluxes in the capillary fringe just above the phreatic surface, which ultimately affects the moisture re-distribution in the whole soil profile. Groundwater extraction pulls the phreatic surface down when lateral inflow cannot meet the artificial extraction rates. The consequence is a soil water flux from the unsaturated zone to the saturated groundwater system, and this is a recharge induced by groundwater pumpage.

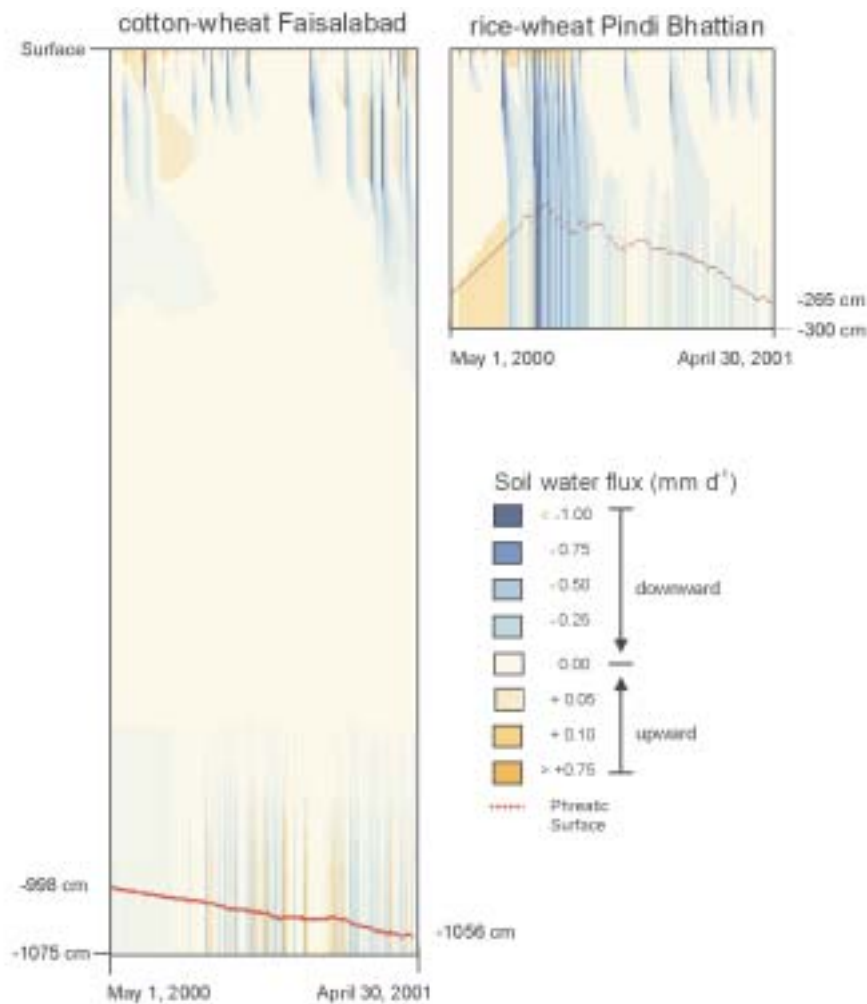


**Figure 4.4** Depth-time domain of vertical soil water fluxes in the unsaturated-saturated zones for a cotton-wheat system at Faisalabad and a rice-wheat system at Pindi Bhattian. The vertical axis represents depth and the horizontal axis time.

A summary of the soil water flux analysis is presented in Tables 4.6 and 4.7 for both Faisalabad and Pindi Bhattian, respectively. These results show that divergence of soil water flux in the sub-root zone occurs, especially in the Faisalabad area. In Faisalabad, the magnitude of the total annual amount of soil water leaving the root zone at 2 m is 8.3 cm higher than the percolating soil water flux ( 6.5 cm) at a depth of 8.7 m, which reveals moisture storage in the subsoil. The soil water flux at the phreatic surface for both cases is much higher than at for a shallow phreatic surface, but this is the result of the groundwater extraction processes explained above. The capillary rise of 5.7 cm is reduced to 0.7 cm at a 8.75 m depth and subsequently to zero at the bottom of the root zone. Hence, there is no direct groundwater contribution to crop

evapotranspiration in Faisalabad. The data from Pindi Bhattian in Table 4.7 show, however, that 7.0 cm of groundwater flows (upward flux) into the root zone at a depth of 2.0 m, which is considerable.

**Table 4.6** Soil water flux at various depths for the cotton-wheat area, Faisalabad.

Month	Soil water flux at 2 m depth (cm)		Soil water flux at 8.75 m depth (cm)		Soil water flux at variable phreatic surface (cm)		Bottom flux $q_{bot}$ at 10.75 m depth (cm)
	$q^{\downarrow}$	$q^{\uparrow}$	$q^{\downarrow}$	$q^{\uparrow}$	$q^{\downarrow}_{(h_m=0)}$	$q^{\uparrow}_{(h_m=0)}$	
May	0.35	0.00	0.68	0.00	1.36	0.00	-1.45
June	1.05	0.00	0.63	0.00	1.35	0.00	-1.51
July	0.44	0.00	0.54	0.00	1.17	0.00	-1.37
Aug.	0.08	0.00	0.59	0.03	1.73	0.20	-1.63
Sep.	0.02	0.00	0.74	0.06	2.42	0.42	-2.32
Oct.	0.00	0.00	0.55	0.11	1.93	0.69	-1.32
Nov.	0.00	0.00	0.71	0.15	3.00	1.12	-2.26
Dec.	0.00	0.01	0.26	0.06	0.89	0.46	-0.47
Jan.	0.00	0.01	0.29	0.14	1.32	0.91	-0.44
Feb.	0.06	0.00	0.53	0.03	2.84	0.50	-2.57
March	3.58	0.00	0.56	0.00	2.79	0.09	-3.02
April	2.74	0.00	0.40	0.11	2.45	1.30	-1.35
Annual	8.32	0.02	6.49	0.69	23.26	5.70	-19.71

**Table 4.7** Soil water flux at various depths for the rice-wheat area, Pindi Bhattian.

Month	Soil water flux at 2 m depth (cm)		Soil water flux at variable phreatic surface (cm)		Bottom flux $q_{bot}$ at 3 m depth (cm)
	$q^{\downarrow}$	$q^{\uparrow}$	$q^{\downarrow}_{(h_m=0)}$	$q^{\uparrow}_{(h_m=0)}$	
May	0.00	1.63	0.00	2.56	2.66
June	0.00	2.30	0.00	2.68	2.68
July	2.52	0.78	2.62	0.78	-1.71
Aug.	16.18	0.20	16.93	0.32	-17.54
Sep.	9.41	0.00	9.63	0.00	-9.53
Oct.	2.10	0.12	2.37	0.06	-2.06
Nov.	0.69	0.91	0.92	0.85	0.17
Dec.	0.61	0.55	1.04	0.38	-0.10
Jan.	1.47	0.28	2.21	0.25	-1.35
Feb.	0.92	0.02	1.29	0.12	-1.15
March	0.48	0.03	1.24	0.18	-1.08
April	0.09	0.14	0.66	0.26	-0.37
Annual	34.48	6.96	38.91	8.44	-29.38



### *Temporal pattern of recharge and groundwater use*

On both experimental sites, a conjunctive use of canal and groundwater resources is practised. The total irrigation in Tables 4.8 and 4.9 was therefore broken down into irrigation with canal water and with groundwater. The net groundwater use is substantially less than the groundwater withdrawals for irrigation  $I_{tw}$  in both cases, because the phreatic aquifer is replenished by recharge.

There is more recharge in Pindi Bhattian (38.9 cm) than in Faisalabad (23.3 cm). Due to the frequent irrigations in rice systems, the monthly rate of recharge ranges between 0.9 to 3.0 cm at Faisalabad and 0 to 16.9 cm at Pindi Bhattian. In Pindi Bhattian, 81% of the annual recharge occurs during the *kharif*. A sharp decline in the phreatic surface is observed in the field during the rice-rowing season. The annual groundwater resource ratio has been found to be 0.2 and 0.6 at Faisalabad and Pindi Bhattian, respectively. This reflects that the rice-wheat systems of Pindi Bhattian rely more on irrigation with groundwater than the cotton-wheat areas of Faisalabad. But an appreciable of groundwater flows back into the aquifer as a result of percolation. The recharge of Faisalabad is rather constant, but high for Pindi Bhattian in August (16.9 cm) and September (9.6 cm).

An annual recharge of 23.3 cm is estimated for the cotton-wheat area. Despite that, a decline in phreatic surface was observed, which indicates that lateral inflow and recharge cannot compensate for the annual groundwater extraction of 27.3 cm. Sustainability will be obtained if the annual groundwater extraction is reduced from 27.3 cm to the net recharge of 17.6 cm, or a reduction of 36%. In the rice-wheat area, irrigation with groundwater (81.1 cm) far exceeds the net recharge of 30.5 cm, but the phreatic surface is not declining. A reduction of 62% in groundwater extraction is necessary in order to reach sustainability of groundwater use at the field scale.

**Table 4.8** Net recharge  $q_{nr}$  and net groundwater use  $I_{ngw}$  in the cotton-wheat system at Faisalabad.

Month	measured		estimated			
	$I_{cw}$	$I_{tw}$	$q_{(h_m=0)}^{\downarrow}$	$q_{(h_m=0)}^{\uparrow}$	$q_{nr}$	$I_{ngw}$
	(cm)	(cm)	(cm)	(cm)	(cm)	(cm)
May	7.62	0.00	1.36	0.00	1.36	-1.36
June	0.00	0.00	1.35	0.00	1.35	-1.35
July	0.00	0.00	1.17	0.00	1.17	-1.17
Aug.	19.28	0.00	1.73	0.20	1.53	-1.53
Sep.	0.00	8.63	2.42	0.42	2.00	6.63
Oct.	5.28	0.00	1.93	0.69	1.24	-1.24
Nov.	0.00	0.00	3.00	1.12	1.88	-1.88
Dec.	10.00	0.00	0.89	0.46	0.43	-0.43
Jan.	0.00	0.00	1.32	0.91	0.41	-0.41
Feb.	0.00	8.44	2.84	0.50	2.34	6.10
March	14.88	3.76	2.79	0.09	2.70	1.06
April	0.00	6.51	2.45	1.30	1.15	5.36
Annual	57.06	27.34	23.26	5.70	17.56	9.78

**Table 4.9** Net recharge  $q_{nr}$  and net groundwater use  $I_{ngw}$  in the rice-wheat system at Pindi Bhattian.

Month	measured		estimated			
	$I_{cw}$	$I_{tw}$	$q_{(h_m=0)}^{\downarrow}$	$q_{(h_m=0)}^{\uparrow}$	$q_{nr}$	$I_{ngw}$
	(cm)	(cm)	(cm)	(cm)	(cm)	(cm)
May	0.00	0.00	0.00	2.56	-2.56	2.56
June	5.00	5.00	0.00	2.68	-2.68	7.68
July	4.07	4.08	2.62	0.78	1.84	2.24
Aug.	9.15	23.16	16.93	0.32	16.61	6.55
Sep.	0.00	14.52	9.63	0.00	9.63	4.89
Oct.	0.00	0.00	2.37	0.06	2.31	-2.31
Nov.	0.00	8.09	0.92	0.85	0.07	8.02
Dec.	0.00	0.00	1.04	0.38	0.66	-0.66
Jan.	0.00	6.98	2.21	0.25	1.96	5.02
Feb.	0.00	6.41	1.29	0.12	1.17	5.24
March	0.00	6.10	1.24	0.18	1.06	5.04
April	0.00	6.75	0.66	0.26	0.40	6.35
Annual	18.22	81.09	38.91	8.44	30.47	50.62

#### 4.4 Conclusions

The aim of this study was to quantify the sub-soil water fluxes in an environment with groundwater irrigation and to understand the impact of surface irrigation with groundwater resources on soil moisture movement. The SWAP model was well calibrated against measurements of actual evapotranspiration computed with the Bowen ratio surface energy balance system and against soil moisture profiles.

The application of the SWAP model provides a quantitative insight of water balance terms and soil water fluxes in the sub-soil, which cannot be straightforwardly measured by field instruments. Detailed time-depth profiles of the sub-soil water fluxes are presented (Figure 4.4). It was found that recharge takes place, even in areas having a deep phreatic surface, due to man-induced groundwater sinks. The percolation flux varies significantly with time and with depth in the unsaturated zone. The flux direction can reverse at greater depths. The water flux leaving the root zone cannot be considered to be the deep percolation rate, especially in deep phreatic surface conditions. As well as applying a transient soil moisture model for water flux determinations, the same model can also investigate the impact of groundwater management scenarios on crop growth and long term aquifer storage.

This case study in Pakistan reveals that a considerable fraction of recharge is due to losses from groundwater irrigation. This reflects that not all groundwater extracted for agriculture is consumed and that irrigation efficiency can be increased.

The sustainability of groundwater irrigation systems is currently studied by means of phreatic surface monitoring networks. Although this is suitable, it does not provide field scale information on the field-scale processes and how rising and falling phreatic surface can be halted. The method shown can help in quantifying the direct interactions at the phreatic surface.



## 5      **SATELLITE SURVEILLANCE OF EVAPORATIVE DEPLETION ACROSS THE INDUS BASIN\***

### 5.1    **Introduction**

The demand for water exceeds its availability in several of the world's large river basins. To determine appropriate water balances and to understand who actually uses the water, it is becoming increasingly important to study spatial patterns of evaporative depletion in the rural parts of river basins. A river basin typically contains irrigated agriculture, rain fed agriculture, forests, native vegetation, wetlands, and other systems, which all transmit water into the atmosphere through evapotranspiration. Digital maps of land use and evaporative water use can be used to determine the depletion of water resources and to study the severity of water shortages and inequities in water use.

Information on water use through evapotranspiration in rural areas is not as commonly available as data on land use and water supply. A classical solution to this problem is the application of distributed hydrological models (e.g. Arnold *et al.*, 1993; Refsgaard, 1997). The evapotranspiration computations in these models depend substantially on the quality of the input data – particularly that of soil and vegetation physical properties – and on the hydrological boundary conditions. It takes considerable effort to collect all the required input data and to calibrate distributed hydrological models (Gupta *et al.*, 1998) for a river basin as huge as the Indus River System (16 million ha). Techniques are needed to diagnose where and how much water has been used, without a dependence on complex and data-demanding simulation models. Satellite remote sensing techniques are widely applied to map crop types, land cover and land use on a regional scale. This paper describes a study designed to diagnose the water use patterns in the Indus basin, and that was part of an overall initiative to determine the agricultural and environmental performance of the Indus basin Irrigation System.

Evapotranspiration mapping using satellite imagery is an expanding research field. The first results were reported in the 1970s (e.g. Hiler and Clark, 1971; Jackson *et al.*, 1977, 1981) and continued in the 1980s (e.g. Soer, 1980; Seguin and Itier, 1983). Despite progress (see Bastiaanssen *et al.*, 1999 for a review), there are few reports of regional-scale applications used to determine water budgets for long periods. The major difficulty is that most remote sensing evapotranspiration algorithms require too much input data such as net radiation, air temperature, and aerodynamic resistances. This paper describes a scientifically proven method that overcomes these constraints by using the concept of evaporative fraction and surface energy balances for entire cropping seasons.

---

\* Adapted version of Bastiaanssen, W.G.M., M.D. Ahmad and Y. Chemin, 2002. Satellite surveillance of evaporative depletion across the Indus basin. *Water Resources Research* (in press)

## 5.2 Study area and climate

The Indus basin contains more than 16 million ha of irrigated land and is one of the largest contiguous irrigation systems in the world. It is located in Pakistan where the climate is semi-arid to arid, with monsoons occurring from June to September. Wheat and fodder are the dominant crops during the dry *rabi* (winter) season. Among other crops, cotton, rice, maize, and fodder are produced during the wet *kharif* (summer) season. In some parts sugarcane is also cultivated which is an annual crop. The large rural population of the Indus basin is directly involved in agriculture, which is important to the economy of the region.

Reference evapotranspiration  $ET_0$ , calibrated from weather data recorded at Faisalabad, Rechna Doab, Pakistan, is presented in Figure 5.1. The standard FAO-56 method for grass as the reference crop was used (Allen *et al.*, 1998) along with the more simplified Priestley and Taylor method (Priestley and Taylor, 1972).

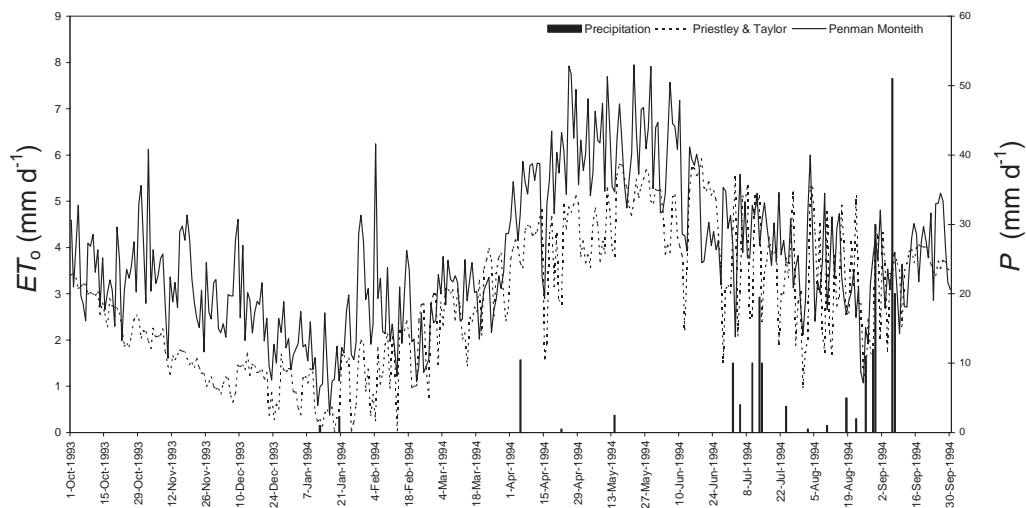


**Figure 5.1** Seasonal variations in reference evapotranspiration  $ET_0$  and precipitation rate  $P$ , Faisalabad, Rechna Doab, Pakistan, October 1993 – 1994.

Penman-Monteith reference evapotranspiration is based on a constant canopy resistance  $r_c=70 \text{ s m}^{-1}$ , independent of weather conditions. This may not be totally correct under high atmospheric vapour pressure deficits ( $>20 \text{ mbar}$ ) (e.g. Stewart, 1988; de Rooy and Holtslag, 1999). Even if the soil moisture conditions are ideal, stomata close if cell moisture depletion is triggered, with a consequent reduction in evapotranspiration. The Priestley and Taylor reference evapotranspiration does not explicitly include the stomatal mechanism, but has a constant resistance contained in the  $\alpha$ -coefficient. The annual reference evapotranspiration computed by Priestley and Taylor's method is  $\Sigma ET_0=1050 \text{ mm}$ , and by Penman-Monteith  $\Sigma ET_0=1367 \text{ mm}$ . This is a noteworthy difference that will be discussed later in this paper.

The computation of actual evapotranspiration  $ET_a$  is based on data from a series of 20 National Oceanic Atmospheric Administration (NOAA) – Advanced Very High Resolution Radiometer (AVHRR) satellite images (Table 5.1). Each AVHRR image covers the entire 16 million ha of the Indus basin. The images were selected for days when there was minimal cloud cover over the basin. October 1993 to October 1994 was chosen for the annual study because additional water balance information was available for this period (Habib *et al.*, 1999). The time between consecutive cloud-free images varies between 2 and 35 days, with an average of 18 days. The selected AVHRR images were first geometrically corrected to remove the effects of the earth's curvature. Thereafter, the spectral radiances for the separate channels of the AVHRR were corrected for absorption and emission by the atmosphere. This was achieved by relating the red channel (band 1) and the near-infrared channel (band 2) to surface reflectances in these bands. Two contrasting surfaces with known surface reflectances were analysed: a wet and a dry surface. The pixels for individual AVHRR images were re-sampled to a resolution of 1 km × 1 km. The ground-based input data consisted of sunshine duration and wind speed measurements collected from 10 different weather stations. Each weather station represents one climatological zone, based on descriptions in the National Climate Atlas of Pakistan.

**Table 5.1** National Oceanic Atmospheric Administration – Advanced Very High Resolution Radiometer (NOAA-AVHRR) acquisition dates during the 1993-94 cropping season.

Oct 10 1993	Jan 21 1994	Apr 4 1994	June 27 1994
Oct 13 1993	Jan 27 1994	Apr 29 1994	July 7 1994
Nov 18 1993	Feb 15 1994	May 16 1994	July 12 1994
Dec 2 1993	Feb 17 1994	May 24 1994	Aug 27 1994
Dec 11 1993	Mar 24 1994	June 13 1994	Sep 24 1994

### 5.3 Theoretical background

Evapotranspiration is related to the surface energy balance, which is expressed as:

$$R_n = G_0 + H + \lambda E \quad (5.1)$$

where  $R_n$  ( $W m^{-2}$ ) is the net radiation flux,  $G_0$  ( $W m^{-2}$ ) is the soil heat flux,  $H$  ( $W m^{-2}$ ) is the sensible heat flux, and  $\lambda E$  ( $W m^{-2}$ ) is the latent heat flux associated with evapotranspiration. Eq. 5.1 can be re-written and expressed as latent heat flux by considering evaporative fraction  $\Delta$  (-) and net available energy ( $R_n - G_0$ ):

$$\lambda E = (R_n - G_0) \quad (5.2)$$

where

$$= \frac{\lambda E}{R_n - G_0} = \frac{\lambda E}{\lambda E + H} \quad (5.3)$$

The net available energy ( $R_n - G_0$ ) in Eq. 5.2 may have different time scales, from instantaneous (at the time of the satellite overpass) to daily-integrated values, or for periods elapsing between two consecutive satellite images. Depending on the time scale chosen, different time integrations of ( $R_n - G_0$ ) need to be obtained. For time scales of 1 day or longer,  $G_0$  can be ignored and net available energy ( $R_n - G_0$ ) reduces to net radiation ( $R_n$ ). For the daily time scale,  $ET_{24}$  ( $\text{mm d}^{-1}$ ) is formulated as:

$$ET_{24} = \frac{86400 \cdot 10^3}{\lambda \rho_w} R_{n24} \quad (5.4)$$

where  $R_{n24}$  ( $\text{W m}^{-2}$ ) is the 24-h average net radiation,  $\lambda$  ( $\text{J kg}^{-1}$ ) is the latent heat of vaporization, and  $\rho_w$  ( $\text{kg m}^{-3}$ ) is the density of water.

For time scales longer than 1 day Eq. 5.4 becomes:

$$ET_{\text{int}} = \frac{dt \cdot 86400 \cdot 10^3}{\lambda \rho_w} R_{n24t} \quad (5.5)$$

where  $ET_{\text{int}}$  ( $\text{mm interval}^{-1}$ ) is actual evapotranspiration during interval  $dt$ ,  $R_{n24t}$  ( $\text{W m}^{-2}$ ) is the average  $R_{n24}$  value for the time interval  $dt$  measured in days.  $R_{n24t}$  is usually lower than  $R_{n24}$  because  $R_{n24}$  is taken from clear-sky satellite overpass days and  $R_{n24t}$  also includes cloud-covered days. The chief assumption in the SEBAL model is that the evaporative fraction specified in Eq. 5.3 remains constant for the time interval between each satellite image. Experimental work has demonstrated that this holds true for environmental conditions where soil moisture does not significantly change (e.g. Shuttleworth *et al.*, 1989; Brutsaert and Sugita, 1992; Nicols and Cuenca, 1993; Kustas *et al.*, 1994; Crago, 1996; Franks and Beven, 1997). Farah (2000) found that the accumulated evapotranspiration for a period of 10 to 20 days can be predicted satisfactory from Eq. 5.5, but that the computation of  $\lambda E$  for a particular day within a 10-day period using the constant value of  $\lambda$  obtained for the time of the satellite overpass is not accurate. This has an important implication:  $\lambda E$  estimates for days with no satellite images can be erroneous, but the temporally integrated value for a week can be sufficiently accurate using a temporally constant value of  $\lambda$ . Apparently, there are some systematic errors that cancel out over longer periods of time.

Eq. 5.2 requires  $\lambda$ ,  $R_n$ , and  $G_0$  to be known. The various components for computing the net radiation flux  $R_n$  can be assessed from remote sensing data. Procedures for computing incoming solar radiation from geo-stationary satellites have been given by Zhang *et al.* (1995) and Diak *et al.* (1996). Surface albedo algorithms have been presented by Valiente *et al.* (1995). Incoming long-wave radiation can be determined from the apparent emissivity of the atmosphere using sounding data (e.g. Diak *et al.*,



2000). Emitted long-wave radiation from the surface can be computed from the radiometric surface temperature (e.g. Kealy and Hook, 1993).

In this case study, surface albedo was determined from AVHRR channels 1 and 2 using the method proposed by Valiente *et al.* (1995). The surface temperature was obtained from AVHRR channels 4 and 5 using the split-window technique proposed by Sobrino *et al.* (1991). The coefficients of the split-window technique were adjusted using measured sea surface temperatures from the Arabian Sea. The required thermal infrared emissivity was computed using the simple method proposed by van de Griend and Owe (1993), that is based on the Normalized Difference Vegetation Index (NDVI). Incoming solar radiation was computed from solar duration measurements, i.e. hours of sunshine ( $n$ ) measured by Gumble Stokes recorders, using the standard conversion equation suggested by Allen *et al.* (1998):

$$K^\downarrow = (0.25 + 0.45 n/N) K_{\text{exo}}^\downarrow \quad (5.6)$$

where  $K^\downarrow$  ( $\text{W m}^{-2}$ ) is the global radiation at the surface level,  $n$  (hr) is the hours of actual sunshine measured in the field,  $N$  (hr) is the theoretical maximum hours of sunshine, and  $K_{\text{exo}}^\downarrow$  ( $\text{W m}^{-2}$ ) is the theoretical extra-terrestrial solar radiation. The coefficient 0.45 in Eq. 5.6 is somewhat lower than the standard coefficient of 0.5 often used, and was determined from pyranometer measurements. The lower value can be ascribed to the dusty atmosphere over the Indus basin (It was not possible to access geo-stationary data from the Indian-owned INSAT satellite to improve the description of spatial variability of solar radiation). The conversion of global radiation into net radiation for time scales of days and longer periods was achieved using a simplified formula (de Bruin and Stricker, 2000):

$$R_{n24} = (1 - r_0) K^\downarrow - 110 K^\downarrow / K_{\text{exo}}^\downarrow \quad (5.7)$$

where  $r_0$  (-) is the surface albedo. The evaporative fraction was computed using the instantaneous surface energy balance residual ( $R_n - G_0 - H$ ), which converts Eq. 5.3 into:

$$= \frac{R_n - G_0 - H}{R_n - G_0} \quad (5.8)$$

The soil heat flux  $G_0$  was computed as a variable fraction of net radiation  $R_n$ , taking into account the presence of leaves through the vegetation index and the surface temperature. It is assumed that warmer surfaces have a higher  $G_0/R_n$  fraction. The largest obstacle in solving  $\lambda$  is the estimation of  $H$ . Various research has been devoted to the assessment of  $H$  from the radiometric surface temperature  $T_0$  (e.g. Sugita and Brutsaert, 1990; Kalma and Jupp, 1990; Brutsaert *et al.*, 1993; Stewart *et al.*, 1994; Troufleau *et al.*, 1997; Chehbouni *et al.*, 1997). Solutions could be found only for sites that were heavily equipped to measure  $H$ , because the  $H(T_0)$  relationship is variable. The complexities of the  $H(T_0)$  relationship are related to the source height

for the radiometric surface temperature,  $z_{0h}$ , which cannot be assessed on the basis of generic rules in heterogeneous landscapes (Carlson *et al.*, 1995). That hampers the interpolation of  $H$  at the regional scale.

The Surface Energy Balance Algorithm for Land (SEBAL) described in Pelgrum and Bastiaanssen (1996), Bastiaanssen *et al.*, (1998), and Bastiaanssen (2000) was developed to overcome the classical problem of relating source height  $z_{0h}$  to radiometric surface temperature  $T_0$ . SEBAL first computes the sensible heat flux  $H$  at extreme dry and wet locations, manually identified on the image by the user. This eliminates the need to install expensive *in situ* equipment to measure  $H$ . Then, by model inversion, a temperature difference  $dT_{air}$  (K), required to match the range of  $H$  in given turbulent conditions, is obtained for these two contrasting surface types using:

$$dT_{air} = \frac{H r_{ah}}{\rho_{air} c_p} \quad (5.9)$$

where  $r_{ah}$  ( $s\ m^{-1}$ ) is the near-surface aerodynamic resistance to heat transfer,  $\rho_{air}$  ( $kg\ m^{-3}$ ) is the moist air density, and  $c_p$  ( $J\ kg^{-1}$ ) is the specific heat at constant pressure. The lower integration constant for  $r_{ah}$  – classically chosen as  $z_1=z_{0h}$  in thermal infrared studies – is conceptualised to be near the surface, to include fluxes originating from local vegetation and soil conditions. In the SEBAL model, a fixed value  $z_1=0.1$  m was chosen. The upper integration constant for  $r_{ah}$  is the reference height (e.g. 2.0 m). (Qualls *et al.*, (1993) also computed  $H$  from near-surface temperature differences.) This implies that  $dT_{air}$  is associated with a vertical column of air between 0.1 and 2.0 m high.

It should be recalled that Eq. 5.9 applies only to two pixels of the image: one pixel that is assumed to be completely wet where  $H \sim 0$  ( $dT_{air} \sim 0$ ), and another pixel that is assumed to be completely dry, so that  $\lambda E \sim 0$ , or  $H = R_n - G_0$ . Eq. 5.9 can be applied only to these two extreme pixels or ‘anchor points’, because  $H$  is not known for all the other pixels.

The identification of the dry pixel with negligible evapotranspiration ( $\lambda E \sim 0$ ) is based on measurements in the thermal infrared channel. First a group of pixels with maximum surface emittance is selected, and visually inspected on the satellite image to identify where they occur in the landscape. Morphological features on the image help to identify dry pixels where  $\lambda E \sim 0$  holds.

The spatial interpolation of  $dT_{air}$  between its two extreme values for a given image and at a certain time is conducted using the radiometric surface temperature image  $T_0$ , being corrected for emissivity to mimic heat release from the land surface into the atmosphere. The assumption is that hot surfaces with high thermal emittance create larger vertical differences in air temperature  $dT_{air}$  than do cold surfaces with minor thermal emittance. Field research has demonstrated that the relationship between  $dT_{air}(T_0)$  is linear (e.g. Wang *et al.*, 1995; Bastiaanssen, 1995; Franks and Beven, 1999):

$$dT_{\text{air}} = a + bT_0 \quad (5.10)$$

The coefficients  $a$  and  $b$  are unique for each satellite image. They are determined from the two pairs  $(dT_{\text{air}}, T_0)$  applicable to the dry and wet pixels. Once the spatial distribution of  $dT_{\text{air}}$  for all pixels is described by means of the  $T_0$ -image and Eq. 5.10, sensible heat flux can be computed for every pixel as:

$$H = \frac{\rho_{\text{air}} c_p}{r_{\text{ah}}} dT_{\text{air}} \quad (5.11)$$

Initially, free convection is assumed, yielding a first estimate of the aerial patterns of sensible heat flux using Eq. 5.11. Thereafter, mixed convection is applied and stability corrections due to buoyancy effects, according to the Monin-Obukhov similarity theory, are applied to the computation of the pixel-dependent aerodynamic resistance to heat transfer  $r_{\text{ah}}$  ( $\text{s m}^{-1}$ ) (Brutsaert, 1982):

$$r_{\text{ah}} = \frac{1}{k u_*} \left( \ln \frac{z_2}{z_1} \right) \left( 1 - \psi_h \right) \quad (5.12)$$

where  $u_*$  ( $\text{m s}^{-1}$ ) is the friction velocity,  $k$  is Von Karman's constant (experimentally equal to 0.41), and  $\psi_h$  (-) is the stability correction for heat transport. Values for  $u_*$  are obtained from the wind speed at the blending height—a value of 100 m was assumed in this study—and the surface roughness length for momentum transport  $z_{0m}$ :

$$u_* = (u_{100} k) / (\ln(100 / z_{0m}) - \psi_m) \quad (5.13)$$

where  $u_{100}$  ( $\text{m s}^{-1}$ ) is the wind speed at the blending height and  $\psi_m$  (-) is the stability correction for momentum transport. The wind speed at the blending height can be estimated from near-surface wind-speed measurements (see Allen *et al.*, 1998). Routine weather station data were used to obtain wind speeds measured at 2.0 m elevation. Using a logarithmic wind profile and a surface roughness length for grass ( $z_{0m}=0.017$  m), wind speed at 2.0 m was converted into wind speed at 100 m.

Eqs. 5.11 to 5.13 require an iterative process to solve for the sensible heat  $H$  using  $u_*$  (through  $\psi_m$ ) and  $r_{\text{ah}}$  (through  $\psi_h$ ).

## 5.4 Results

A total of 60 evapotranspiration maps were created, encompassing the entire Indus basin. This large area consisted of 160,000 pixels, each of 100 ha. First, 20 instantaneous latent heat flux maps  $\lambda E$  were made, followed by 20 daily integrated evapotranspiration maps  $ET_{24}$ , and 20 maps each covering a fraction of the annual evapotranspiration cycle  $ET_{\text{int}}$ . The results for the *rabi* and *kharif* are shown in Figure 5.2. The actual evapotranspiration for *rabi* is between 300 to 400 mm. It should be

noted, even though it is not shown, that the  $ET_a$  of the Punjab exceeds the  $ET_a$  of the Sindh during *rabi*. The stronger extra-terrestrial solar radiation, increased precipitation, and cultivation of rice and sugarcane crops during *kharif* explain why evapotranspiration is higher (600 mm). The evaporative fraction is likely to increase during the rainy season when plant canopies and soils are wet; but, clear satellite images are limited, due to the persistent cloud cover. The range of evapotranspiration levels occurring in *kharif* is wider than that in *rabi*. This can be explained by the high spatial variability of cloud cover combined with the stronger extra-terrestrial solar radiation. Actual evapotranspiration is reduced in cloud-covered regions and enhanced in cloud-free regions. Figure 5.3 provides a map of annual  $ET_a$ , computed using the SEBAL model described above.

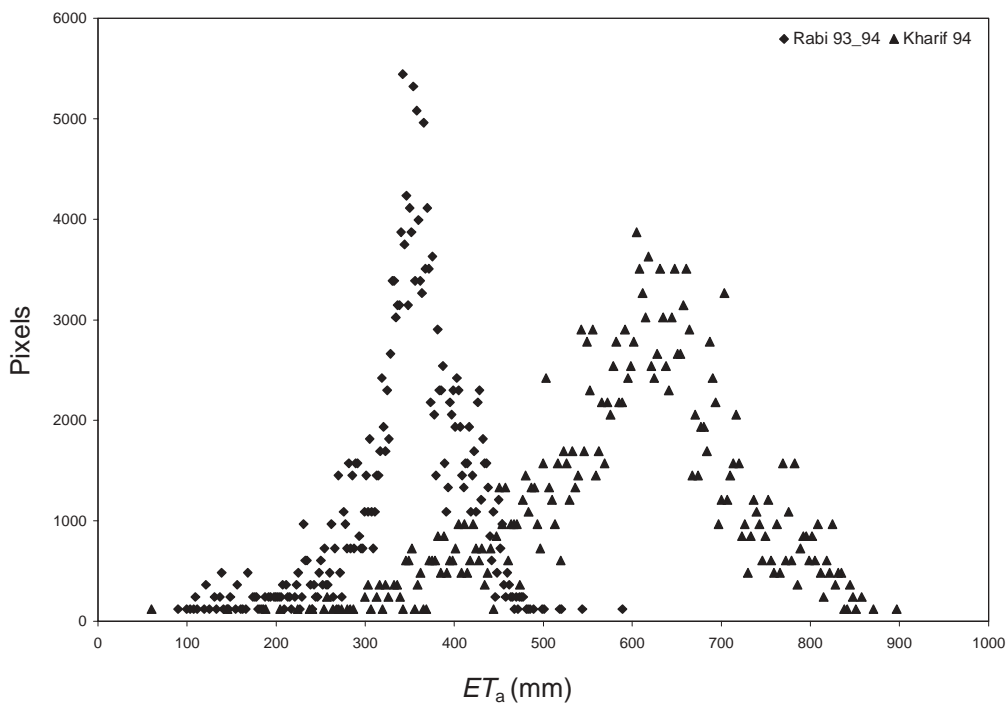


**Figure 5.2** Frequency distribution of the cumulative actual evapotranspiration  $ET_a$  for the *rabi* and *kharif* seasons for 16 million ha of the Indus basin, Pakistan, at the spatial resolution of one pixel, i.e. 1 km  $\times$  1 km for 100 ha.

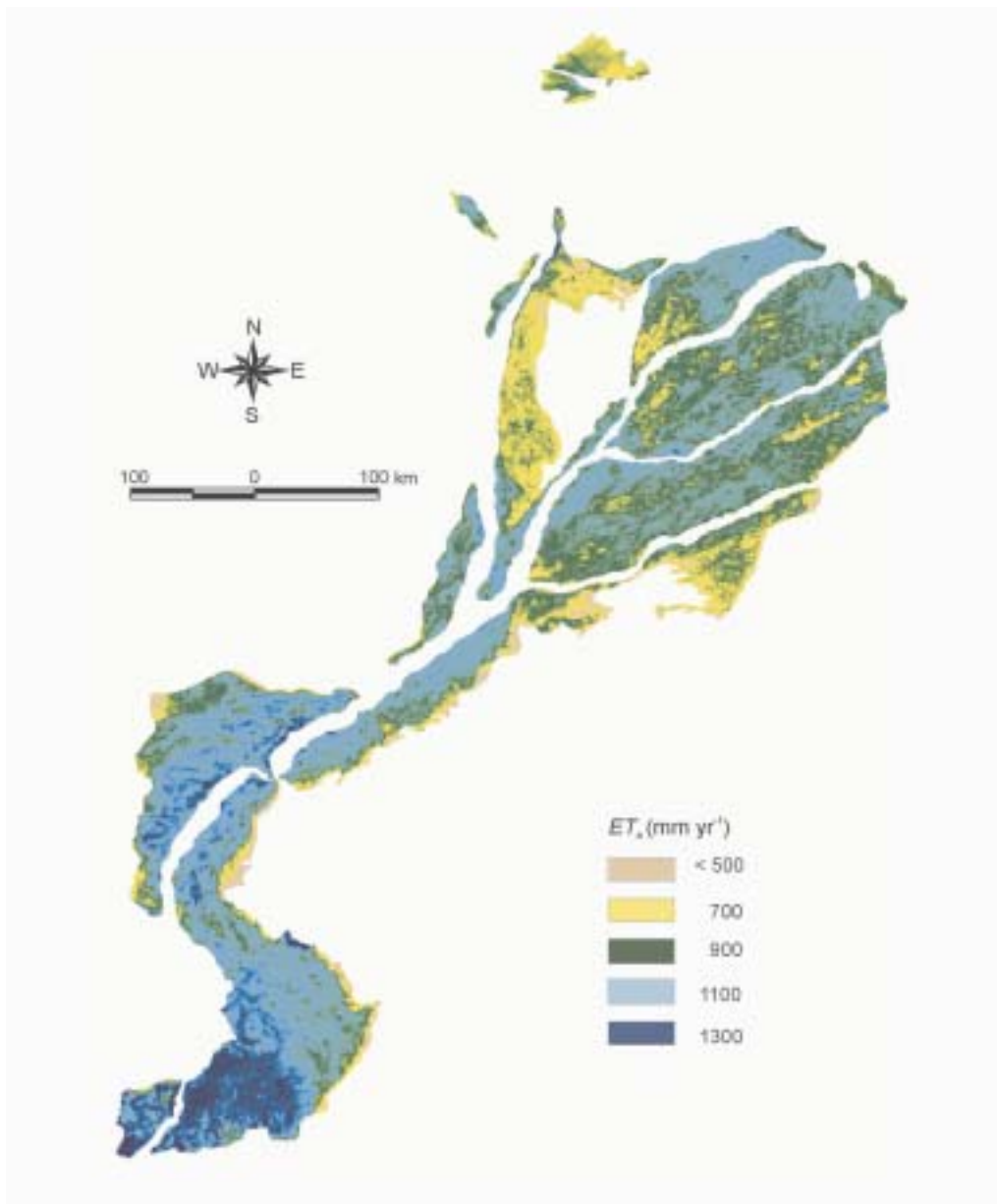


**Figure 5.3** Annual actual evapotranspiration  $ET_a$  for the Indus Basin, Pakistan, between October 1993 and October 1994.

Water quality reduces across the Indus basin towards the outflow into the Indian Ocean. The downstream end of the basin contains poor-quality water and is generally waterlogged for long periods during *khariif*. The southern part of the Sindh Province contains mangroves, flooded areas, and rice paddies, and has shallow phreatic

surfaces. It exhibits the highest  $ET_a$  rates in the basin and represents the wetter end of the frequency distribution of Figure 5.2. The second highest evapotranspiration zone is found on the right bank of the Indus River in the Sindh, where rice is the major staple crop during the monsoon season.

The frequency distribution of annual evapotranspiration is shown in Figure 5.4. The minimum for a NOAA-AVHRR pixel (100-ha area) is 230 mm and the maximum is 1460 mm. The reference evapotranspiration according to Penman-Monteith was 1367 mm, which deviates 7 % from the maximum value. This is equal to a crop coefficient of 1.07, which is a likely value for vegetated surfaces and is consistent with the SEBAL results. The values from Penman-Monteith may be slightly overestimated due to the constant canopy resistance. The cumulative values as determined by Priestley and Taylor seem to underestimate the annual  $ET_a$ , hence the standard  $\alpha=1.26$  coefficient may be higher under the semi-arid conditions of Pakistan.

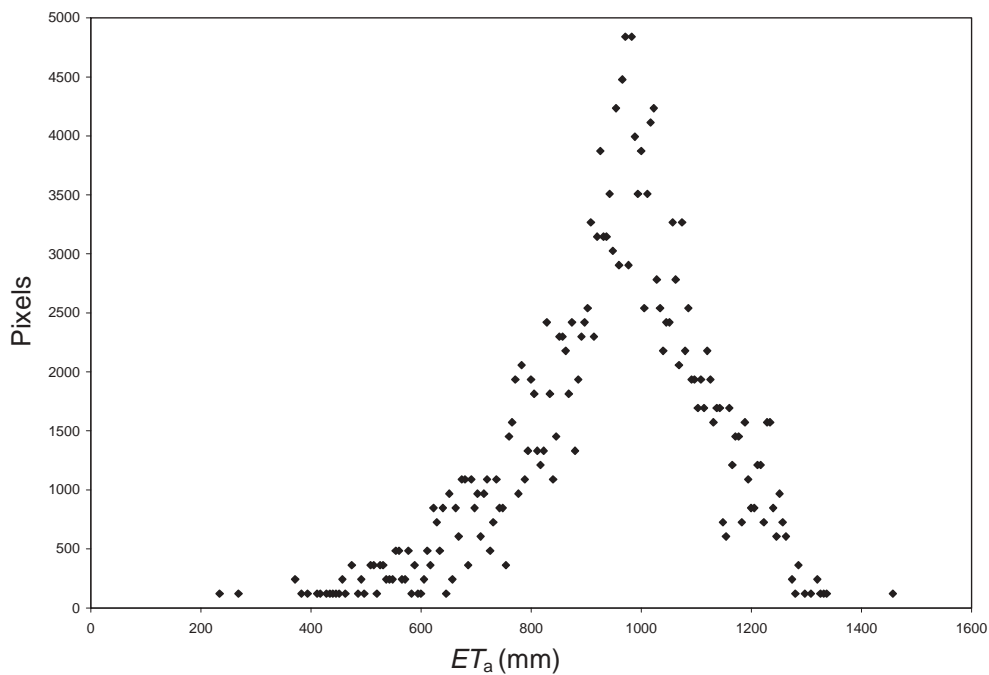


**Figure 5.4** Frequency distribution of annual actual evapotranspiration  $ET_a$  in the Indus basin, Pakistan.

It is interesting to investigate the temporal behaviour of actual evapotranspiration in three particular sub-areas located in the Indus basin. These sub-areas reflect the best, average and poorest conditions in irrigation, crop, drainage, and soil management. The sub-areas are all land surfaces. The sub-area where evapotranspiration was in the lowest 5% ( $\Sigma ET_a = 500$  mm) is at the downstream end of canal commands in the Punjab Province. Limited canal water and the presence of saline groundwater and

soils could be a problem in this area. The sub-area where evapotranspiration was average ( $\Sigma ET_a = 955$  mm) lies in the Punjab near Faisalabad. Pixels with average evapotranspiration can also be found in the North West Frontier Province and the Sindh Province. The sub-area where consumptive use was in the highest 5% ( $\Sigma ET_a = 1275$  mm) is located at the downstream end of the Indus basin in canal commands, where shallow water tables and waterlogging are common.

Figure 5.5 shows that the lowest  $ET_a$  for all three sub-areas (best, average, and poorest) was found in January, and is related to low ambient temperatures and to canal closing for routine annual maintenance.  $ET_a$  starts to increase during March when solar radiation increases steeply. The widest variation in  $ET_a$  occurs during June, prior to the onset of the monsoon. It seems that pixels with the lowest  $ET_a$  are fallow during *kharif* since  $ET_a$  drops below  $1 \text{ mm d}^{-1}$ , whereas rice systems have an  $ET_a$  of almost  $6 \text{ mm d}^{-1}$ .

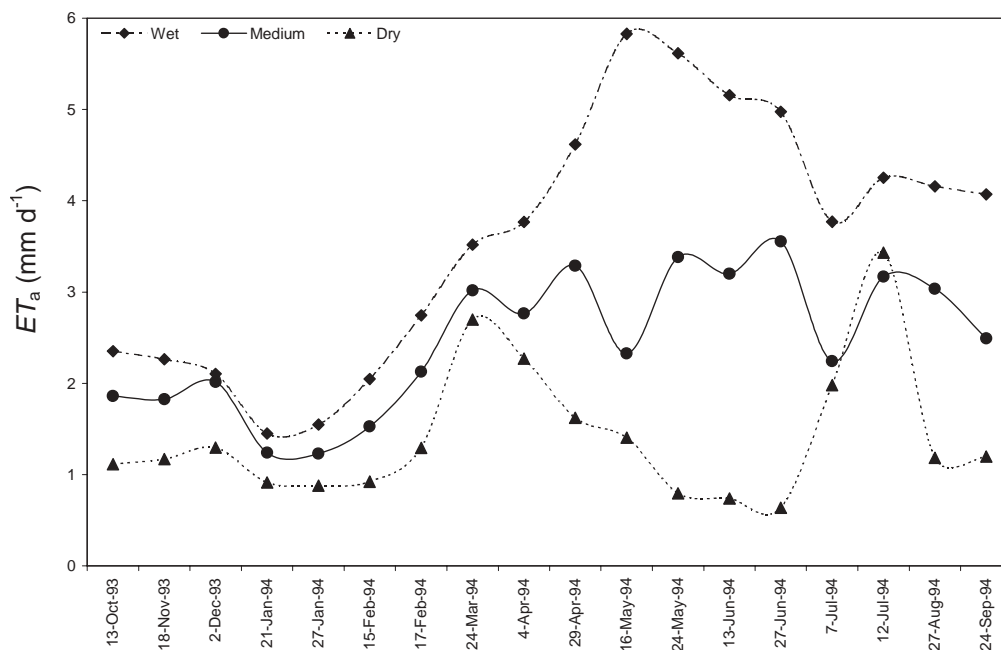


**Figure 5.5** Annual variability in actual evapotranspiration  $ET_a$  for wet, medium and dry sub-areas covering a range of soil wetness conditions in the Indus basin, Pakistan, October 1993 – October 1994.

## 5.5 Validation

Sarwar *et al.*, (2000) modelled the soil water balance of two large plots near Faisalabad using the one-dimensional transient moisture and salinity flow model Soil-Water-Atmosphere-Plant (SWAP) (Belmans *et al.*, 1983; Kroes *et al.*, 2000). The

model requires the following input data: Routine weather data, irrigation applications, Leaf Area Index development, root development, measured soil water retention characteristics, and saturated hydraulic conductivity. The unsaturated hydraulic conductivity was calibrated from observations of the phreatic surface and vertical soil moisture distribution. Measurements of soil moisture profiles and soil matric pressure head profiles and drainage outflow, over a period of almost 2 years, were used to validate SWAP. The root mean square error (RMSE) in drainage outflow was  $0.013 \text{ mm d}^{-1}$ . The RMSEs for daily soil moisture were  $0.02 \text{ cm}^3 \text{ cm}^{-3}$ , soil matric pressure head  $-26 \text{ cm}$ , soil salinity  $0.15 \text{ dS m}^{-1}$ , and phreatic surface fluctuations  $15 \text{ cm}$ . A RMSE of  $15 \text{ cm d}^{-1}$  for the phreatic surface may pose a threat to the accuracy of  $ET_a$  predictions by SWAP for short time-scales. In a different SWAP study, also conducted in the Punjab, Ahmad *et al.*, (2002) noted that daily  $ET_a$  for the SWAP model was less accurate. They demonstrated that the RMSE in actual evapotranspiration between SWAP and the Bowen ratio energy balance method varies between 0.9 for shallow and  $1.1 \text{ mm d}^{-1}$  for deep phreatic surface conditions. In conditions with deep phreatic surfaces, Ahmad *et al.*, found the RMSE for soil moisture varied between  $0.022$  and  $0.027 \text{ cm}^3 \text{ cm}^{-3}$ , similar to that found by Sarwar and co-workers. Hence, the actual evapotranspiration predicted by SWAP is only suitable for comparison against remote-sensing results when  $ET_a$  is integrated over time intervals longer than one month.

SWAP model-simulated evapotranspiration values, together with the single matching remote-sensing pixel evapotranspiration, are shown in Figure 5.6. The total  $ET_a$  for a time interval centred on the instant of every NOAA-AVHRR image was first computed assuming a constant evaporative fraction (see Eq. 5.5). Combining all the time intervals from the 20 NOAA-AVHRR images produced the step-wise graph shown in Figure 5.6. A pixel represents 100 ha, and the SWAP model covers a drainage plot of 70 ha. The accumulated evapotranspiration for a wheat-cotton rotation was found to vary between 980 and 1070 mm, depending on the irrigation water quality and the depth of irrigation applied (Sarwar *et al.*, 2000). Under farmer management, where phreatic surfaces are shallow and there is a sub-surface drainage system, the cumulative actual evapotranspiration (according to SWAP) for a period of 351 days was  $-ET_a = 1010 \text{ mm}$ . The SEBAL results for the same period were  $\Sigma ET_a = 1010 \text{ mm}$ , i.e., no difference could be detected. Figure 5.6 demonstrates that the two methods are in close agreement throughout the year, except during monsoon showers, and that SEBAL is not biased by land wetness or weather. The study area for the SWAP model in terms of soil wetness is somewhere between the dry and wet pixels chosen for the SEBAL procedure. The fact that SEBAL results agree closely to SWAP results confirms that the assumptions upon which it is based are correct. Hence, the assumptions that  $H=0$  for wet surfaces and  $\lambda E=0$  for dry surfaces seem to be reasonable.

During the year 2000, Bowen ratio surface energy balance measurement systems to directly measure actual evapotranspiration were set up in a cotton field at Faisalabad and a rice paddy at Pindi Bhattian (Ahmad *et al.*, 2002). Although this was for a different period than the remote-sensing study, it is worth comparing the results with the SEBAL estimations of 1994. The weather during these two study periods was not identical. Annual precipitation over the entire Rechna Doab was 315 mm from June



1993 to June 1994, whereas the Faisalabad station recorded 290 mm from May 2000 to May 2001. These differences mainly occur during the hot, wet *kharif* season. Excluding *kharif* leaves a period of approximately 8 months for comparison. The measured total evapotranspiration for this period was 570 mm, whereas the SEBAL estimates were 626 mm. This difference of 10% on a field scale is satisfactory, considering the differences in weather, inaccuracies in the Bowen-ratio method, and scale differences between the field apparatus and the pixel size (1 km × 1 km).

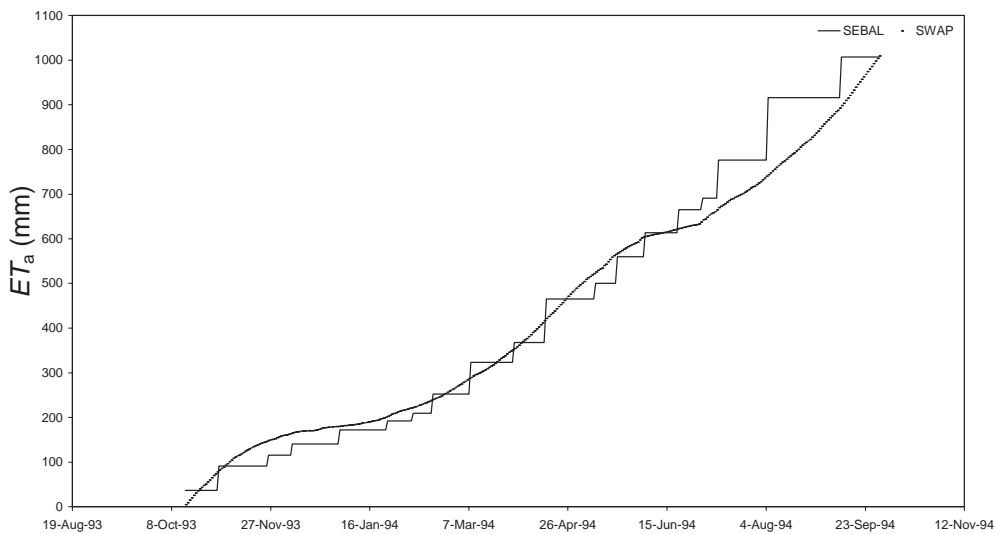


**Figure 5.6** Cumulative actual evapotranspiration  $ET_a$  estimated by the locally calibrated transient model Soil Water Atmosphere Plant (SWAP) and the Surface Energy Balance Algorithm for Land (SEBAL) for the Fourth Drainage Project near Faisalabad, Pakistan, October 1993 – October 1994. The size of each step in the SEBAL results represent the interval for which evapotranspiration is estimated from Eq. 5.5 (plotted at the midpoint of each interval between AVHRR image dates in Table 5.1).

The Rechna Doab occupies an area of approximately 2.97 million ha between the Ravi and Chenab rivers. A long-term water balance for the Rechna Doab between 1980 and 1995 was prepared using precipitation data  $P$  from selected weather stations. The piezometric readings were from approximately 900 stations; and, canal water deliveries  $I_{CW}$  were measured at six major off- take points using calibrated  $Q(h)$  relationships. All point data were interpolated into a raster map using a kriging geo-statistical procedure. By ignoring groundwater lateral inflows and outflows, the net groundwater use  $I_{ngw}$  (Eq. 3.20) was computed from phreatic surface fluctuations using a specific yield  $S_y$  of 13 %. The average values of the water-balance terms were computed and are presented in Table 5.2. Thereafter, by neglecting runoff and soil moisture storage changes on an annual basis, an actual evapotranspiration rate  $ET_a$  was computed (Eq. 3.23) as a water balance residual. The long-term actual

evapotranspiration for the entire Rechna Doab was found from Eq. 3.23 to be  $\Sigma ET_a = 1100 \text{ mm yr}^{-1}$  (1980–95) and  $\Sigma ET_a = 900 \text{ mm yr}^{-1}$  (June 1993 to June 1994). The mean SEBAL estimates of actual evapotranspiration for Rechna Doab were  $\Sigma ET_a = 940 \text{ mm yr}^{-1}$  from October 1993 to October 1994, with a standard deviation of  $80 \text{ mm yr}^{-1}$ . Hence, the 5% difference noticed between SEBAL (from October 1993 to October 1994) and the water balance (from June 1993 – to June 1994) can be considered small and within the error margins of both methods. It can therefore be concluded, that a satisfactory water balance was calculated.

**Table 5.2** Long-term average (1980–95) water balance for Rechna Doab, Pakistan, obtained from point observations and geo-statistical interpolation techniques.

	Depth ( $\text{mm yr}^{-1}$ )		
	1980–95	June 1993–June 1994	June 1994–June 1995
Precipitation	435	315	420
Irrigation	605	558	560
Net groundwater use	10	30	-5
Evapotranspiration	1050	900	970

## 5.6 Evaporative depletion in the Indus Basin

Doorenbos and Kassam (1979) collected and consolidated field experimental data from various places across the world. Table 5.3 presents a comparison of their results with those obtained from SEBAL and SWAP modelling of Sarwar and Bastiaanssen (2001).

**Table 5.3** Actual water use measured by remote sensing technology (Surface Energy Balance Algorithm for Land; SEBAL), a transient moisture flow model (Soil-Water-Atmosphere-Plant; SWAP) and the generalized crop water requirements of Doorenbos and Kassam (1979) for four crops and mangrove areas within the Indus Basin, Pakistan.

Crop	SEBAL (mm)		SWAP (mm)	FAO-33* (mm)
	Mean	Standard deviation		
Cotton	580	80	610 - 720	700–1300
Rice	410	60	n.a.**	450– 700
Wheat	360	40	380–400	450– 650
Sugarcane	970	130	n.a.	1500– 2500
Mangroves	1300–1500	n.a.	n.a.	n.a.

\* FAO 33 is the Food and Agricultural Organization of the United Nations (Doorenbos and Kassam, 1979)

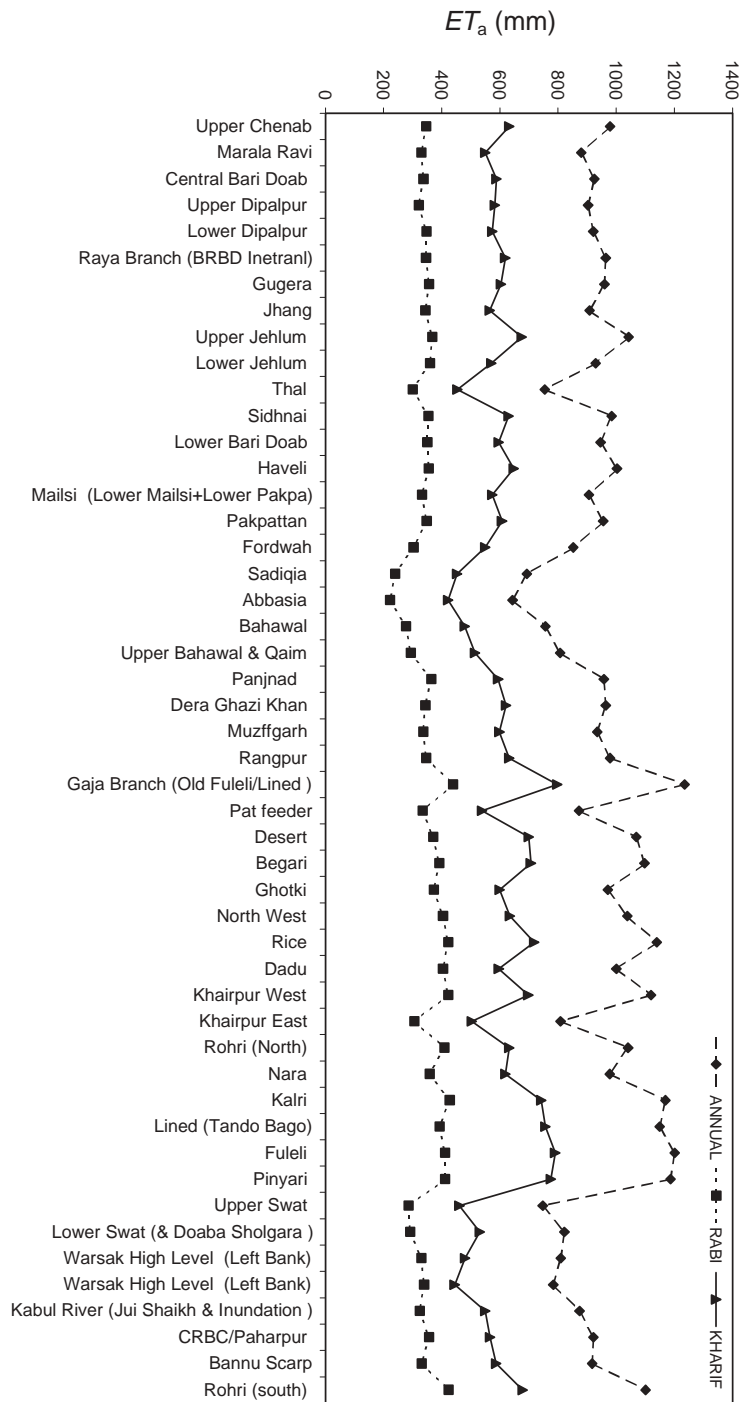
\*\* Not applicable

Pixels covering predominantly cotton, rice, wheat and sugarcane crops were identified on the basis of their temporal crop growth rhythms in relation to the cropping calendar. The recommended water use of Doorenbos and Kassam (1979) is not achieved in the Indus basin, which is reflected in the prevailing water deficits. The data show that sugarcane has the widest gap between the recommended water use to maintain potential crop growth and the actual amount of water used. The mangroves in the southern Sindh are the largest water consumers in Pakistan, accounting for 1300-1500 mm yr<sup>-1</sup>.

The *warabandi* irrigation system in the Indus basin, aims to supply all riparian users with an equitable amount of water (Berkoff and Hupert, 1987). Water consumption as computed from satellite data for an annual cycle provides critical information on equity in evaporative depletion. A summary for the various canal commands is provided in Figure 5.7. These are averages for each entire canal command, and may therefore be lower than the averages for irrigated crops presented in Table 5.3. Large differences can be noted: peak water consumption occurs in the Gaja Branch (Old Fuleli/Lined Canal) canal with an average value of  $ET_a = 1240$  mm yr<sup>-1</sup>. Water consumption in the Sindh is generally high, but the variability among the canal projects is also high in that Province. Evapotranspiration from the Abbasia, Sadiqia, Upper Swat, and Bahawal canal commands is less than 800 mm yr<sup>-1</sup>. Another important observation is that the water use during *rabi* is more homogeneous than during *kharif*. The lowest water user in the basin is the Abbasia Canal that consumes only 640 mm yr<sup>-1</sup>. This implies that even between huge canal commands with an average coverage of 360,000 ha, significant differences in water use can be detected. These variations relate to groundwater pumping as well as to the management, allocation, and distribution of canal water.

Figure 5.7

Annual actual evapotranspiration  $ET_a$  in various canal commands of the Indus basin, Pakistan.



## 5.7 Conclusions

Spatial patterns of actual annual evapotranspiration can be assessed by the SEBAL remote-sensing technique using a minimum of weather input data (solar duration and wind speed). At a field scale, no difference between annual actual evapotranspiration computed by remote sensing and by the transient model SWAP could be detected. Errors occur when the time scale is shorter than a year, but the overall agreement with SWAP for periods of 1 month and longer is quite good. The Bowen-ratio field-measurement technique gave results that varied from SEBAL results by 10% during a season, but the comparison was for different years. The Rechna Doab residual water balance showed a difference of only 5% over 2.97 million ha. This implies that easily available remote-sensing images can be used to compute the evaporative depletion in large river basins where a minimum of ground data is available.

When water is scarce, the supply is insufficient to cover all demands. Strategic management should then be based on water resource depletion. Equitable access to water resources by all users can be evaluated once the evaporative depletion is known (see Fig. 5.7 for example). Large variations between crop types, canal commands and upstream-downstream effects can be determined. Areas receiving less water resources can be easily identified.

Frameworks to evaluate productive and effective use of water resources exist. Irrigation performance and water-producing indicators are available to assist water policy makers and water resource managers in their decision-making. The implementation of these frameworks relies on accurate and up to date water-balance data. Satellite-based computations can provide this information and eliminate the need to rely on field databases.



## 6 RETRIEVING SOIL MOISTURE STORAGE IN THE UNSATURATED ZONE FROM SATELLITE IMAGERY AND BI-ANNUAL PHREATIC SURFACE FLUCTUATIONS\*

### 6.1 Introduction

Groundwater irrigation has been the heart of the “*green revolution*” in agriculture across many Asian nations, and has permitted the cultivation of high-value crops in various arid regions. Groundwater has also provided security against drought when irrigation with surface water resources has been deficient (e.g. Foster *et al.*, 2000). Groundwater use in the Indus river basin has resulted in increased irrigation efficiency and water productivity (Bastiaanssen *et al.*, 2002a). Sustainability of such conjunctive use systems requires net recharge to be in equilibrium with groundwater withdrawals. Both groundwater withdrawals and net recharge are affected by changes in soil moisture storage; hence, the estimation of soil moisture storage changes is essential.

Conventionally, changes in soil moisture storage are accounted for using the concept of the *storage coefficient*. In unconfined aquifers, the storage coefficient relates to the unsaturated zone, usually extending from the phreatic surface to the ground surface. The storage coefficient is generally calculated either by simultaneously measuring phreatic surface fluctuations and drain discharges over a certain time period, or from water retention characteristics of the soil profile (De Ridder and Boonstra, 1994). Calculation of the storage coefficient by these methods is impractical for large areas, so often a constant value ranging from less than 5% for clayey material to 35% for coarse sand and gravel sand is used in groundwater studies. However, since the storage coefficient varies with the depth to the phreatic surface, a constant value may result in considerable error in water balance estimates (Ritzema, 1994).

In areas where the phreatic surface is deep, with negligible capillary rise, changes in the phreatic surface depth and changes in total soil moisture storage have less effect on each other. The processes in the upper part of unsaturated zone are hydrologically disconnected from the processes near the phreatic surface. This implies that for areas where the phreatic surface is deep, it is not practical to calculate the soil moisture storage changes in the unsaturated zone from changes in the phreatic surface depth. Independent from these concepts, conventional techniques also fail to spatio-temporally describe the variability of soil moisture storage in the root zone from rainfall and irrigation practices.

Remote sensing techniques have made tremendous progress in assessing spatial and temporal variation of soil moisture (Moran *et al.*, 2002). A variety of both infrared and microwave sensors have been tested, but their application is confined to near surface

---

\* Adapted version of Ahmad, M.D. and W.G.M. Bastiaanssen, 2002. Retrieving soil moisture storage in the unsaturated zone from satellite imagery and bi-annual phreatic surface fluctuations. *Irrigation and Drainage Systems (Submitted)*

soil moisture computations. Soil moisture content in the unsaturated zone does not vary linearly between the root zone and the saturated zone. The shape of the soil moisture profile depends on the water retention characteristics of the soil.

This paper intends to compute the monthly variability of soil moisture storage by means of a new parameterisation of soil moisture storage combined with limited phreatic surface observation data for both shallow and deep phreatic surfaces.

## 6.2 Soil moisture

Conventionally, under shallow phreatic surface conditions, changes in the soil moisture storage of the unsaturated zone,  $dW_u$ , are determined from observations of phreatic surface fluctuations,  $dh$ , and a constant value of the storage coefficient,  $\mu$ . In unconfined aquifers, the storage coefficient ( $\mu = dW_u/dh$ ) depends on the soil hydraulic properties and depth to the phreatic surface. Under transient conditions, the depth to the phreatic surface is variable ( $z_1$  to  $z_2$ ) during the time interval ( $t_1$  to  $t_2$ ). It should be noted that the integration depths for the soil moisture storage computation at  $t_1$  and  $t_2$  are not necessarily similar; therefore, both the shape of the profile and the total depth vary over time. Because the shape of the soil moisture profile,  $\theta(z)$ , varies,  $\mu$  cannot be a constant. The shaded portion in Figure 6.1 represents the change in soil moisture storage,  $dW_u$ , between  $t_1$  and  $t_2$ . Mathematically it can be expressed as:

$$\frac{dW_u}{dt} = \int_{z=-z_2}^{z=0} \theta(z, t_2) dz - \int_{z=-z_1}^{z=0} \theta(z, t_1) dz = \mu \frac{dh}{dt} \quad (6.1)$$

where  $\theta$  ( $\text{cm}^3 \text{cm}^{-3}$ ) is the volumetric soil moisture content.

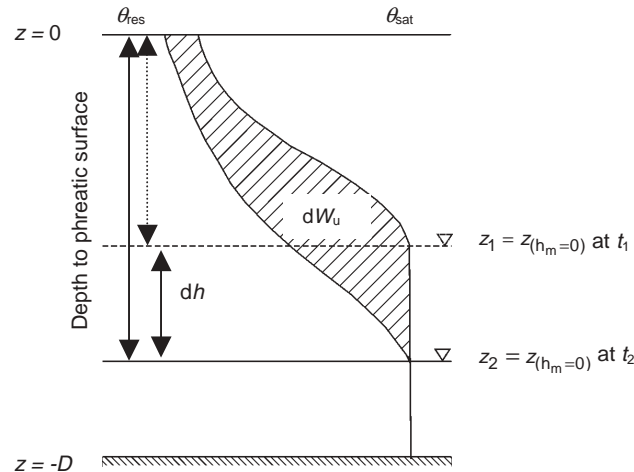


**Figure 6.1** Schematisation of change in unsaturated zone storage  $dW_u$  with change in phreatic surface  $dh$  in unconfined aquifers.



Soil wetness is manifested in the surface energy balance by the magnitude of sensible heat  $H$  ( $W m^{-2}$ ) and latent heat fluxes  $\lambda E$  ( $W m^{-2}$ ), which are governed by soil moisture content. *In situ* measurements of  $H$  and  $\lambda E$ , can therefore be used to estimate soil moisture content. The Bowen ratio  $\beta$  (-) is determined from the difference in vapour pressure  $de$  and temperature  $dT_{air}$  between the two observed levels:

$$\beta = \frac{H}{\lambda E} = \gamma \frac{T_{air_1} - T_{air_2}}{e_1 - e_2} = \gamma \frac{dT_{air}}{de} \quad (6.2)$$

where  $\gamma$  ( $Pa K^{-1}$ ) is the psychrometric coefficient,  $T_{air}$  ( $K^\circ$ ) is air temperature and  $e$  ( $Pa$ ) the vapour pressure, and subscript 1 and 2 indicate the lower and upper levels respectively. From  $\beta$ , the evaporative fraction  $\Lambda$  (-) can be computed as:

$$\Lambda = \frac{\lambda E}{\lambda E + H} = \frac{1}{1 + \beta} \quad (6.3)$$

The value of  $\Lambda$  under non-advective conditions ranges between 0 to 1, which represents zero to maximum evapotranspiration. Since  $\Lambda$  can also be calculated over large areas using satellite imagery by solving the surface energy balance (Bastiaanssen *et al.*, 1998), attempts to relate soil moisture content to surface energy balance parameters were investigated by Davies and Allen (1973), De Bruin (1983), Owe and Van De Griend (1990) and Bindlish *et al.*, (2001). Using a similar concept, an empirical relationship between evaporative fraction  $\Lambda$  (latent heat/net available energy) and volumetric soil moisture content  $\theta$  was developed using data from two large climate-hydrology studies investigating soil moisture-evaporation-biomass interactions [First ISCLCP (International Satellite Land Surface Climatology Project) Field Experiment FIFE (Sellers *et al.*, 1992) and ECHIVAL Field Experiment in Desertification-Threatened Areas EFEDA (Bolle *et al.*, 1993)]. Scott *et al.*, (2002) modified the  $\theta$  ( $\Lambda$ ) relationship by normalizing  $\theta$  with saturated soil moisture content  $\theta_{sat}$ :

$$\frac{\theta}{\theta_{sat}} = e^{\{(-1.0)/0.42\}} \quad (6.4)$$

The value of relative soil moisture content  $\theta/\theta_{sat}$  (-) varies between 0 (oven dry) to 1 (full saturation) and is a standard relationship which can be applied to a wide range of soils. This relationship explains the dependence of the evaporative fraction on root zone soil moisture content and vice versa, which means that by estimating  $\Lambda$  from remote sensing, we can estimate relative soil moisture content  $\theta/\theta_{sat}$  in the root zone.

### 6.3 Study area

This research work was carried out in the Rechna Doab area of the Indus river basin irrigation system. For a detailed analysis and understanding of the various components, at a field level, two experimental sites near *Pindi Bhattian* and *Faisalabad* were selected (Figure 2.4), representing shallow (2 m) and deep (10 m) phreatic surface conditions respectively. Rice-wheat crop rotation was practised during the *kharif* and *rabi* seasons respectively at Pindi Bhattian, while cotton-wheat rotation was practiced at Faisalabad. The detailed description of these sites is presented in section 2.3.1.

Field data on various agronomic aspects and water balance components were collected for two growing seasons, *kharif* 2000 and *rabi* 2000-01. At both experimental plots, Bowen ratio towers were installed and operated from June 21, 2000 to March 21, 2001. Near-surface atmospheric profiles of temperature, humidity and wind speed were measured, along with precipitation and incoming solar radiation. For missing days, climatic data from the nearest meteorological stations were collected. Daily phreatic surface fluctuations were precisely recorded with a *Diver* (automatic recorder) and with manual measurements using sounding devices. Soil moisture content in the root zone (up to 100 cm) was monitored in the field with the help of a theta probe using the frequency domain technique. The theta probe measures the volumetric soil moisture content by measuring changes in the dielectric constant.

### 6.4 Field scale results

The relative moisture content  $\theta/\theta_{\text{sat}}$  was determined by dividing the measured  $\theta$  in the root zone depth of 100 cm with a saturated soil moisture content  $\theta_{\text{sat}}$  of  $0.35 \text{ cm}^3 \text{ cm}^{-3}$  for *Faisalabad* and  $0.40 \text{ cm}^3 \text{ cm}^{-3}$  for *Pindi Bhattian*. The evaporative fraction  $\Lambda$  was calculated by applying Eqs. 6.2 and 6.3 to the measurements from the Bowen ratio towers at both experimental plots. The values of  $\theta/\theta_{\text{sat}}$  were plotted against the evaporative fraction  $\Lambda$  for both experimental sites (Figure 6.2). The comparison of field measurements with the standard curve (from Eq. 6.4) reveals a deviation of  $\pm 20\%$ . The deviation from the standard curve could be the result of the combined effect of several factors, such as instrumental error in measuring  $\theta$  and  $\Lambda$ , or non-compatible of scales between  $\theta$  and  $\Lambda$ . A logarithmic trend line fitted to field observations was compared with the standard theoretical curve (Eq. 6.4). A close correlation was found between the curve derived from field measurements and the standard theoretical curve.

The range of error between theoretical and measured  $\theta$  values was plotted in Figure 6.3. It shows that estimated  $\theta$  could maximally differ from actual measurements by  $\pm 0.12 \text{ cm}^3 \text{ cm}^{-3}$ . The overall root mean square error (RMSE) of  $0.05 \text{ cm}^3 \text{ cm}^{-3}$  has been found for wheat, cotton and rice areas in Rechna Doab for  $\Lambda$  values between 0.48 and 0.94. Moreover, there is a systematic trend in the error: a lower error in  $\theta$  ( $\pm 0.03 \text{ cm}^3 \text{ cm}^{-3}$ ) is found when  $\Lambda$  ranges from 0.65 to 0.85, the usual range of  $\Lambda$  under irrigated agriculture (e.g. Kustas *et al.*, 1990; Dugas, *et al.*, 1991; Bink, 1996, Wang *et al.*,

1998). The error increases at high and low values of  $\lambda$ . Values of  $\lambda$  greater than 0.85 typically occur in rice crop areas and in wetlands.

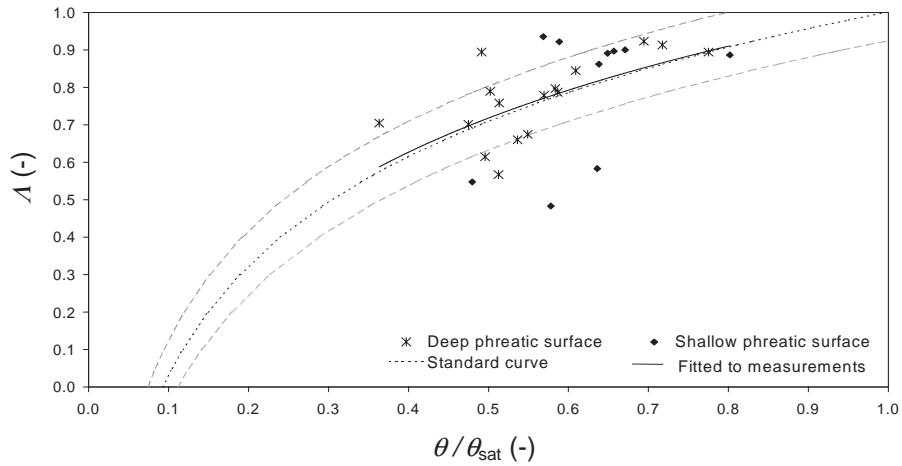


**Figure 6.2** The empirical relationship between relative soil moisture content ( $\theta/\theta_{\text{sat}}$ ) in the root zone and evaporative fraction  $\lambda$  for wheat, rice, and cotton areas at Rechna Doab in relation to the standard curve from other studies.

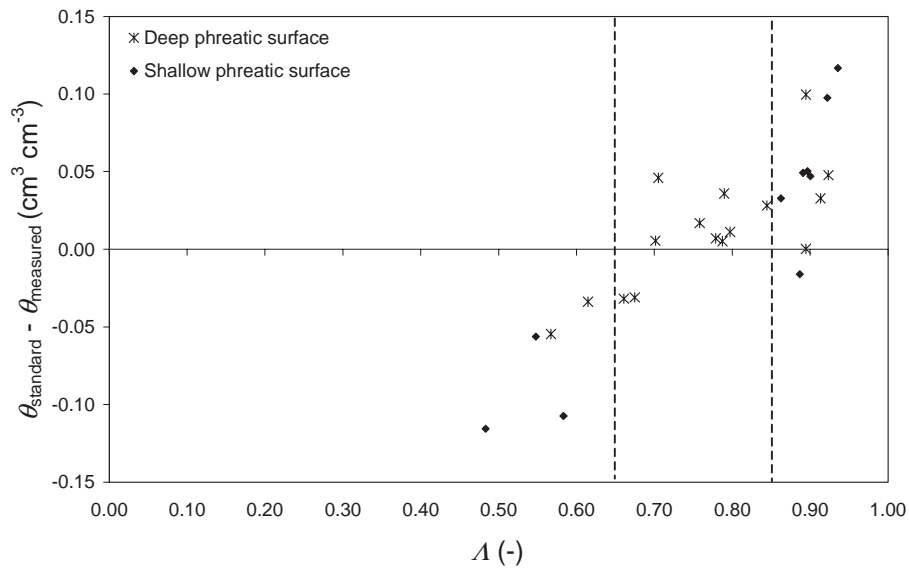


**Figure 6.3** Difference between root zone soil moisture content estimated from standard relationship ( $\theta_{\text{standard}}$ ) and field measurement ( $\theta_{\text{measured}}$ ) over a range of evaporative fractions  $\lambda$  for Rechna Doab.

## 6.5 Outline of a new simple parameterisation of matric pressure head distribution

The computation of unsaturated soil moisture storage  $W_u$  using satellite imagery is not straightforward and field measurements of  $W_u$  for large depths are impractical to achieve. For these reasons, a physically based transient Soil-Water-Atmosphere-Plant model (Van Dam *et al.*, 1997) was used to compute the day-to-day variations of  $W_u$  for deep phreatic surface conditions. The SWAP model was calibrated and validated with *in situ* measurement of root zone  $\theta$  and actual evapotranspiration  $ET_a$  for cotton-wheat and rice-wheat cropping systems with deep and shallow phreatic surface conditions respectively (Ahmad *et al.*, 2002). The root mean square error (RMSE) between measured and computed soil moisture contents were found to be  $0.02 \text{ cm}^3\text{cm}^{-3}$  for Faisalabad and  $0.03 \text{ cm}^3\text{cm}^{-3}$  for Pindi Bhattian. The RMSE for actual evapotranspiration were respectively  $1.07$  and  $0.99 \text{ mm d}^{-1}$  which is a difference of approximately 16 % at an evapotranspiration rate of  $6 \text{ mm d}^{-1}$ . The difference between measured and computed accumulated annual evapotranspiration was much smaller (1.5 to 3%).

The results of the SWAP model have been used to develop a new simple parameterisation of matric pressure head distribution to calculate  $W_u$ . For this, the unsaturated zone was divided into two zones: a *root zone* of constant depth (100 cm below the surface), and a variable *intermediate zone* (between the root zone and the phreatic surface). The root zone soil moisture storage  $W_{rz}$  can be computed using remote sensing by applying Eq. 6.4 and the  $\lambda$  map derived from satellite data with reasonable accuracy for large areas (as demonstrated in Figure 6.2).

The largest variability in soil water fluxes occurs in the root zone, especially near the soil surface. At larger depths, the fluxes are quasi-state, and a simplified solution using pseudo steady-state fluxes – both upward and downward - can be applied (e.g. de Laat, 1976). Above the phreatic surface, water will enter the capillary zone until the reduction of the air-water interfacial energy becomes equal to the increase of the gravitational energy of the water. The hydraulic conductivity in the capillary fringe above the phreatic surface is near that for full saturation. As long as the potential is below the air entry point, the gradient of the soil water head is negligible and hydrostatic equilibrium exists with  $h_m = -z^*$  (Jury *et al.*, 1991), where  $z^*$  is the height above the phreatic surface.

The validity of  $h_m = -z^*$  varies with soil types and depth to the phreatic surface, e.g. for clay: no equilibrium exists; for coarse sand:  $z^* = 50 \text{ cm}$ ; and for fine sand:  $z^* = 100$  to  $200 \text{ cm}$  (Koorevaar *et al.*, 1983). Extensive modelling exercises with SWAP have demonstrated that  $h_m = -z^*$  can be applied to the sub-soil in Rechna Doab, and that two depths need to be considered with respect to the phreatic surface: up to 750 cm and greater than 750 cm from ground surface. Where the phreatic surface is within 750 cm from ground surface, a linear decrease in matric pressure head  $h_m$  from phreatic surface ( $h_m = 0$ ,  $z^* = 0$ ) to the bottom of root zone is likely (with a minimum value of  $h_m = -650 \text{ cm}$  when the phreatic surface is 750 cm below the ground surface).

The soil matric pressure head profile  $h_m(z)$  can be transferred into a soil moisture profile  $\theta(z)$  using the well-known relationship between  $h_m$  and  $\theta$  proposed by Van Genuchten (1980).

$$\theta(h_m) = \theta_{res} + \frac{\theta_{sat} - \theta_{res}}{\left(1 + |\alpha h_m|^n\right)^{\frac{n-1}{n}}} \quad (6.5)$$

where  $\alpha$  and  $n$  are variables that determine the shape of the water retention curve. We introduce here the intermediate zone, which is the layer between the root zone and the phreatic surface. For areas with very deep phreatic surfaces (over 750 cm), the intermediate zone is further sub-divided into a lower layer, which goes from the phreatic surface to a constant height of 650 cm above the phreatic surface, and an upper layer that represents the area above (Figure 6.4). The depth of this upper layer of the intermediate zone is variable and is equal to the difference between the phreatic surface depth and 750 cm.

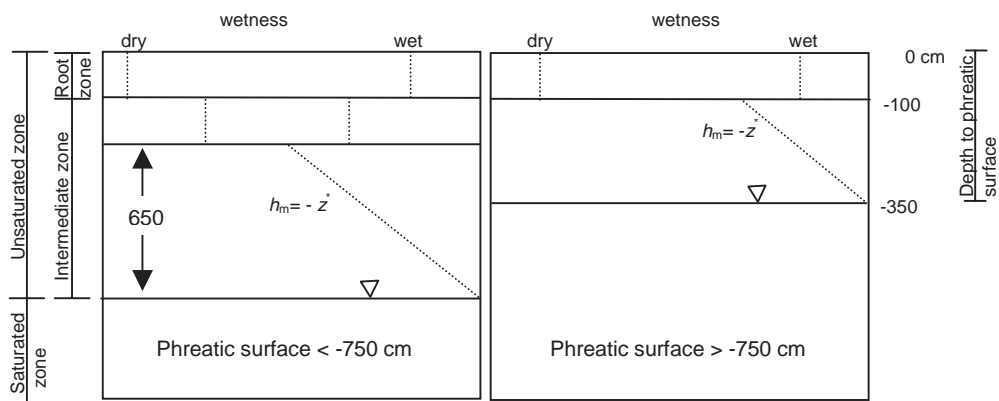


**Figure 6.4** Schematic diagram showing the new, simple parameterisation scheme for matric pressure head  $h_m$  distribution in the unsaturated zone.  $z$  is height above the phreatic surface.

In the lower layer of the intermediate zone,  $h_m = -z$  is assumed; whereas in the upper layer, the average value of  $h_m$  is calculated from  $h_m$  of the root zone and  $h_m = -650$  cm  $[(-650 + h_m \text{ of root zone}) / 2]$  (see Figure 6.4).

To verify the accuracy of this new, simple parameterisation of matric pressure head distribution, it was compared to the daily model output of  $W_u$  from SWAP (Figure 6.5). A good agreement with an absolute RMSE of 7 cm is found at an average soil moisture storage of  $W_u = 110$  cm, this is a difference of 6%. No systematic deviations between shallow and deep phreatic surface conditions can be found.

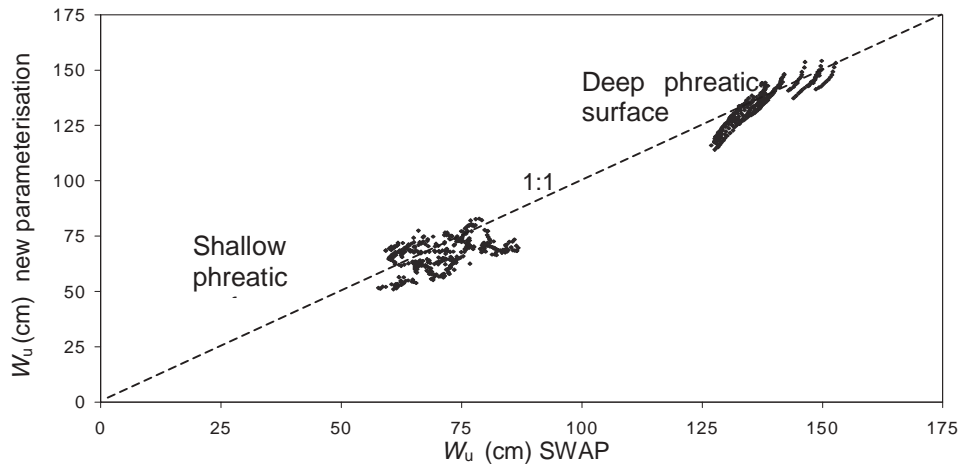


**Figure 6.5** Comparison of unsaturated zone soil moisture storage ( $W_u$ ) from the new simple parameterisation scheme for matric pressure head distribution with the agro-hydrological model (SWAP) in Rechna Doab, Pakistan.

Two arbitrary days, Aug. 1, 2000 (*kharif*) and Jan. 10, 2001 (*rabi*) were selected to compare the  $\theta(z)$  profile from the new parameterisation and the SWAP model for deep and shallow phreatic surface conditions (shown in Figure 6.6 and 6.7).

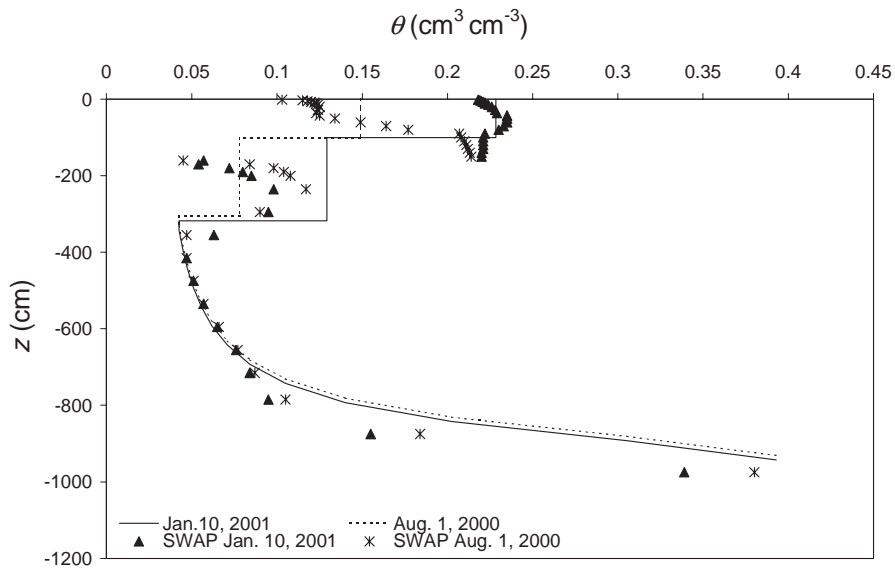


**Figure 6.6** Soil moisture content profile  $\theta(z)$  resulting from new simple parameterisation (see Figure 6.4) and detailed agro-hydrological model (SWAP) for the Faisalabad. The root zone is 100 cm thick.

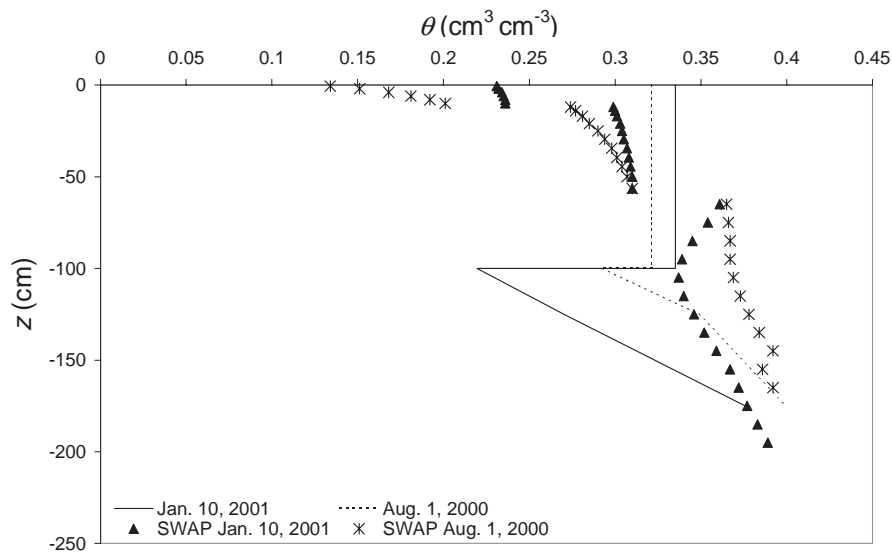


**Figure 6.7** Soil moisture content profile  $\theta(z)$  resulting from new parameterisation (see Figure 6.4) and detailed transient agro-hydrological model (SWAP) for the Pindi Bhattian. The root zone is 100 cm thick.

It is important to know the absolute error that could occur at different levels of probability of exceedance. The absolute deviation in daily  $W_u$  between the new parameterisation and the SWAP model was computed for each day of the year for both shallow and deep phreatic surface conditions and was plotted against its probability of occurrence (Figure 6.8). With the new parameterisation, the maximum error that could occur in the  $W_u$  estimation is  $18.24 \text{ cm d}^{-1}$ . However, there is an 85% chance that the error in  $W_u$  will be within the range of  $0\text{-}10 \text{ cm d}^{-1}$ . The average error at 50% probability is less than  $5 \text{ cm d}^{-1}$ .

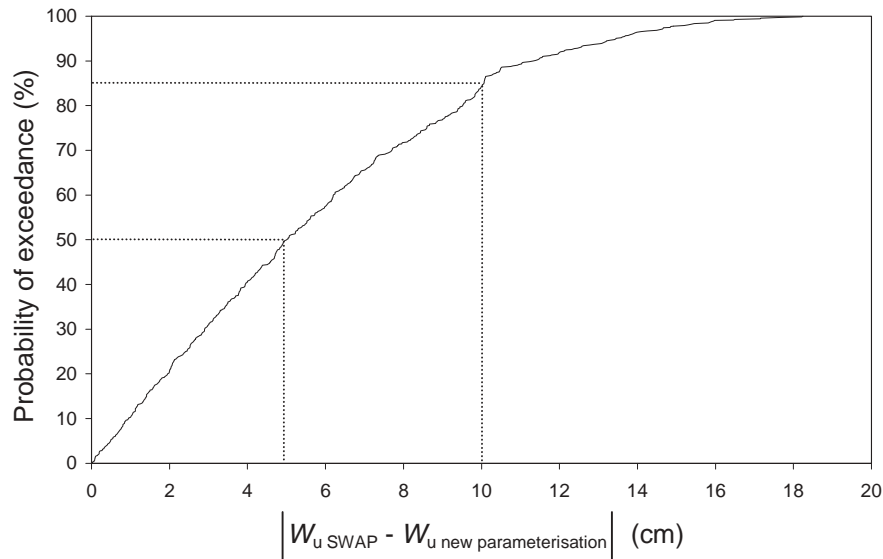


**Figure 6.8** Distribution of daily absolute deviation of unsaturated soil moisture storage  $W_u$  between the new, simple parameterisation and the detailed transient agro-hydrological (SWAP) model.

## 6.6 Application of new parameterisation at regional scale

Computation of a spatially distributed  $W_u$  at a regional scale by applying the new parameterisation developed and verified at field scale requires the input of a distributed  $W_{rz}$  and the depth to phreatic surface at regional scale.

In this study, the Surface Energy Balance Algorithm for Land (SEBAL) developed by Bastiaanssen *et al.*, (1998) to compute the actual evapotranspiration  $ET_a$ . NOAA-AVHRR images covering the complete annual growing cycle (October 1993 to October 1994) were processed and the evaporative fraction  $\lambda$  was computed using 18 cloud-free images for Rechna Doab (Bastiaanssen *et al.*, 2002b: Chapter 5). The period from October 1993 to October 1994 was chosen for the annual study because additional water balance information was available for that year.

From these  $\lambda$  maps, the relative soil moisture content  $\theta / \theta_{sat}$  in the root zone was computed for Rechna Doab using Eq. 6.4. The soils of Rechna Doab are predominantly coarse to moderately coarse. An average value of  $\theta_{sat} = 0.35 \text{ cm}^3 \text{ cm}^{-3}$  was used to compute the root zone  $\theta$  for all 18 images of Rechna Doab. The soil moisture storage in the root zone  $W_{rz}$  (cm) was determined from root zone  $\theta$  using a constant depth of 1 meter.

The temporal variation in  $W_{rz}$  is plotted in Figure 6.9 for rice-wheat and cotton-wheat areas of Rechna Doab. Monthly changes in  $W_{rz}$  were between 10.0 to 32.1 cm: from near residual to near saturation conditions. The lowest soil moisture storage values in



both cropping systems occurred during May. This is the end of the *rabi* when the crops are harvested. Land preparation and basin irrigation are not common during this period, and areas are intentionally kept drier. The first irrigation is usually done 10-12 weeks after sowing, which is also manifested in Figure 6.9 by a slow increase of wetness in the cotton fields. Rice-wheat areas reveal a drastic increase in soil moisture storage from June to September because of frequent basin irrigation.

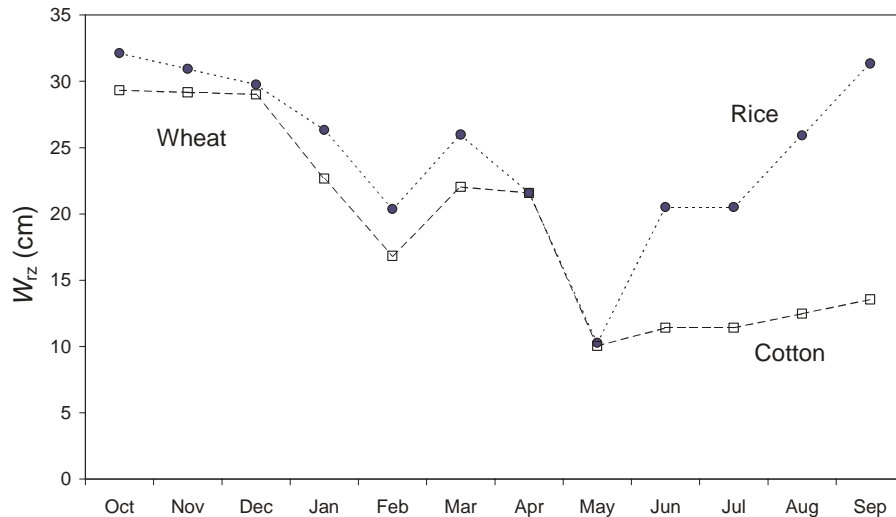


**Figure 6.9** Temporal variation in root zone soil moisture storage  $W_{rz}$  (0-100 cm) in the rice-wheat (longitude 74.24°E latitude 31.84°N) and cotton-wheat (longitude 73.04°E latitude 31.36°N) areas of Rechna Doab.

In order to compute  $W_u$  with the new parameterisation, depth to phreatic surface is also required in addition to  $W_{rz}$ . Within Rechna Doab, there is an intensive nodal network of 981 piezometers (Figure 6.10). The depth of the phreatic surface is measured twice a year, pre- and post-monsoon, by the SCARP Monitoring Organization (SMO) of the Water and Power Development Authority (WAPDA). Using this data, digital maps of the depth to the phreatic surface for October 1993, May 1994, and October 1994 were created by kriging. Monthly estimates of  $W_u$  require monthly information on the depth to the phreatic surface. This is obtained by linear interpolation between the available measurements: post- to pre-monsoon and pre- to post-monsoon measurements.

Daily field measurement of phreatic surfaces with automatic divers and sounding devices for *kharif* 2000 and *rabi* 2001 at Pindi Bhattian and Faisalabad area were used to estimate the expected range of error emerging from temporal linear interpolation of the bi-annual phreatic surface measurements. Annual precipitation over the entire Rechna Doab from June 1993 to June 1994 was 315 mm, whereas from May 2000 to May 2001 the Faisalabad station recorded 290 mm. Although this was a different year from the remote sensing (evapotranspiration) study, it is assumed

that phreatic surface changes for the year 1993-94 will have a similar trend as in year 2000-01. On a monthly basis, RMS errors of 20 cm and 3 cm were found for areas of shallow phreatic surfaces and deep phreatic surfaces respectively. The higher RMS error for areas of shallow phreatic surfaces was the result of larger soil water fluxes between the unsaturated and saturated zone under rice growing areas.

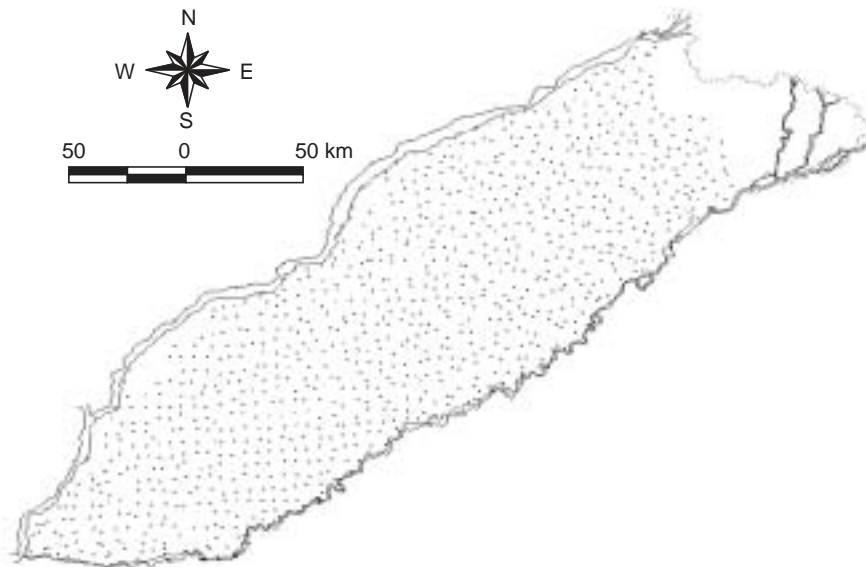


**Figure 6.10** Nodal network of piezometers in the Rechna Doab, Pakistan.

The monthly values of  $W_{rz}$  and depth to phreatic surface were used to estimate the  $W_u$  with the new parameterisation method by using average values of van Genuchten-Mualem (VGM) parameters (Table 6.1) for the entire Rechna Doab. The resulting maps of October 1993 and February 1994 are presented in Figure 6.11. They depict that the depth to phreatic surface has more influence on the spatial variation of soil moisture storage than root zone soil moisture storage: the deeper the phreatic surface, the higher the unsaturated zone storage. However, monthly changes in the storage are mainly influenced by variation in root zone soil moisture content, which is also witnessed in Figure 6.9.

**Table 6.1** Van Genuchten-Mualem (VGM) parameters (Eq. 6.5) for Rechna Doab.

VGM Parameters	Root zone	Intermediate Zone	
		Upper layer	Lower layer
$\theta_{res}$ ( $\text{cm}^3 \text{cm}^{-3}$ )	0.035	0.033	0.028
$\theta_{sat}$ ( $\text{cm}^3 \text{cm}^{-3}$ )	0.354	0.369	0.400
$n$ ( $\text{cm}^{-1}$ )	0.018	0.016	0.011
$n$ (-)	1.260	1.733	2.680

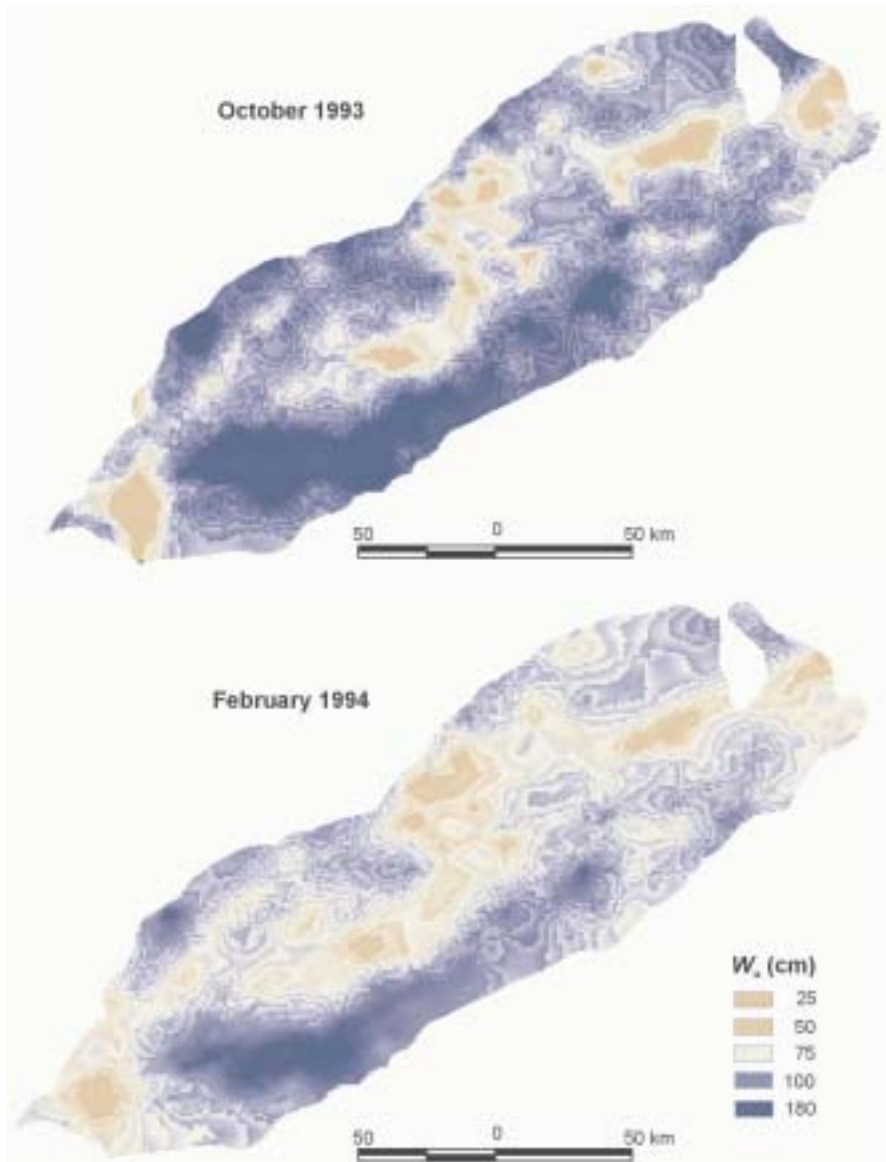


**Figure 6.11** Spatial variations in soil moisture storage  $W_u$  for the entire unsaturated zone in Rechna Doab.

The monthly changes in phreatic surface  $dh$  and unsaturated soil moisture storage  $dW_u$  for areas of shallow and deep phreatic surfaces are summarized for two locations in Table 6.2. A considerable change in monthly  $W_u$  was observed during May.

**Table 6.2** Monthly changes in depth of phreatic surface  $dh$  and unsaturated zone soil moisture storage  $dW_u$  in the areas of shallow and deep phreatic surfaces in Rechna Doab.

Month	Shallow phreatic surface Pixel (100 ha) at longitude 73.32°E latitude 31.78°N				Deep phreatic surface Pixel (100 ha) at longitude 72.59°E latitude 30.90°N			
	Depth to phreatic surface	$dh$	$W_u$	$dW_u$	Depth to phreatic surface	$dh$	$W_u$	$dW_u$
	cm	cm month <sup>-1</sup>	cm	cm month <sup>-1</sup>	cm	cm month <sup>-1</sup>	cm	cm month <sup>-1</sup>
Oct. 93	184.2	+7.1	65.9	-1.3	1040.5	-9.7	154.4	-15.3
Nov. 93	191.3	+6.9	64.6	-1.4	1030.8	-9.4	139.1	-10.0
Dec. 93	198.2	+7.1	63.2	-5.7	1021.4	-9.7	129.2	-6.7
Jan. 94	205.4	+7.1	57.5	-5.5	1011.7	-9.7	122.5	-6.8
Feb. 94	212.5	+6.4	52.0	-0.3	1002.0	-8.8	115.7	+15.8
March 94	218.9	+7.1	51.7	+19.8	993.2	-9.7	131.5	-1.6
April 94	226.0	+6.9	71.5	-12.7	983.5	-9.4	129.9	-33.8
May 94	232.9	-1.6	58.8	+6.6	974.1	-14.7	96.1	+13.8
June 94	231.4	-1.5	65.4	+0.3	959.4	-14.2	109.9	-1.0
July 94	229.8	-1.6	65.7	-0.3	945.2	-14.7	108.8	-8.9
Aug 94	228.2	-1.6	65.4	-0.3	930.4	-14.7	100.0	-6.6
Sep 94	226.7		65.1		915.7		93.4	

The frequency distribution of monthly changes in  $W_u$  from October 1993 to November 1993 and February 1994 to March 1994 for the 2.97 million ha area of Rechna Doab is presented in Figure 6.12. For this large area,  $W_u$  decreased from October 1993 to November 1993 by an approximate value of 5 cm month<sup>-1</sup>. This was apparently due to post monsoon conditions at the end of the rice-growing season. However, from February 1994 to March 1994, there was a considerable increase in  $W_u$ . This increase was apparently the result of intensive groundwater irrigation in the middle of the *rabi*, when wheat is in the heading stage. The positive change in  $W_u$  is approximately 5 cm month<sup>-1</sup>. The magnitude of these changes is approximately 1.5 mm d<sup>-1</sup> on a monthly basis, and is a significant component of the soil water balance.

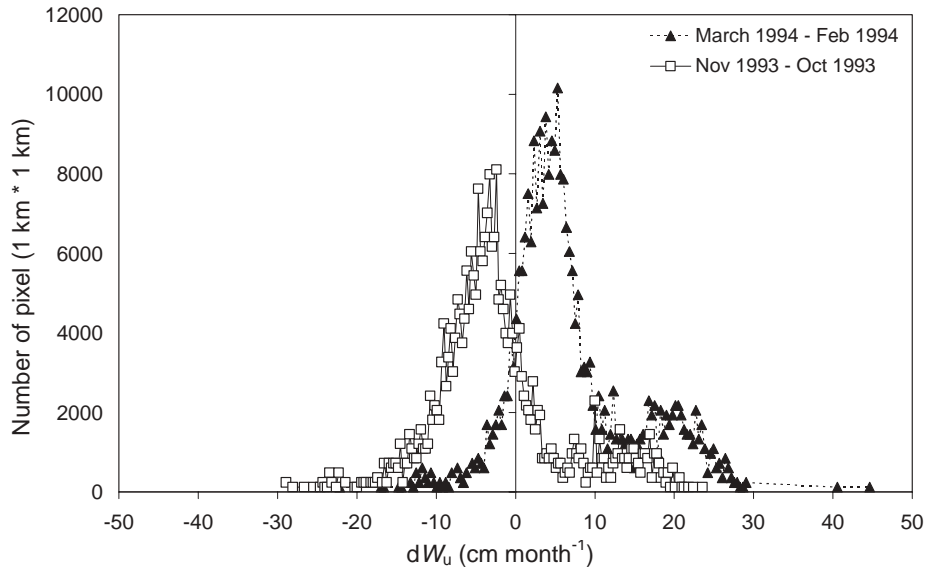


**Figure 6.12** Frequency distribution of monthly change in unsaturated zone soil moisture storage  $dW_u$  for the 2.97 million ha area of Rechna Doab.

The average changes in depth of the phreatic surface  $dh$ , root zone soil moisture storage  $W_{rz}$ , and unsaturated zone soil moisture storage  $W_u$  for the 2.97 million ha area is presented in Table 6.3. The  $dW_u$  values range between  $-12.1$  and  $+7.1$   $\text{cm month}^{-1}$ , but the cumulative change in storage is approximately  $-8.1$   $\text{cm}$  from October 1993 to September 1994 (Table 6.3). There are both negative and positive changes in monthly  $W_{rz}$  and  $W_u$  for the Rechna Doab. The positive and negative variations of  $W_u$  coincide with changes of  $W_{rz}$ . For conditions where the phreatic surface is deep, the change in  $W_{rz}$  resulted from precipitation and different irrigation and agronomic practices, as discussed earlier. *Cumulative change does not amplify over a longer timeframe due to the cancelling effect of positive and negative changes in  $W_u$ .*

**Table 6.3** Average monthly changes in phreatic surface  $dh$ , root zone soil moisture storage  $W_{rz}$ , and unsaturated zone soil moisture storage  $W_u$  in the 2.97 million ha area of Rechna Doab based on geo-information techniques.

Month	Depth to phreatic surface	$dh$	$W_{rz}$	$dW_{rz}$	$W_u$	$dW_u$	Cumulative change in $W_u$
	cm	cm month <sup>-1</sup>	cm	cm month <sup>-1</sup>	cm	cm month <sup>-1</sup>	cm
Oct. 93	464.3	+8.4	30.9	-3.3	93.6	-2.3	-2.3
Nov. 93	472.8	+8.2	27.5	-0.8	91.4	+0.3	-1.9
Dec. 93	480.9	+8.4	26.8	-4.2	91.7	-3.4	-5.4
Jan. 94	489.3	+8.4	22.6	-4.6	88.3	-4.2	-9.5
Feb. 94	497.8	+7.6	18.0	+5.7	84.1	+7.1	-2.4
Mar. 94	505.4	+8.4	23.7	-2.8	91.2	-2.1	-4.5
April 94	513.8	+8.2	21.0	-11.2	89.2	-12.1	-16.5
May 94	521.9	-6.6	9.7	+6.8	77.1	+6.8	-9.7
June 94	515.4	-6.4	16.5	+0.3	83.9	-0.2	-9.9
July 94	509.0	-6.6	16.8	+1.4	83.7	+0.7	-9.2
Aug. 94	502.4	-7.6	18.2	+1.7	84.5	+1.1	-8.1
Sep. 94	495.8		19.9		85.6		

## 6.7 Summary and conclusions

This study calculated the spatio-temporal changes in soil moisture storage in the unsaturated zone for large irrigated areas by using public domain remotely sensed satellite data and bi-annual field measurements of the depth to the phreatic surface. Soil moisture content in the root zone was computed from satellite imagery, using a universal standard relationship between evaporative fraction and relative soil moisture content (Eq. 6.4). The error in such estimation is about  $0.03 \text{ cm}^3 \text{ cm}^{-3}$  for typically irrigated regions. The RMSE is  $0.05 \text{ cm}^3 \text{ cm}^{-3}$  for a range of evaporative fractions between 0.48 to 0.94. Hydrological studies in irrigated river basins require values for soil moisture storage changes in the complete unsaturated zone. To address this, a new simple parameterisation of matric pressure head distribution was developed which accurately calculates the unsaturated zone storage using root zone storage and depth to the phreatic surface data. The traditional storage coefficient is too simplistic to compute unsaturated zone storage changes for canal and groundwater irrigation systems, especially when the phreatic surface is deep. Transient processes in the unsaturated zone prevail and significant storage changes occur on monthly basis, which can only be computed with a more sophisticated methodology. This analysis shows that in Rechna Doab, soil moisture storage changes in the unsaturated zone range from  $\pm 5$  to  $\pm 10$  cm per month. It is important to describe these soil moisture storage changes in all water balance and water accounting studies.

## 7 ESTIMATION OF DISAGGREGATED CANAL WATER DELIVERIES IN PAKISTAN USING GEOMATICS\*

### 7.1 Introduction

Irrigated agriculture plays an important role in global food production. Today, an estimated 40 percent of agricultural products and 60 percent of the world's grain are grown on irrigated lands (Meinzen-Dick and Rosegrant, 2001). However, in many parts of the world, poor management of irrigation systems has resulted in the degradation of precious water and land resources. Conjunctive use of canal and groundwater resources can improve environmental sustainability and financial viability of irrigated agriculture. The concept of integrated water resources management has not yet been implemented on large irrigation systems. Lack of data on availability and use of both canal water and groundwater at various levels makes the concept of integrated water resources management difficult to implement in a complex river basin. Even if such information is available, it is often incomplete, unreliable, or not easily accessible (Murray-Rust and Merry 1994).

Classically, discharges are measured at the canal head. The accuracy of such discharge measurements depends upon a number of factors and is questionable. (For an overview on possible errors in discharge measurements, see Bos, 1976). Open channel flows are transient in nature, causing fluctuations in the delivery flow rates (Clemmens and Dedrick, 1984). Studies of the impact of these processes on water distribution in Pakistan reported *that 20-30% daily discharge fluctuations are common in irrigation canals* [Sarwar *et al.*, (1997) and Khan *et al.*, (1998). Skogerboe *et al.*, (1998)]. For single measurements of discharge with current meters and flumes, an accuracy of 95% can be attained (Hersch, 1995). The estimation and interpretation of canal deliveries for a longer time period from a single daily measurement requires proper attention and careful interpretation.

Discharge measurement structures in smaller canals providing water to tertiary systems are less common. The volume of water flowing through smaller canals is usually estimated using a proportionality factor for the area under service. This information does not reflect how the canal water is actually spread within the area being served. *A benefit of knowing the canal water distribution is that the use of groundwater can then be assessed.* Ahmad and Bastiaanssen (2002) showed that net groundwater use can be assessed from information on actual evapotranspiration, which can be computed from remotely sensed land surface parameters and canal water distribution information. Growing evidence shows that in many large gravity irrigation systems, an uneven water distribution between head and tail occurs, particularly in secondary and tertiary canals (Bhutta and Vander Velde, 1992 and Latif and Sarwar, 1994). This lack of performance may be the result of deteriorating

---

\* Adapted version of Ahmad, M.D., A. Stein and W.G.M. 2002. Estimation of disaggregated canal water deliveries in Pakistan using Geomatics. *Irrigation Science* (submitted)

infrastructure due to poor maintenance of irrigation canals and illegal water offtakes by farmers attempting to expand irrigated areas and to grow more profitable high delta crops.

Most previous attempts to estimate actual water distribution in irrigation systems were based on hydrodynamic simulation models (e.g. Bhutta and Vender Velde, 1992; Schuurmans and Pichel, 1996; Van Waijjen *et al.*, 1997). The simplest form of a water distribution model is to assume a homogenous distribution of canal water over the entire irrigated area. This type of model has limited utility for the management of bifurcating water distribution systems because it does not account for spatial variation of canal water distribution. However, they are widely used for data-scarce environments. Complex mathematical models, often based on Manning's and Saint Venant equations, can simulate the water profile and velocities in the canal and can be used for a variety of applications including canal water distribution (e.g. Malaterre and Baume, 1997; Kuper, 1997). The development and calibration of such models requires detailed information on canal geometry and irrigation structures, which is not readily available for most irrigation systems (Visser *et al.*, 1997; Ahmad *et al.*, 1998).

Until now, international literature has placed limited emphasis on exploring the potential of geo-information techniques for assessing canal water distribution in data scarce environments. The scarce literature dealing with this issue is found in technical reports, rather than in review journal articles. Pioneering work was done by Menenti *et al.* (1989), who defined the equity in water supply as the volume of canal water applied per unit of irrigated land at different hierarchical levels in a water distribution system. Case studies by Menenti *et al.*, (1989, 1996) discern irrigated areas from non-irrigated areas using Landsat based vegetation indices. Bastiaanssen *et al.*, (1999) found systematic differences in wheat yield using from remote sensing, and they related canal water availability and wheat yield to the distance from the distributaries. In arid and semi-arid regions, groundwater is widely used in conjunction with canal water for irrigation. *This makes the task of solving canal water distribution using satellite imagery more complex: most of the irrigated area may actually be receiving water from both canal and groundwater, with varying proportion.*

The aim of this study is to determine response and explanatory variables, such as shape and size of soil cover, from satellite images and GIS analysis. The hypothesis of this paper is that by knowing these variables one can improve the quantification of the actual canal water distribution. *In this study, we developed a GIS/RS-based water disaggregation approach that estimates the distributed water flows in a certain irrigation canal command area using discharge measurements at the main inlet of the irrigation system and satellite imagery.*



## 7.2 Materials and methods

### 7.2.1 Data collection

#### *Field Data*

This study focuses on the Ghour Dour and Gajiana distributaries, both off-taking from the upper Gugera Branch of the Lower Chenab Canal East (LCC East) irrigation system in the Rechna Doab (Figure 7.1).

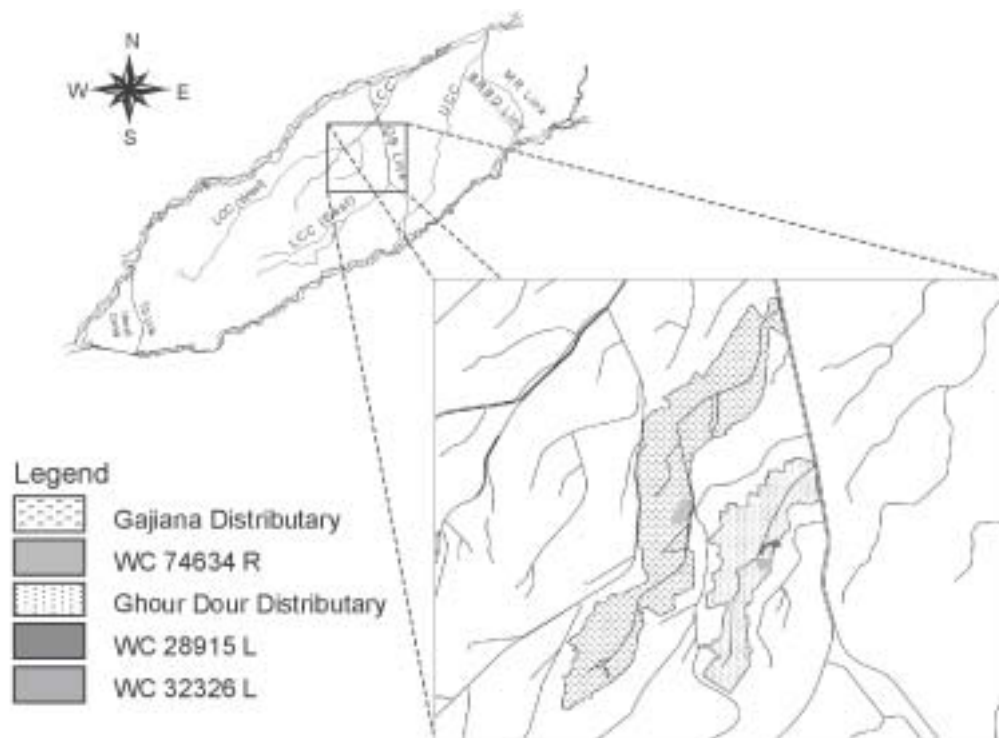


**Figure 7.1** Location of sample distributaries and watercourses in the Rechna Doab, Pakistan.

The gross command areas of these distributaries are 8,756 ha and 19,111 ha respectively. Of the three sample watercourses (WC), two receive water from the Ghour Dour Distributary and one from the Gajiana Distributary. The distance between the head of the sample distributaries and the sample watercourses varies between 9 to 23 km. Their area represents only 2.2% and 1.6% of the gross area. Hence, field data for a very small scale are collected and compared to field data for a very large scale.

GIS information on watercourse boundaries, cropping patterns, and tubewell locations were obtained for the sample watercourses. The sample watercourses have varying

numbers of tubewells for irrigation: sample WC 28915L and WC 32326L of Ghour Dour have 2 and 17 tubewells respectively, whereas WC 74634R of Gajiana Distributary, has 38 tubewells. This implies that the crops in the Ghour Dour distributary rely more on canal water resources than in the Gajiana distributary, and that the presence of crops is not related to canal water alone.

Data collected for this study includes daily canal discharge  $Q_{cw\_h}$  ( $LT^{-3}$ ) into Gajiana and Ghour Dour distributaries for *kharif* 2001. For the same period, daily watercourse head discharge  $Q_{cw\_wc}$  ( $LT^{-3}$ ) was also collected. The distributary and watercourse discharges were computed from water level gauge readings and application of the relationship between water level and discharge. Discharge measurements were taken to calibrate this relationship (Qureshi *et al.*, 2001).

A general balance equation sets the canal head discharge  $Q_{cw\_h}$  equal to the summation of the watercourse discharge  $Q_{cw\_wc}$  and conveyance losses  $Q_{cl}$  in the canal:

$$Q_{cw\_h} = Q_{cw\_wc1} + Q_{cw\_wc2} + \dots + Q_{cw\_wcn} + Q_{cl} \quad (7.1)$$

where  $Q_{cw\_wci}$  is the watercourse discharge for the  $i^{th}$  watercourse ( $i = 1, 2, \dots, n$ ). Conveyance losses from the irrigation canal are mainly due to evaporation and seepage. These losses in an irrigation canal depend on a number of factors, including discharge rate, length of the canal, wetted perimeter, and soil type. In the secondary canals of the Punjab, conveyance losses are approximately  $0.025 \text{ m}^3 \text{ m}^{-2} \text{ s}^{-1}$  or  $6.82 \text{ l km}^{-1} \text{ s}^{-1}$  (Tareen *et al.*, 1996, Skogerboe *et al.*, 1999). The total water available at the head of all watercourses ( $Q_{cw\_wcn}$ ) in the distributary command  $Q_T$  ( $L^3T^{-1}$ ) is computed as follows:

$$Q_T = Q_{cw\_h} - 0.00682 L_d \quad \text{m}^3 \text{ s}^{-1} \quad (7.2)$$

where  $L_d$  is the length of the distributary (km).

Figure 7.2 shows the daily variation in distributary head discharge and watercourse discharge during the *kharif* 2001. Maximum temporal deviation occurred in October 2001, when (due to water shortage in the system) no canal water was diverted to the Gajiana and Ghour Dour distributaries for 19 and 11 days respectively. The higher variability between head and watercourse discharges in the Gajiana distributary than in the Ghour Dour distributary was the result of canal breaches.

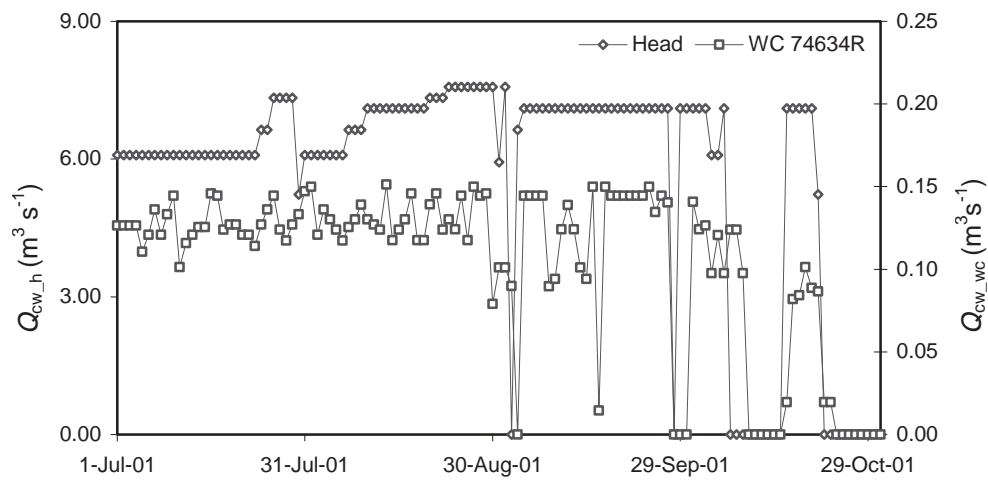
#### Remote Sensing/Satellite Data

A Landsat-7 Enhanced Thematic Mapper (ETM) image from path/row (149/38) acquired on 24 August 1999, covering the Upper Gugera Branch, was used to compute crop growth by means of the Normalized Difference Vegetation Index (NDVI). This computed crop growth was then related to discharge measurements at the head of the distributary. 24 August 1999 coincides with the middle of the *kharif*, when rice is at the heading stage (see Figure 2.2). The discharge measurements were

for 2001 rather than 1999 and this unavoidable discrepancy needed proper attention in the data analysis.

The digital numbers for band 3 (red) and band 4 (near infrared) of Landsat-7 ETM were first converted to spectral radiances using standard calibration coefficients and then to spectral reflectances ([http://ftpwww.gsfc.nasa.gov/IAS/handbook/handbook\\_toc.html](http://ftpwww.gsfc.nasa.gov/IAS/handbook/handbook_toc.html)). These reflectance values were used to calculate the NDVI, which was later used for the identification of cropped areas.

#### Gajiana Distributary



#### Ghour Dour Distributary

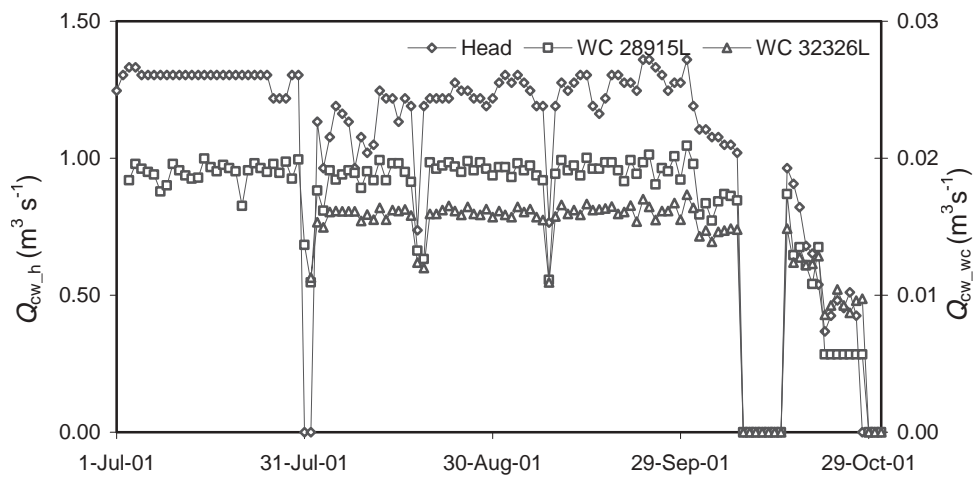


**Figure 7.2** Comparison of distributary head discharge ( $Q_{cw\_h}$ ) vs sample watercourse head discharge ( $Q_{cw\_wc}$ ).

### 7.2.3 Water distribution models

Several factors help describe irrigation practices in a distributary: NDVI, size of actual irrigated area\*  $A$  ( $L^2$ ), its perimeter  $P$  ( $L$ ), distance of an irrigated pixel from the distributary head  $d_h$  ( $L$ ) and from distributary canal  $d_d$  ( $L$ ). Using this information, six different conceptual geomatic models were formulated. The level of the model increases with complexity (Table 7.1).

**Table 7.1** Alternative models to test the new canal water distribution model.  $Q_{cw,h}$  is distributary head discharge,  $A$  is irrigated area,  $d_h$  is distance of irrigated pixel from the head of distributary,  $d_d$  is distance of irrigated pixel from the distributary canal, NDVI is Normalized Difference Vegetation Index, and  $P$  is perimeter of irrigated area.

Model	Field	Geo-information				
	Observation	$A$	$d_h$	$d_d$	NDVI	$P$
Model 1 $I_{cw}^{(1)}(x)$	$Q_{cw,h}$	J				
Model 2 $I_{cw}^{(2)}(x)$	J	J	J			
Model 3 $I_{cw}^{(3)}(x)$	J	J	J	J		
Model 4 $I_{cw}^{(4)}(x)$	J	J			J	
Model 5 $I_{cw}^{(5)}(x)$	J	J	J	J	J	
Model 6 $I_{cw}^{(6)}(x)$	J	J	J	J	J	J

The **first model** is based on the discharge at the distributary head  $Q_{cw,h}$  and the total size of actually irrigated area  $A_T$  in a distributary. The canal water irrigation rate  $I_{cw}(x)$  ( $LT^{-1}$ ) to a point  $x$ , in a command area  $A_T$  is calculated as:

$$I_{cw}^{(1)}(x) = \frac{Q_T}{A_T} \quad (7.3)$$

where the super-script 1 represents the model number.

This is a simple and widely used approach for data-scarce environments, in which an equitable distribution of canal water over the entire irrigated area is assumed.

The **second model** relates the relative distance between an irrigation point  $x$  and the distributary head ( $d_h$ ). For any location  $x$ , in a command area  $A_T$ ,  $M_{A_T}(x)$  is the distance of point  $x$  to the distributary head  $d_h$ :

\* It is important to differentiate between *actually irrigated area from irrigable area*. Actual irrigated area depends upon available resources, particularly water and is *always less than the irrigable area*.

$$M_{A_T}(x) : d(x, d_h) \quad ; x \in A_T \quad (7.4)$$

This distance can be computed for each command area as:

$$\tilde{M}_{A_T}(x) = \frac{M_{A_T}(x)}{\max_{x \in A_T}(M_{A_T}(x))} \quad (7.5)$$

The canal water availability Index  $CWAI_{d_h}$  is defined as:

$$CWAI_{d_h}(x) = \frac{\frac{1}{|A_T|} \int_{A_T} \tilde{M}_{A_T}(x) dx}{\tilde{M}_{A_T}(x)} \quad (7.6)$$

which relates canal water availability to a point  $x$  with reference to  $d_h$ . The areas close to the canal head will have a lower fraction of  $\tilde{M}_{A_T}(x)$  and will have much higher values of  $CWAI_{d_h}$  than far locations. To reduce the effect of this numerical instability, a logistic transformation is used:

$$C\tilde{W}AI_{d_h}(x) = \frac{CWAI_{d_h}(x)}{1 + CWAI_{d_h}(x)} \quad (7.7)$$

The irrigation rate with canal water  $I_{cw}(x)$  to a point  $x$  in  $A_T$  is calculated as:

$$I_{cw}^{(2)}(x) = Q_T \frac{C\tilde{W}AI_{d_h}(x)}{\int_{A_T} C\tilde{W}AI_{d_h}(x) dx} \quad (7.8)$$

Unlike  $I_{cw}^{(1)}(x)$ , this model assumes that water distribution is un-even, with a decreasing trend from head to tail in a distributary command.

The **third model** relates the access of canal water to a point  $x$  as a function of two distances: distance to distributary head  $d_h$  and shortest distance to distributary/minor  $d_d$ . For any location  $x$ ,  $N_{A_T}(x)$  is the shortest distance of point  $x$  to the distributary  $d_d$ :

$$N_{A_T}(x) : d(x, d_d) \quad ; x \in A_T \quad (7.9)$$

The relative distance  $\tilde{N}_{A_T}(x)$  is defined as:

$$\tilde{N}_{A_T}(x) = \frac{N_{A_T}(x)}{\max_{x \in A_T}(N_{A_T}(x))} \quad (7.10)$$

By adding  $\tilde{M}_{A_T}(x)$  and  $\tilde{N}_{A_T}(x)$ , Eqs. 7.5 and 7.10, a relative location map  $d_{rel}(x)$  is computed:

$$d_{rel}(x) = \tilde{N}_{A_T}(x) + \tilde{M}_{A_T}(x) \quad (7.11)$$

The canal water availability Index  $CWAI_{d_{rel}}$  is defined by:

$$CWAI_{d_{rel}}(x) = \frac{\frac{1}{|A_T|} \int_{A_T} d_{rel}(x) dx}{d_{rel}(x)} \quad (7.12)$$

which relates canal water availability to a point  $x$  with reference to  $d_{rel}(x)$ . Similar to model 2, a logistic transformation to reduce numerical instability is performed to yield  $C\tilde{W}AI_{d_{rel}}(x)$ .

The irrigation rate with canal water  $I_{cw}(x)$  to a point  $x$  in  $A_T$  is calculated as:

$$I_{cw}^{(3)}(x) = Q_T \frac{C\tilde{W}AI_{d_{rel}}(x)}{\int_{A_T} C\tilde{W}AI_{d_{rel}}(x) dx} \quad (7.13)$$

This model is an extension of  $I_{cw}^{(2)}(x)$  which incorporates  $d_d$ . This assumes that similar to  $d_h$ , water availability also decreases with an increasing value of  $d_d$ .

The **fourth model** relates crop greenness, expressed through NDVI, to the canal water application rate. Using this criterion, the canal water irrigation rate to any point  $x$  in  $A_T$  is computed as:

$$I_{cw}^{(4)}(x) = Q_T \frac{NDVI(x)}{\int_{A_T} NDVI(x) dx} \quad (7.14)$$

which assumes that canal water has a relationship with crop presence in semi-arid zones.

The **fifth model** combines  $I_{CW}^{(3)}(x)$  and  $I_{CW}^{(4)}(x)$  by considering both NDVI and the location of point  $x$  within  $A_T$ . Relating the presence of vegetation with distance from a distributary and its head, a Canal Water Availability Index ( $CWAI_{NDVI}$ ) is defined by combining NDVI and the  $\tilde{M}_{A_T}(x)$  and  $\tilde{N}_{A_T}(x)$  maps:

$$CWAI_{NDVI}(x) = \frac{NDVI_{A_T}(x)}{(\tilde{M}_{A_T}(x) + \tilde{N}_{A_T}(x))} \quad (7.15)$$

The areas close to a distributary and its head will have a lower value of  $d_{rel}$  (Eq. 7.11) and therefore, will have much higher values of  $CWAI_{NDVI}$  than locations of a higher relative distance at the same NDVI value. Similar to models 2 and 3, a logistic transformation yields  $C\tilde{W}AI_{NDVI}(x)$ . The canal water irrigation rate to a pixel at location  $x$  in  $A_T$  is computed as:

$$I_{CW}^{(5)}(x) = Q_T \frac{C\tilde{W}AI_{NDVI}(x)}{\int_{A_T} C\tilde{W}AI_{NDVI}(x) dx} \quad (7.16)$$

The hypothesis is that a high NDVI at the tail end of distributary and watercourse command is the result of water availability from other sources, such as groundwater. Areas with high NDVI that are close to a distributary or minor canal and its head receive more canal water than areas with a similar NDVI but are located further from the canal head.

The **sixth model** assumes that spatial NDVI patterns are associated with the presence of irrigation. To compute the distribution of canal water with respect to the shape of cultivated crops, different variables are defined that describe the presence of irrigation at different threshold  $y_k$  values of NDVI. An indicator variable  $U(x, y_k)$  for irrigation threshold  $y_k$ , location  $x$ , and variable NDVI( $x$ ) are defined as:

$$U(x, y_k) = \begin{cases} 0 & \text{if } NDVI(x) < y_k \\ 1 & \text{if } NDVI(x) \geq y_k \end{cases}, \text{ for } x \in A_T \quad (7.17)$$

where sub-script  $k$  is the number of threshold used and  $y_1 > y_2 > \dots > y_k$ .

A common measure for expressing shape statistics is *compactness*  $\eta$ , defined as *the ratio of the area of an object to the area of a circle with the same perimeter* (Glasbey and Horgan, 1995). If the area of an irrigated polygon  $i$  equals  $A_i$  and its perimeter equals  $P_i$ , then the compactness  $\eta_{y_k}^i$  can be expressed as:

$$\eta_{y_k}^i = 4\pi \frac{A_i}{(P_i)^2} ; U(x, y_k) = 1 \quad (7.18)$$

The maximum value of  $\eta_{y_k}^i$  is 1, representing a circle. Highly irregular structures have a  $\eta_{y_k}^i$  value close to 0. A final compactness map  $\eta_{A_T}^{i'}$  is calculated by:

$$\eta_{A_T}^{i'}(x) = \begin{cases} \eta_{y_1}^i & \text{if } U(x, y_1) = 1 \\ \eta_{y_k}^i & \text{if } U(x, y_k) = 1 \text{ and } U(x, y_{k-1}) = 0 \text{ for } k = 2, 3, \dots, n \\ 0 & \text{otherwise} \end{cases} \quad (7.19)$$

where  $i'$  belongs to the collection of all integrated polygons taken from each of the  $\eta_{y_k}^i$  maps. Finally, the canal water irrigation rate  $I_{CW}(x)$  to a pixel at location  $x$  in  $A_T$  is computed:

$$I_{CW}^{(6)}(x) = Q_T \frac{1}{\eta_{A_T}^{i'}(x) \int_{A_T} \frac{1}{\eta_{A_T}^{i'}(x)} dx} \quad (7.20)$$

The basic difference with  $I_{CW}^{(4)}(x)$  is that spatial structure, i.e. coherent patterns, is included. The hypothesis of  $I_{CW}^{(6)}(x)$  is that circular patterns of NDVI represent areas that have no long watercourses and that rely on groundwater from tubewells. Pumped groundwater is often used in the vicinity of the source of extraction to minimize conveyance losses, and as a result, the shape of irrigated areas is close to a circle. Elongated patterns of NDVI in this model are associated with the presence of long watercourses and areas relying dominantly on canal water resources.

This study considers four threshold values for  $I_{CW}^{(6)}(x)$ :  $y_1 = 0.6$ ,  $y_2 = 0.5$ ,  $y_3 = 0.4$ , and  $y_4 = 0.3$ , representing the area of different categories of irrigated crops. Each  $U(x, y_k)$  map has a number of isolated irrigated polygons, as shown in Figure 7.3. Using Eq. 7.18), the compactness of resultant polygons in  $U(x, y_k)$  is then computed. Finally  $\eta_{A_T}^{i'}(x)$  is obtained (Eq. 7.20) by superimposing  $\eta_{0.4}^i$ ,  $\eta_{0.5}^i$  and  $\eta_{0.6}^i$  respectively on  $\eta_{0.3}^i$ . This represents the shape (circular or irregular) of irrigate areas under different crop categories.



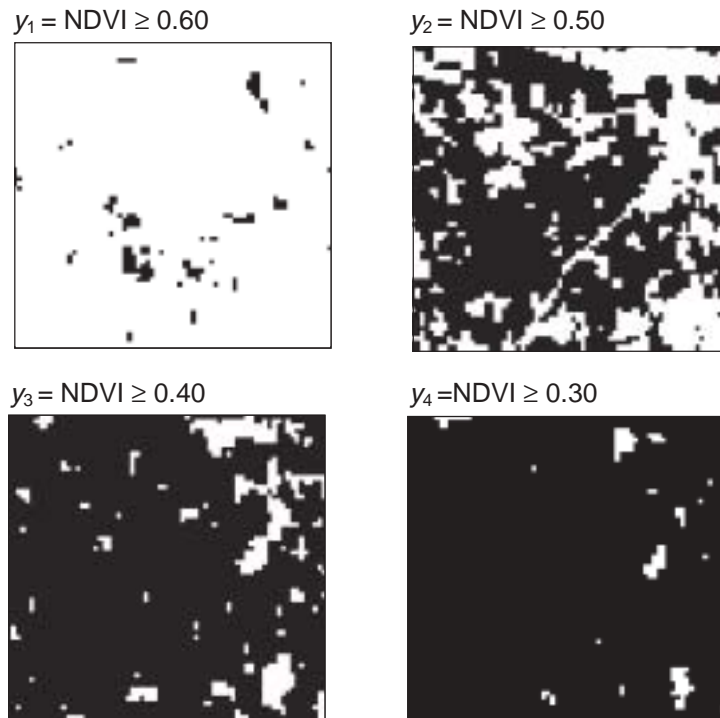


**Figure 7.3** Indicator variable map  $U(x, y_k)$  representing irrigated areas at 0.6, 0.5, 0.4 and 0.3 NDVI thresholds ( $y_k$ ).

### 7.3 Results and discussion

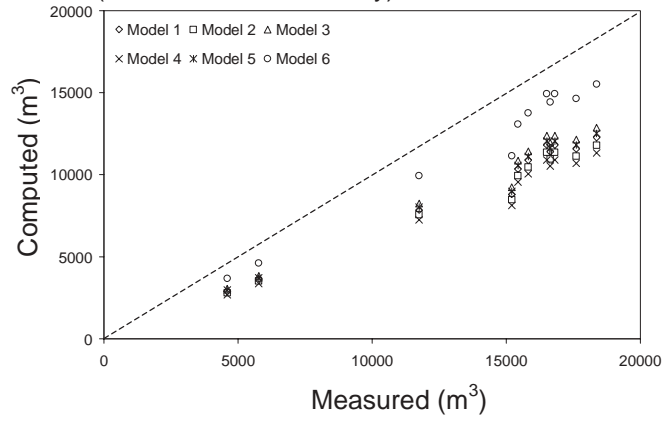
A comparison of NDVI data from Landsat-7 images with land use maps of the sample watercourses, reveals that irrigated crops have a minimum NDVI = 0.3. Hence, all pixels with a NDVI less than 0.3 are excluded from receiving canal water. Isolated areas less than 5 ha that are not connected with the main irrigation system are regarded as areas being irrigated with groundwater. After excluding the areas without irrigation and areas extracting groundwater only, the remaining areas are investigated for canal water use.

The six models were applied to the selected distributaries to disaggregate the canal water deliveries  $Q_{cw\_h}$  designated for the various watercourses of the total irrigated area (18755 ha) from August to October 2001. The sample watercourse coverage were overlaid on the  $I_{cw}(x)$  maps obtained from six different models to spatially integrate the volume of canal water delivered to the three watercourses investigated. The computed volume of water to a watercourse with canal irrigated area  $A_{wc}$ ,

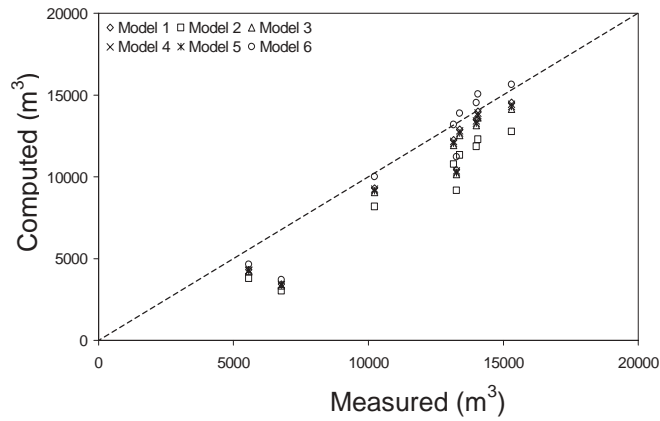
$$\int_{A_{wc}} I_{cw}(x) dx, \text{ is compared with field measurements on a 10-day interval (Figure 7.4).}$$

The reason for choosing a 10-day interval was to represent the conditions after a complete water turn within a watercourse. Before comparing the performance of the six conceptual geomatic models, it is essential to remember that the field measurements are also subject to errors (up to 30%). A deviation of 0.82% (wc74634R for  $I_{CW}^{(5)}(x)$ ) to 70% (wc32326L for  $I_{CW}^{(2)}(x)$ ) from field measurements is observed over the 10-day interval. The higher errors occurred in the month of October, when a canal is occasionally closed due to water shortage or breaches. In general, an underestimation of watercourse discharge is noticed. This peculiar phenomenon may be the result of a change in cropping pattern from 1999 to 2001.

a) WC 28915 L (Ghour Dour Distributary)



b) WC 32326L(Ghour Dour Distributary)



c) WC 74634R (Gajiana Distributary)

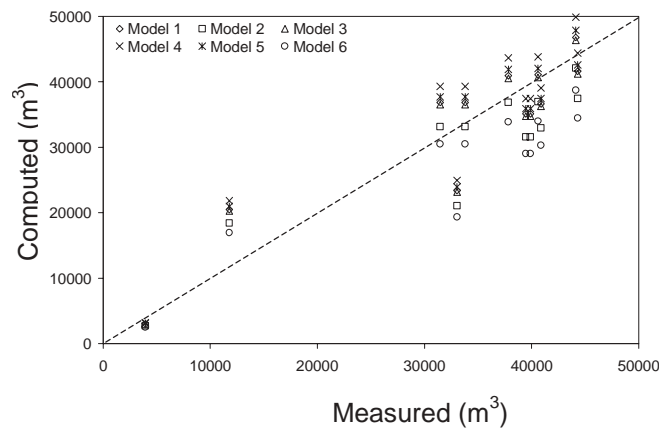


**Figure 7. 4** Computed vs measured canal water diversion to sample watercourses at a 10 day interval.

The overall comparison and accuracy assessment of the different models over a monthly time period is presented in Table 7.2. The absolute deviation varies between different models and between different months (4%:  $I_{CW}^{(4)}(x)$  during September to 53 %:  $I_{CW}^{(4)}(x)$  during October). This reflects the performance stability of the various models. By looking at the average and standard deviation of monthly absolute deviations, we have ranked models from best to least accurate:  $I_{CW}^{(6)}(x)$ ,  $I_{CW}^{(3)}(x)$ ,  $I_{CW}^{(2)}(x)$ ,  $I_{CW}^{(1)}(x)$  &  $I_{CW}^{(5)}(x)$ , and  $I_{CW}^{(4)}(x)$  respectively. This indicates which hypothesis worked better than others.

**Table 7.2** Absolute deviations of computed discharge from measured discharge. (Comparison of 6 geo-information based water distribution models)

Water-course	Model 1 $I_{CW}^{(1)}(x)$ (%)	Model 2 $I_{CW}^{(2)}(x)$ (%)	Model 3 $I_{CW}^{(3)}(x)$ (%)	Model 4 $I_{CW}^{(4)}(x)$ (%)	Model 5 $I_{CW}^{(5)}(x)$ (%)	Model 6 $I_{CW}^{(6)}(x)$ (%)
<b>Ghour Dour Distributary Watercourse 28915L</b>						
July	43	45	40	47	41	27
August	40	42	37	45	39	24
September	43	45	40	47	42	28
October	49	51	47	53	48	36
<b>Ghour Dour Distributary Watercourse 32326L</b>						
July	25	35	27	26	27	20
August	16	26	18	16	17	9
September	23	33	25	24	25	17
October	41	48	43	42	42	37
<b>Gajiana Distributary Watercourse 74634R</b>						
July	27	35	28	23	26	40
August	18	27	19	13	17	33
September	8	17	9	4	6	24
October	42	41	42	43	43	41
<b>Overall Performance of Models</b>						
Average Deviation	31	37	31	32	31	28
Standard Deviation of Deviations	13	10	12	16	13	10

$I_{CW}^{(6)}(x)$  gave the best performance for the estimation of disaggregated canal water deliveries with the lowest monthly deviation (28%) and the lowest standard deviation of monthly absolute deviation (10%). This indicates that the shape (compactness) of an irrigated area is one of the most important variables (which explain the proportion of canal water and groundwater as a source of irrigation water) in estimating canal water deliveries to a particular area.  $I_{CW}^{(4)}(x)$ , which is based solely on NDVI, is the least accurate and very unstable with a 32% absolute deviation and a 16% standard deviation of absolute deviations (these errors are acceptable for wc32326L but not for wc28915L). This indicates that variation in NDVI values is primarily due to groundwater irrigation flows rather than canal water irrigation flows.

The Root Mean Square Error (RMSE) at time intervals of 10, 20 and 30 days were computed for a maximum period of two months (see Table 7.3) in order to determine whether the errors cancel with time integration. The highest relative error (RMSE = 6%) was observed in watercourse 28915L of Ghour Dour distributary. There are no significant changes in relative RSME between smaller (10 day) to larger (30 days) time intervals. This indicates that the models perform equally well at all time steps on a watercourse spatial scale, and that the degree of randomness is limited. The errors have a systematic behaviour because random errors decrease when integrated over a longer period.

**Table 7.3** Variation in relative root mean square error (RMSE) at different time steps (Aug. 1 to Sep.29, 2001).

Watercourse	Model 1 $I_{CW}^{(1)}(x)$ (%)	Model 2 $I_{CW}^{(2)}(x)$ (%)	Model 3 $I_{CW}^{(3)}(x)$ (%)	Model 4 $I_{CW}^{(4)}(x)$ (%)	Model 5 $I_{CW}^{(5)}(x)$ (%)	Model 6 $I_{CW}^{(6)}(x)$ (%)
<b>Ghour Dour Distributary Watercourse 28915L</b>						
10 days	42	44	39	46	41	26
20 day	42	44	39	46	40	26
30 day	42	44	39	46	40	26
<b>Ghour Dour Distributary Watercourse 32326L</b>						
10 days	19	29	21	20	20	14
20 day	19	28	21	19	20	13
30 day	19	28	21	19	20	13
<b>Gajiana Distributary Watercourse 74634R</b>						
10 days	17	25	17	12	15	31
20 day	16	24	17	11	14	30
30 day	16	24	17	10	14	30

The result of  $I_{CW}^{(6)}(x)$ , being the most accurate model, is presented in Figure 7.5 to show intra-distributary canal water distribution for the month of September 2001. Both the intensity of irrigated area and canal irrigation is significantly less in the tail end of both distributaries. This was the basis in development of  $I_{CW}^{(3)}(x)$ , which is the second highly accurate model.

*The results shows that errors in the models are similar to the field accuracies, and this is a big achievement as millions of points can be computed from the remotely sensed data.* Further verification of these approaches is recommended in irrigation systems where comprehensive and accurate databases are available.

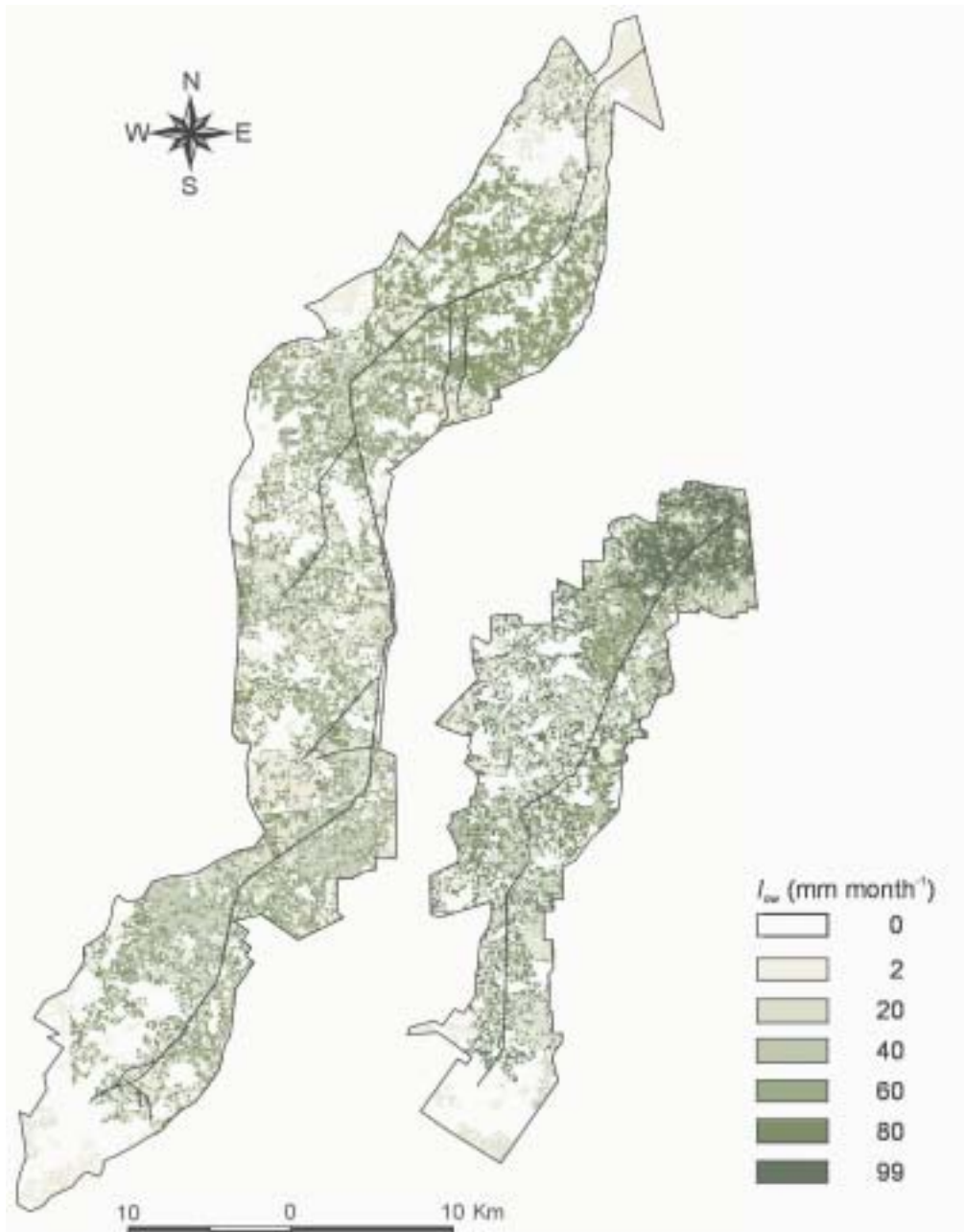


**Figure 7.5** Estimated monthly irrigation rate with canal water  $I_{cw}$  in September 2001 using model 6 ( $I_{cw}^{(6)}(x)$ ) in the Gajiana and Ghour Dour distributaries.

## **7.4 Conclusions**

This study shows that geomatics can be used to estimate disaggregated canal water deliveries from head discharge with 28% accuracy at areas having size equal to 1-1.6% of overall canal irrigated area. The magnitude of error in estimation is of a comparable size as obtained with field measurements at the same scale. Linking NDVI with canal water deliveries is not very successful. The shapes of isolated irrigated area derived from NDVI however are suitable for estimating canal water deliveries. The combined distance function as defined in this study is a promising variable to be included in geomatic modelling. All geomatic models perform equally well at 10, 20 and 30 days time interval. This shows that randomness in the errors is of little importance. The systematic underestimation of the measured flow of 28% is not clearly understood. Finally we conclude that geo-information techniques can be used to compute water distribution in large irrigation systems with a minimum of field data if an appropriate geomatic model is selected.



## 8 NET GROUNDWATER USE IN RECHNA DOAB FOR SUSTAINABLE POLICY AND DECISION MAKING\*

### 8.1 Concept and basic equations for net groundwater use

In Chapter 3, the concept of net groundwater use  $I_{ngw}$  at a field scale was introduced as:

$$I_{ngw} = I_{tw} - q_{nr} \quad (3.19)$$

which describes the moisture exchanges between the saturated and unsaturated zones, as shown in Figure 8.1.

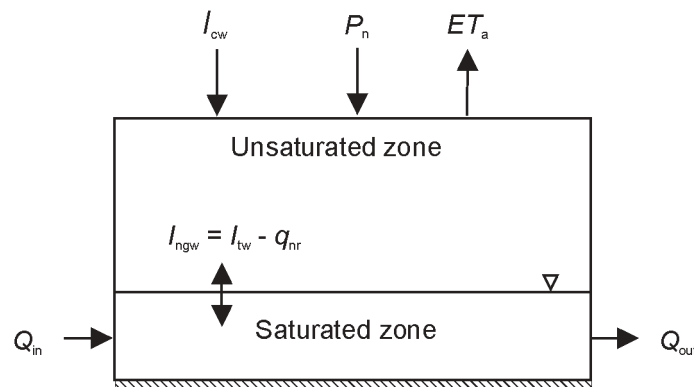


**Figure 8.1** Schematic diagram representing the net groundwater use  $I_{ngw}$  and other water fluxes which include:  $I_{cw}$  rate of irrigation with canal water,  $P_n$  rate of net precipitation,  $ET_a$  rate of actual evapotranspiration,  $I_{tw}$  rate of irrigation with groundwater withdrawal from tubewells,  $q_{nr}$  net recharge, and  $Q_{in}$  and  $Q_{out}$  lateral in-flow and out-flow in the saturated zone.

At a *regional or basin scale*,  $I_{ngw}$  can be computed (See Box. 3.1) in two different ways:

1. *Transient water balance of the **saturated** zone:*

$$I_{ngw} = \frac{Q_{in} - Q_{out}}{A} - S_y \frac{dh}{dt} \quad (3.20)$$

\* Adapted from Ahmad, M.D., W.G.M. Bastiaanssen and R.A. Feddes, 2002. Net groundwater use in Rechna Doab for sustainable policy and decision making. *Ground Water (to be submitted)*

where  $Q_{in}$  and  $Q_{out}$  represent lateral groundwater inflow and outflow respectively,  $S_y$  is the specific yield,  $dh$  is the change in the depth of the phreatic surface, and  $dt$  is the change in time.

## 2. Transient water balance of *unsaturated* zone:

$$I_{ngw} = ET_a - P_n - I_{cw} + \frac{dW_u}{dt} \quad (3.23)$$

where  $ET_a$  is the rate of actual evapotranspiration,  $P_n$  the rate of net precipitation,  $I_{cw}$  the rate of irrigation with canal water and  $dW_u$  the change in soil moisture storage during time  $dt$ .

The main advantage of computing  $I_{ngw}$  with Eq. 3.23 is that the lateral groundwater movement in the saturated zone does not have to be quantified.

## 8.2 Conventional techniques

### *Specific yield $S_y$ -method*

For large areas, conventional techniques for estimating distributed groundwater use and recharge depend on the analysis of the fluctuation of the depth to the phreatic surface (Healy and Cook, 2002). Such an approach is based on the assumption that the rise or fall of the phreatic surface is due to recharge or groundwater use only, i.e., lateral groundwater movement  $\frac{Q_{in} - Q_{out}}{A} = 0$ . Hence, net groundwater use  $I_{ngw}$  is then simply calculated as:

$$I_{ngw} = -S_y \frac{dh}{dt} \quad (8.1)$$

This approach uses a gross simplification of very complex upward movement of water from and downward movement to the phreatic surface. To apply this method for a large area, an estimate of specific yield  $S_y$  is required in addition to the monitoring of the phreatic surface depth by a network of piezometers.

Across Rechna Doab, the depth of the phreatic surface was measured twice a year, pre- and post-monsoon, with a nodal network of 981 piezometers (Figure 6.10) by the SCARP Monitoring Organization (SMO) of Water and Power Development Authority (WAPDA) of Pakistan. They also conducted pumping tests at 47 different locations to calculate the specific yield  $S_y$  for Rechna Doab (Khan, 1978). This point data of specific yield and piezometric levels for October 1993 and October 1994 were acquired from WAPDA and interpolated using the kriging method. Thereafter, the annual change in phreatic surface depth  $dh$  was calculated from the maps

representing the depth of phreatic surface in October 1993 and October 1994. Finally, using  $dh$  and  $S_y$  maps, the annual net groundwater use  $I_{ngw}$  was computed (Eq. 8.1) from October 1993 to October 1994 (Figure 8.2). The gradual trends of  $I_{ngw}$ , having positive as well as negative values, are the inherent limitation of this method, as it results from the spatial averaging which is dependent on the density of the observation points.

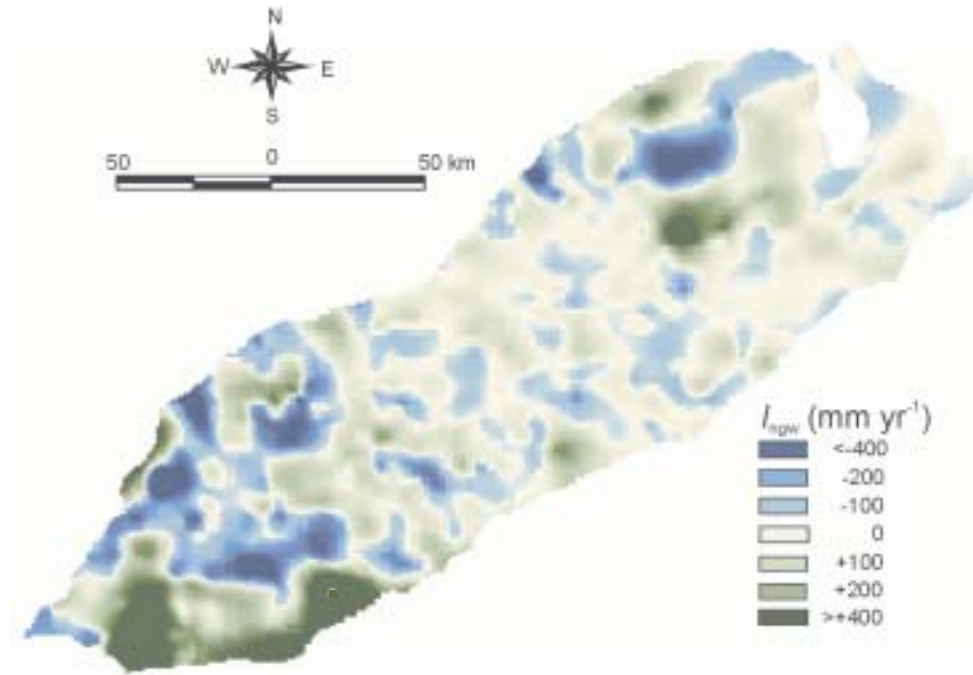


**Figure 8.2** Annual net groundwater use  $I_{ngw}$  (Eq. 8.1) (obtained from measurement of the phreatic surface on October 1993 and October 1994 and specific yield  $S_y$  data in Rechna Doab). Positive values show net groundwater use and negative values show net replenishment.

#### *Statistical Method (Utilization Factor $U_F$ -Method)*

Sometimes groundwater use for agriculture is referred to as the groundwater withdrawal by tubewells for irrigation  $I_{tw}$ . In large irrigation schemes, statistical methods are used to define the relationship between  $I_{tw}$  and tubewell utilization time, as well as site characteristics (NESPAC-SGI, 1991; Maupin, 1999). Tubewell utilization time is calculated from electricity/fuel usage bills or through field surveys.

In the Punjab of Pakistan, use of private tubewells has rapidly increased (Figure 1.2); and farmers operate their tubewells from a number of energy sources including: diesel engines, tractor power take-offs and electric motors (Perry and Hassan, 2000). Due to

unplanned and rapid development, no mechanism is in place to calculate electricity or fuel usage of tubewells in Pakistan. Therefore NESPAK-SGI (1991) has worked out factors  $U_F$  (ratio of daily tubewell working hours to number of hours in a day) through field surveys in different areas of Pakistan.  $U_F$  can be used to compute  $I_{tw}$  from the number of tubewells  $N_{tw}$  in an irrigated area  $A$  and their average discharge capacity  $Q_{tw}$  as:

$$I_{tw} = \frac{U_F N_{tw} Q_{tw}}{A} \quad (8.2)$$

This statistical approach is known in Pakistan as the *Utilization Factor  $U_F$ -method*.

Tahir and Habib (2001) used  $U_F$ ,  $N_{tw}$  and  $Q_{tw}$  data (GOP, 1994) for the approximation of  $I_{tw}$  in the Punjab. As tubewell statistics were available for large aggregated districts, they first calculated  $I_{tw}$  for the district and then transformed it to a canal command scale, according to the proportion of the district to the specific command area. Estimated annual  $I_{tw}$  values for different canal commands of Rechna Doab are summarized in table 8.1.

**Table 8.1** Annual estimates of groundwater withdrawal for irrigation  $I_{tw}$  for the year 1993-94, (according to Eq. 8.2) using utilization factors  $U_F$  in different canal commands of Rechna Doab. Marala-Ravi Link MR Link, UCC Upper Chenab Canal, BRBD Bambanwala-Ravi-Bedian-Depalpur Canal, LCC Lower Chenab Canal and Haveli Canal. (partly after Tahir and Habib, 2001)

	Canal Command				
	MR	UCC	BRBD	LCC	Haveli
$I_{tw}$ (mm yr <sup>-1</sup> )	932	629	729	460	540

The highest  $I_{tw}$  was found in the non-perennial canal commands that are located in the upper Rechna Doab: MR, UCC and BRBD (see Figure 2.4). This area is in the rice-wheat agro-climatic zone of the Punjab and most groundwater withdrawals are for rice cultivation.

### 8.3 Geo-information techniques for unsaturated zone water balance

The transient unsaturated zone water balance approach (Eq. 3.23) to assess the distribution of  $I_{ngw}$  over large irrigated river basins is not commonly used, because conventional means for obtaining distribution information for Eq. 3.23 fail. For example, evapotranspiration – one of the largest water balance components – is often estimated by reference crop evapotranspiration  $ET_0$  (Allen *et al.*, 1998), which differs considerably from *actual* evapotranspiration  $ET_a$ . Note: for certain land use classes,  $ET_0$  can be as large as 10 mm d<sup>-1</sup> and  $ET_a$  can be as small as 1 mm d<sup>-1</sup>.

Present day *geo-information techniques* can be used to estimate water balance components with acceptable accuracy (Bos *et al.*, 2001) and makes it attractive to calculate  $I_{ngw}$  from the unsaturated zone water balance according to Eq. 3.23. The actual evapotranspiration rate  $ET_a$  is computed from the Surface Energy Balance Algorithm for Land (SEBAL) using NOAA-AVHRR satellite imagery (described in Chapter 5). Since there is a direct link between  $ET_a$  and volumetric soil moisture content  $\theta$  at various stages in the growing season,  $ET_a$  data also provide information on  $\theta$ . Using the  $ET_a$ - $\theta$  relationship, unsaturated zone soil moisture storage  $W_u$  can be computed as shown in Chapter 6. On an annual basis in Rechna Doab, the net precipitation rate  $P_n$  is not a major water balance component. Therefore, monthly estimates of precipitation on a pixel-wide basis were obtained from linear interpolation of gauge readings collected at 8 meteorological stations throughout Rechna Doab. Since Rechna Doab is relatively flat and irrigation fields have bunds, runoff has been ignored. In Chapter 7, different models were developed to compute canal water distribution on a pixel-wide basis using canal flow data at main diversions and satellite imagery. Canal water diversions to all major irrigation canal systems of Rechna Doab have been measured at the head works by the Punjab Irrigation department and WAPDA. With the lack of high-resolution satellite images covering the entire Rechna Doab for a complete annual cycle (October 1993- October 1994), canal water distribution was estimated by relating NDVI with canal water availability, using Model 4 (Eq. 7.14) of Chapter 7. The maps showing the spatial distribution of the various water balance components derived from remote sensing and geo-information techniques are presented in Figure 8.3.

The spatial variability in annual  $I_{cw}$ , in canal commands is mainly the result of the non-perennial system (little or no water supplies in *rabi*) in the upper Rechna Doab. Despite the low canal water supplies, the upper Rechna Doab (served by Marala-Ravi MR Link, Bambanwala-Ravi-Bedian-Depalpur BRBD Link and Upper Chenab Canal UCC) is the most intensively cultivated area. The crop water requirement is met by additional supply from groundwater extraction by tubewells, with some contribution from precipitation. Upper Rechna Doab, in particular the MR canal command, receives 2 to 3 times more precipitation than the middle and lower part of the Doab. The highest rate of irrigation with canal water  $I_{cw}$  was estimated in the Haveli canal, because there are large uncertainties in the gross areas as reported by the irrigation department and WAPDA (calculated from canal command coverage).

Spatial distributions of  $ET_a$ , varying from 600 to 1100 mm yr<sup>-1</sup>, are found in the cultivated areas across Rechna Doab. The canals, having high  $ET_a$ , are distinct. A large tract with higher  $ET_a$  exists in the rice growing area in the upper Rechna Doab. The variation in  $I_{cw}$ ,  $P_n$  and  $ET_a$  causes positive as well as negative changes in soil moisture storage  $W_u$  in Rechna Doab.

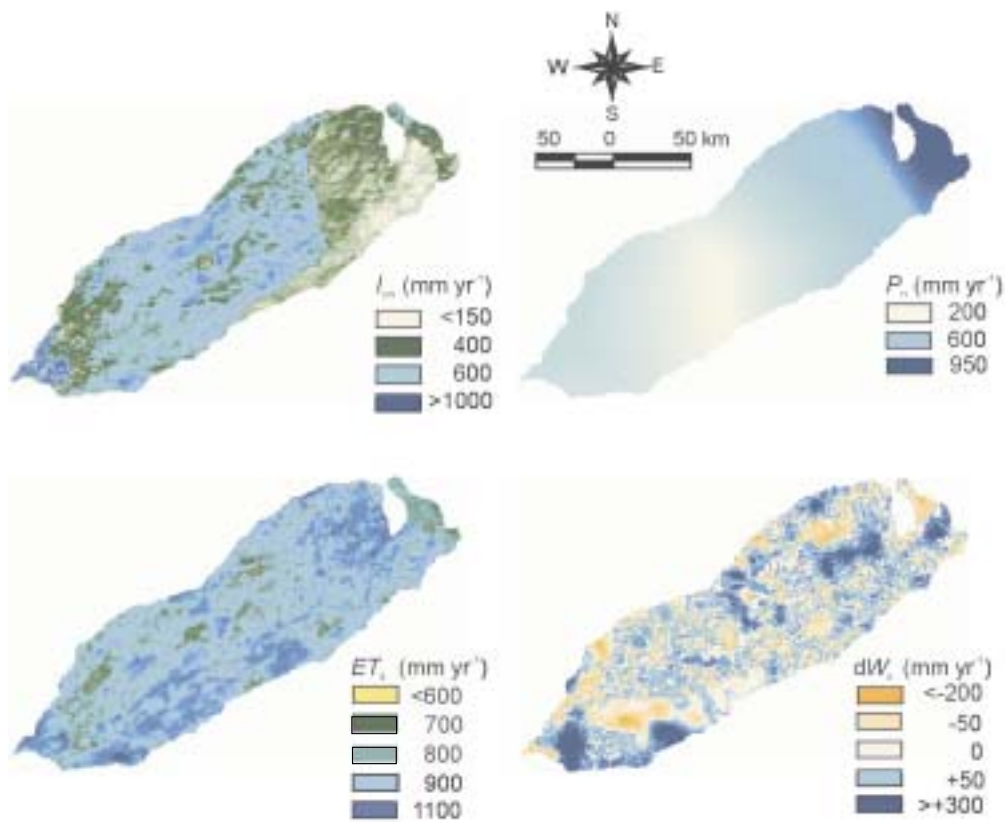


**Figure 8.3** Maps showing the distribution of annual irrigation rate with canal water  $I_{cw}$ , net precipitation rate  $P_n$ , actual evapotranspiration rate  $ET_a$  and change in the unsaturated zone soil moisture storage  $dW_u$  from October 1993 to October 1994 in Rechna Doab.

Finally, for each pixel, net groundwater use  $I_{ngw}$  was estimated by means of Eq. 3.23. First monthly values were calculated and then aggregated to annual values (Figure 8.4). Positive  $I_{ngw}$  values in Figure 8.4 represent net groundwater use, negative values represent net replenishment. It appears that in cultivated areas the largest variability of  $I_{ngw}$  stems from  $dW_u/dt$  (varying between  $-200$  and  $+300 \text{ mm yr}^{-1}$ ) and  $ET_a$  (varying between  $600$  to  $1100 \text{ mm yr}^{-1}$ ). The  $I_{cw}$  component can generally be computed with better precision using high-resolution satellite imagery in combination with field data collection.

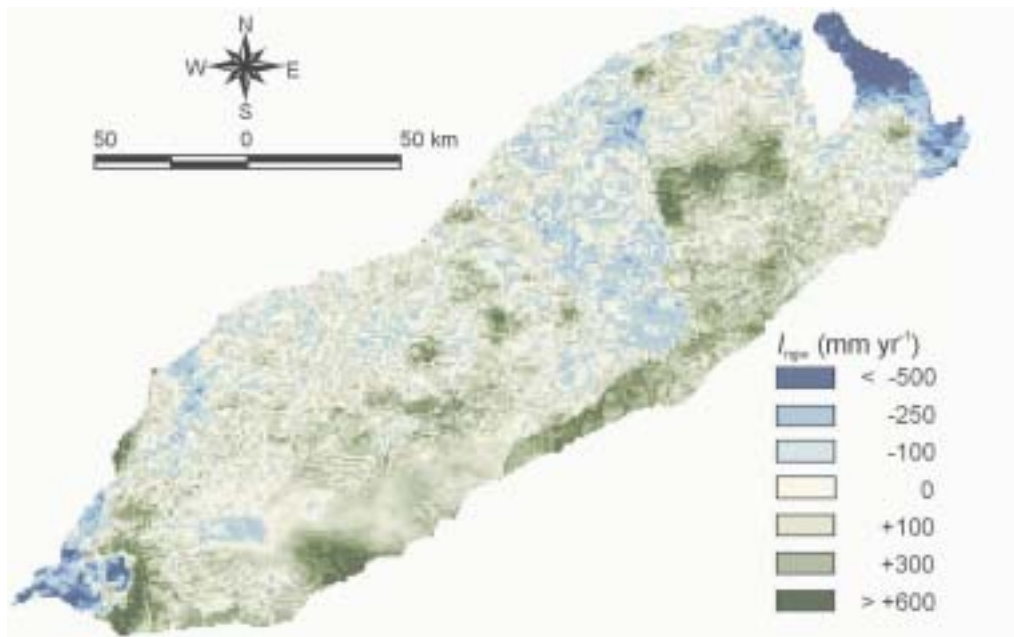


**Figure 8.4** Distributed *annual* net groundwater use  $I_{ngw}$  (Eq. 3.23) from October 1993 to October 1994, as computed using remote sensing and geo-information techniques in Rechna Doab.

The highest  $I_{ngw}$  is observed in the UUC and BRBD, which are areas containing non-perennial canals. Other fragmented pockets of high  $I_{ngw}$  are in the LCC (East), which have higher annual  $ET_a$  because of rice cultivation or higher cropping intensities. Scattered patterns of groundwater replenishment (negative values of  $I_{ngw}$ ) are also observed across the LCC system, particularly in the head reach with a rice-wheat cropping system. But, most of the groundwater replenishment occurs in the command areas of MR and Haveli. The replenishment in MR is mainly because of a higher net precipitation rate  $P_n$ , while in Haveli it is because of higher canal water supplies. Most of the replenishment occurs during the monsoon months, when canals are flowing at peak discharge (see Figure 2.6). This water is not necessarily lost as groundwater, as it may be used elsewhere at a latter time.

Results at canal command level

Monthly estimates of  $I_{ngw}$  in different canal commands of Rechna Doab, as calculated from the geo-information based water balance analysis, are presented in Figure 8.5.

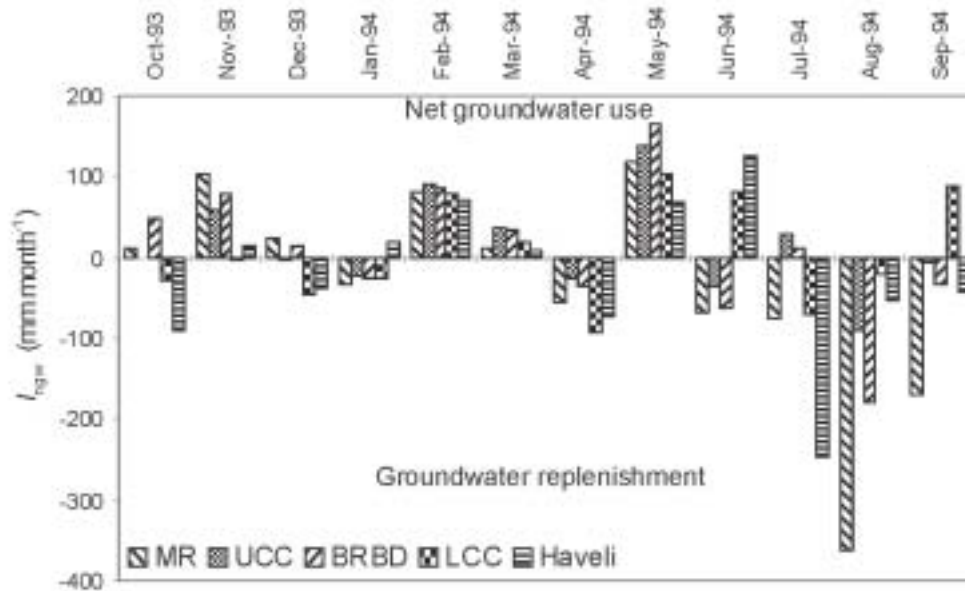


**Figure 8.5** Monthly net groundwater use  $I_{ngw}$  in different canal commands of Rechna Doab. Net groundwater use occurs during crop sowing periods while replenishment occurs during monsoon periods. Marala-Ravi Link MR, UCC Upper Chenab Canal, BRBD Bambanwala-Ravi-Bedian-Depalpur Canal, LCC Lower Chenab Canal and Haveli Canal.

Positive and negative values of  $I_{ngw}$  were observed in all canal commands during both the *rabi* and *kharif*. The highest values are found in *kharif* (July to September) due to the high crop water requirement (more pumping, positive  $I_{ngw}$ ) and the monsoon period (more precipitation, negative  $I_{ngw}$ ). Most of the groundwater use  $I_{ngw}$  was during November and May in all canal commands. This coincides with the higher water demand for land preparation for timely sowing of *rabi* and *kharif* crops. The values of  $I_{ngw}$  in MR, UCC, and BRBD are much higher than in other canal commands during the *rabi*, since little or no canal water is being diverted to these canal commands (see Figure 2.6). During the monsoon months,  $I_{ngw}$  was often negative (July, August and September), which implies that groundwater systems are replenished in most of the canal commands. Aggregated results on an annual basis reveal that, in the three canal commands of UCC, BRBD and LCC, considerable amounts of net groundwater



were used: 170, 108 and 85 mm yr<sup>-1</sup> respectively. In MR and Haveli, the groundwater aquifer was replenished with 405 and 201 mm yr<sup>-1</sup> respectively.

If independent data on the depth of the phreatic surface and specific yield  $S_y$  are also available, the values of  $I_{ngw}$  can be further used to assess the magnitude of the in-flow or out-flow of groundwater by lateral movement at a particular location. This is accomplished by re-arranging Eq. 3.20 as:

$$\frac{Q_{in} - Q_{out}}{A} = I_{ngw} + S_y \frac{dh}{dt} \quad (3.24)$$

Using the results from the geo-information techniques with raster maps of  $S_y$  and  $dh/dt$ , annual lateral groundwater movements were computed for Rechna Doab (Figure 8.6). These results show the annual lateral in-flow or out-flow for a particular area. For comparison, a phreatic surface height map was calculated (October 1993) by the kriging method using point observations of the phreatic surface depth and the natural surface level (Figure 8.7). Groundwater flow occurs from the Upper Rechna to the lower Rechna Doab; a similar trend is shown in Figure 8.6.

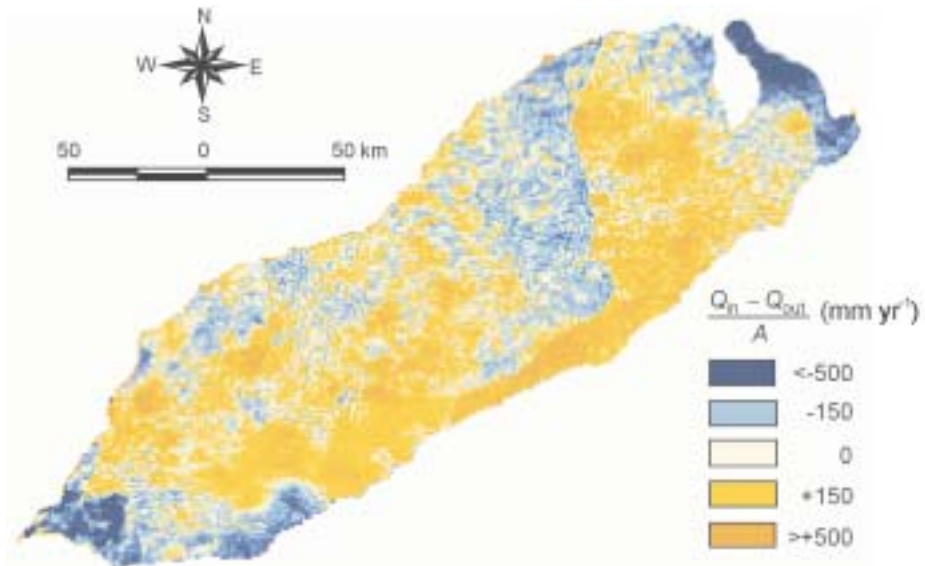


**Figure 8.6** Annual net lateral groundwater flow ( $\frac{Q_{in} - Q_{out}}{A}$ ) during October 1993-October 1994 in Rechna Doab estimated Eq. 3.24 applying *geo-information techniques*.

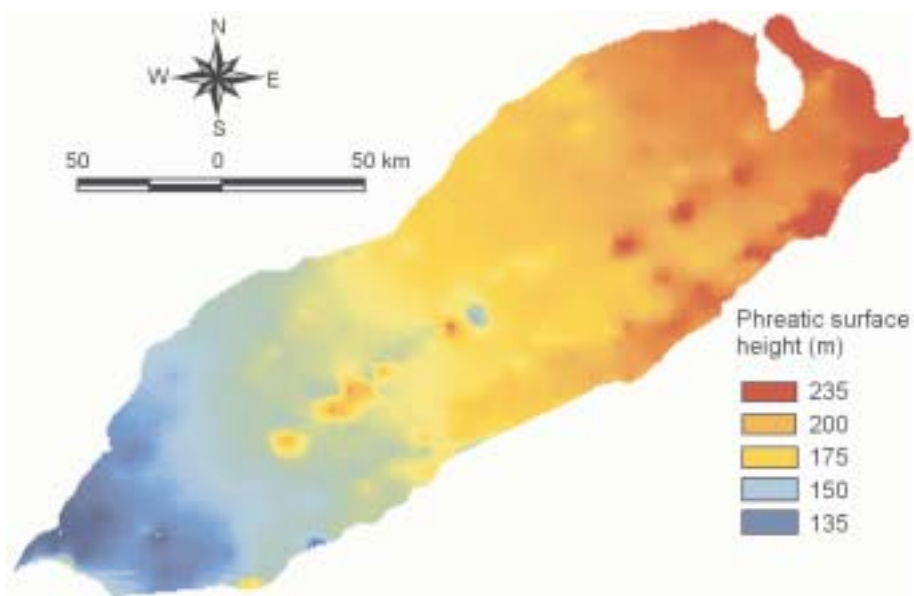


**Figure 8.7** Height of the phreatic surface above mean sea level in Rechna Doab for October 1993.

#### 8.4 Comparison between conventional and geo-information techniques

A comparison between Figure 8.2 and 8.4 shows that the geo-information based analysis produce  $I_{ngw}$  values that give different spatial shapes, with more abrupt changes than the gradual patterns of Figure 8.2. The effect of change in land use, soil types and irrigation practices on  $I_{ngw}$  is more pronounced in the geo-information based analysis. Figure 8.8 shows the frequency distribution of  $I_{ngw}$  values from  $S_y$ -method (Eq. 8.1), as well as the results of the unsaturated zone water balance analysis (Eq. 3.23) using the geo-information techniques. Figure 8.8 shows that the geo-information based water balance analysis has a wide spread of values as compared to the  $S_y$  method. In the positive range, the values from the geo-information technique are significantly higher than the values from the  $S_y$  method, and thus the values of the  $S_y$ -method are systematically underestimated.

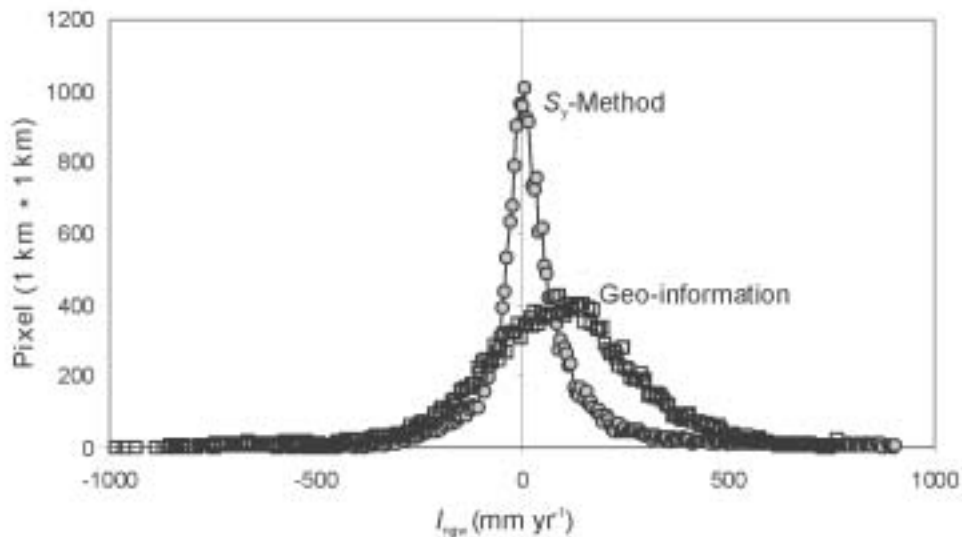


**Figure 8.8** Frequency distributions of *annual* net groundwater use  $I_{ngw}$  using either the specific yield  $S_y$ -method (Eq. 8.1) or the remote sensing and geo-information technique (Eq. 3.23), October 1993 to October 1994 in Rechna Doab.

The main difference between the two methods is that the conventional approach ( $S_y$ -method) neglects groundwater lateral flow. *This also confirms that in highly permeable aquifers, such as in Rechna Doab, lateral groundwater flow cannot be ignored. Any localized change in the phreatic surface depth caused by groundwater withdrawals or irrigation activity tends to be stabilised by groundwater flows into and from surrounding areas; this cannot be observed with occasional monitoring of the phreatic surface depth.*

It is interesting to compare values for groundwater withdrawal by tubewells  $I_{tw}$  (a traditional way of referring to groundwater use for irrigation in Pakistan) using the  $U_F$ -method (Eq. 8.2) with net groundwater use  $I_{ngw}$  obtained by both the geo-information and the  $S_y$ -Method (Table 8.2). Except for Haveli, the geo-information and  $S_y$ -method show similar trends of annual net groundwater use in all commands. The results from the  $U_F$  method are significantly higher (550%) than the results obtained from the geo-information technique. This could be due to incorrect computations or because the net recharge component is not considered in  $U_F$ -Method. The  $S_y$ -method, which ignores lateral groundwater flow, yielded a 65% underestimation of net groundwater use. Net laterals flows to Rechna Doab from October 1993 to October 1994 amounted to 1193 million  $m^3 yr^{-1}$  (from the average of 53 mm  $yr^{-1}$ ). The largest inflows were found in the LCC and UCC respectively.

**Table 8.2** Comparison of annual net groundwater use  $I_{ngw}$  computations from the geo-information techniques (Eq. 3.23) and the  $S_y$ -method (Eq. 8.1) with groundwater withdrawal by tubewells  $I_{tw}$  calculated using the utilization factors  $U_F$  (Eq. 8.2) in the different canal commands of Rechna Doab from October 1993 to October 1994.  $Q_{in}$  and  $Q_{out}$  represent respectively the groundwater lateral in-flow and out-flow. (Marala-Ravi MR Link, UCC Upper Chenab Canal, BRBD Bambanwala-Ravi-Bedian-Depalpur Canal, LCC Lower Chenab Canal and Haveli Canal.)

Canal commands	Geo-information	$S_y$ -Method	$U_F$ -Method	Geo-information	$S_y$ -Method	$U_F$ -Method	Geo-information
	$I_{ngw}$	$I_{ngw}$	$I_{tw}$	$I_{ngw}$	$I_{ngw}$	$I_{tw}$	$Q_{in} - Q_{out}$
	mm yr <sup>-1</sup>	mm yr <sup>-1</sup>	mm yr <sup>-1</sup>	10 <sup>6</sup> m <sup>3</sup> yr <sup>-1</sup>	10 <sup>6</sup> m <sup>3</sup> yr <sup>-1</sup>	10 <sup>6</sup> m <sup>3</sup> yr <sup>-1</sup>	10 <sup>6</sup> m <sup>3</sup> yr <sup>-1</sup>
MR	-405	-54	+932	-264	-35	+606	-229
UCC	+170	+24	+629	+732	+103	+2702	+629
BRBD	+108	+13	+729	+191	+23	+1292	+168
LCC	+85	+34	+460	+1289	+511	+6979	+778
Haveli	-201	+65	+540	-115	+37	+308	-152
Rechna Doab				+1833	+639	+11882	+1193
				+82	+28	+529	+53
							10 <sup>6</sup> m <sup>3</sup> yr <sup>-1</sup>
							mm yr <sup>-1</sup>

## 8.5 Summary and conclusion

In this Chapter net groundwater use  $I_{ngw}$  was computed using the specific yield method (Eq. 8.1), and the remote sensing and geo-information method for calculating the unsaturated zone water balance (Eq. 3.23). The annual average water balance components in Rechna Doab are summarized in Figure 8.9. On the average, the specific yield method produced a 65% under estimation of net groundwater use as compared to the geo-information technique. This difference is explained by groundwater lateral flows, which are ignored in the specific yield method. Therefore, even at an annual scale, the effect of groundwater withdrawal by tubewells or net recharge from irrigated fields in highly permeable phreatic aquifers is difficult to observe and quantify with occasional monitoring of the phreatic surface depth.

Also, groundwater withdrawal computations using utilization factors (Eq. 8.2) differ greatly from the net groundwater use calculations (Eq. 3.23) and do not provide useful information for groundwater policy makers.

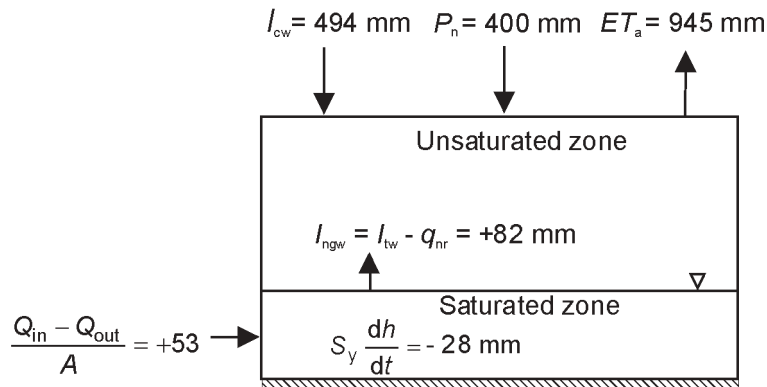


**Figure 8.9** Annual water balance from October 1993 to October 1994 over the Rechna Doab as estimated from geo-information techniques, where  $I_{ngw}$  is net groundwater use,  $I_{cw}$  is rate of irrigation with canal water,  $P_n$  is rate of net precipitation,  $ET_a$  is rate of actual evapotranspiration,  $I_{tw}$  is rate of irrigation with groundwater withdrawal from tubewells,  $q_{nr}$  is net recharge, and  $Q_{in}$  and  $Q_{out}$  are lateral in-flow and out-flow in the saturated zone.

Even at canal command level, geo-information techniques provide more accurate results than the conventional techniques. This is because geo-information based net groundwater use combined with the  $S_y$ -method depicts whether the rise or fall of the phreatic surface can be ascribed to net lateral groundwater flow or to vertical interactions. Such information is of strategic importance when considering localized or regional options for sustainable groundwater management.

In conclusion, geo-information techniques provide a comprehensive, efficient, and standardized opportunity of quantifying the net groundwater use for agriculture with a minimal need of field data.

## 9 SUMMARY AND CONCLUSIONS

### *Problem Statement*

The food-producing regions of the world increasingly rely on irrigation from groundwater resources. Therefore, the achievement of sustainable groundwater use has become a key element of global food security. Poor planning and inadequate water management have resulted in rises and falls of the phreatic surface in arid regions such as Pakistan. Lack of accurate information on net groundwater use – the difference between groundwater withdrawal by tubewells and net recharge (Eq. 3.19) – is the main hindrance to effective management and protection of precious water resources. Net groundwater use has a dynamic nature and is difficult to quantify for irrigated agriculture. Conventional methods used to assess net groundwater use for large areas are based on statistical methods like the tubewell utilization factor method (Eq. 8.2) and the saturated zone water balance method (Eq. 3.20).

The tubewell utilization factor method (Section 8.2) approximates groundwater withdrawal for irrigation using tubewell inventory data and utilization time calculated either from fuel/electricity usage or through field surveys. This approach provides a gross picture of extracted water for irrigation in large areas but does not describe net groundwater use, because the net recharge (Eq. 3.18) – the difference between recharge and capillary rise – is not considered.

In saturated zone water balance analysis, rise and fall of the phreatic surface is linked to net groundwater use. The basic problems with this method are due to the linkages between (i) lateral groundwater movement, (ii) vertical exchanges with the unsaturated zone and (iii) change in soil moisture storage. Groundwater simulation models are complex and can solve (i) but are less suitable for solving (ii).

*This thesis attempts to develop a methodology (Chapter 3), which relies on the combined use of remotely sensed information and GIS techniques for the estimation of net groundwater use, without the inclusion of complex groundwater models.*

### *Study Area*

The investigations were conducted in Rechna Doab, which is located in the heart of the Indus basin irrigation system (Chapter 2). Rechna Doab is the interfluvial area between the Chenab and Ravi Rivers (Figure 2.1). The gross area of this Doab is 2.97 million ha, with a maximum length of 403 km and maximum width of 113 km, including 2.3 million hectares of cultivated land. The climate is semi-arid, with annual potential evapotranspiration ( $1400 \text{ mm yr}^{-1}$ ) far exceeding annual precipitation ( $400 \text{ mm yr}^{-1}$ ). Due to both scant and erratic precipitation, successful agriculture is only possible by means of irrigation. In Rechna Doab, the canal irrigation system was introduced in 1892 with the construction of the Lower Chenab Canal and is one of the oldest and most

intensively developed irrigated areas of Punjab, Pakistan. Both canal water and groundwater, with varying proportion, are now jointly used for irrigation across Rechna Doab. The study area lies in the rice-wheat and sugarcane agro-ecological zones of the Punjab province. Rice, cotton and forage crops dominate in the summer season (*kharif*). Wheat and forage are the major crops in the winter season (*rabi*). In some areas, sugarcane, an annual crop, is also cultivated.

### Field Scale Analysis

Field level analysis of soil water flow and soil moisture dynamics in Rechna Doab have been discussed in Chapter 4. Two fields representing the rice-wheat and cotton-wheat cropping system were selected for thorough field measurements in shallow and deep phreatic surface areas (lasting from June 2000 to May 2001). A physically based numerical model termed SWAP (Soil-Water-Atmosphere-Plant) was applied to compute soil moisture content and vertical soil water fluxes in the unsaturated zone of these two fields. SWAP has been calibrated and verified with *in situ* measurements of soil moisture content (using a theta probe with the frequency domain technique) and evapotranspiration fluxes (using the Bowen ratio surface energy balance technique). This is the first attempt in Pakistan to verify the unsaturated zone model SWAP using the Bowen ratio technique. The root mean square errors (RMSE) between measured and computed soil moisture contents were found to be  $0.02 \text{ cm}^3 \text{ cm}^{-3}$  for Faisalabad and  $0.03 \text{ cm}^3 \text{ cm}^{-3}$  for Pindi Bhattian. The RMSE for actual evapotranspiration were respectively  $1.07$  and  $0.9 \text{ mm d}^{-1}$ , which is a difference of approximately 16% at an evapotranspiration rate of  $6 \text{ mm d}^{-1}$ . The difference between measured and computed accumulated annual evapotranspiration was much smaller (1.5 to 3%).

The calibrated SWAP model provided an insight into capillary rise and groundwater recharge patterns, as well as daily changes of soil moisture profiles and soil moisture storage. *The simulation results for Pakistani conditions show that recharge cannot always be estimated solely from root zone water balances; and therefore, advanced simulation techniques are necessary to compute the interaction between the unsaturated and saturated zone.* The results also indicated that a considerable amount of groundwater extracted through irrigation tubewells returns to the same unconfined aquifer. This phenomenon is more pronounced in shallow phreatic surface conditions (2 m deep), especially for rice crops, where almost 50% of the groundwater withdrawal flows back to the aquifer. For year 2000-01, an annual recharge of 38.9 cm was estimated for rice-wheat systems; a reduction of 62% in groundwater extraction is required for sustainability of groundwater use at a field scale. An annual recharge of 23.3 cm was computed for the cotton-wheat area; sustainability of groundwater use at a field scale will be obtained only with a reduction of 36% in groundwater extraction.

### Basin Scale Analysis

For basin level groundwater management analysis, a *regionalization method* must be developed that extrapolates field conditions to the regional scale. This study explores



a remote sensing based regionalization method that estimates most of the water balance components in the unsaturated zone, i.e. actual evapotranspiration, soil moisture storage, and canal water supplies.

#### *Actual Evapotranspiration*

Under semi-arid conditions, actual evapotranspiration is one of the largest water balance components for irrigated areas. Chapter 5 presents the Surface Energy Balance Algorithm for Land (SEBAL) method for computing actual evapotranspiration over large areas based on public domain National Oceanic and Atmospheric Administration – Advanced Very High Resolution Radiometer (NOAA-AVHRR) satellite data. Methods for computing actual evapotranspiration using satellite data have been developed over the last 20 years. Only a minimum of ground data, sunshine duration and wind speed, are necessary as input for the SEBAL remote sensing method.

The SEBAL results were validated with the (i) SWAP model, (ii) *in situ* Bowen ratio measurements, and (iii) residual water-balance analysis for an area of 2.97 million ha. The accuracy of the time-integrated annual actual evapotranspiration computations varied from 0% to 10% on the field scale to 5% at the regional scale. Spatio-temporal values for actual evapotranspiration help to evaluate water use distribution, (which is related to groundwater withdrawal for irrigation), as well as management, allocation and distribution of canal water. Over the entire Rechna Doab, variations of 600 to 1100 mm yr<sup>-1</sup> in actual evapotranspiration were found for the irrigated areas. This type of information can help improve water allocation planning.

#### *Soil Moisture Storage*

Soil moisture storage is a parameter that is often neglected in hydrological studies because it is difficult to quantify. Satellite remote sensing data can now be applied to compute near-surface (root zone) soil moisture content. In this study, a standard relationship between the relative moisture content in the root zone and the evaporative fraction was validated using *in situ* measurements of root zone soil moisture content and the evaporative fraction for two locations in Rechna Doab. The results show that the application of a standard curve to relative moisture content and evaporative fraction (Eq. 6.4) yields an overall root mean square error (RMSE) of 0.05 cm<sup>3</sup>cm<sup>-3</sup> for cotton, rice, and wheat areas in the Rechna Doab.

In this thesis, a new method was developed (see chapter 6) to compute soil moisture storage values for the entire unsaturated zone from both root zone soil moisture content and depth to phreatic surface information, the latter collected twice a year. Transient soil moisture profiles from the validated SWAP model for the shallow and deep phreatic surface conditions have been used to develop and verify the results of a new and simple parameterisation of soil water distribution (Figure 6.4). The absolute root mean square error of daily estimates of unsaturated zone storage was found to be 7 cm (for an average soil moisture storage of 110 cm, this is a difference of 6%). No systematic deviations between shallow and deep phreatic surface conditions were noticed.

This method for computing monthly storage changes in the unsaturated zone has been applied to the entire Rechna Doab. Piezometric levels were spatially interpolated using the kriging geo-statistical procedure to obtain digital maps of phreatic surface depth. It was concluded that the *spatial variation* of total unsaturated zone soil moisture storage largely depends on the depth of the phreatic surface, whereas the *temporal variation* depends on monthly variations in root zone soil moisture storage (being a function of the irrigation regime applied). The analysis showed (Table 6.3) that soil moisture storage changes are in the range of  $\pm 10 \text{ cm month}^{-1}$ , a large value for a monthly analysis.

### *Canal Water Supplies*

Accurate information on the distribution of canal deliveries within an irrigation system is essential to understand where the water is following to. Numerical techniques to estimate canal water distribution require large amounts of data with respect to hydraulic parameters and operation of the hydraulic structures; and these data are not available for large irrigation systems. In this study, six quantitative geomatic models, with varying complexity and physical representation, have been formulated (see Chapter 7). The models use high-resolution Landsat-7 images and a canal network stored in a GIS. The distribution models require only the flow rates at the head of the distribution system. Results were compared with discharge measurements for three tertiary watercourses within two selected secondary distributary-canal (Gajiana and Ghour Dour) in Rechna Doab. The total area that these distributaries feed are 19111 ha and 8756 ha respectively. The distance between the head of the sample distributaries and the sample watercourses varied from 9 to 23 km. The model that computed canal water distribution using the shape of the irrigated area was the most accurate at the watercourse scale, with an overall deviation of 28%. This level of deviation is also seen in poorly calibrated discharge measurement devices; hence, the results are not necessarily poor. In conclusion, remote sensing and geo-information techniques can be used to compute disaggregated canal water diversions in large irrigation systems, using a minimum input of field data. However, testing with more extensive datasets is deemed necessary.

### *Net groundwater use*

Chapter 8 integrates the approaches and results presented in Chapters 5 through 7 in order to compute net groundwater use. This requires maps showing the distribution of the various water balance components (i) actual evapotranspiration, (ii) net precipitation, (iii) canal water for irrigation, and (iv) unsaturated zone soil moisture storage changes – for the entire Rechna Doab. Net precipitation maps were calculated from linear interpolation of gauge readings across Rechna Doab. Canal water distribution was estimated using Model 4 (Eq. 7.14) of Chapter 7, i.e. relating the Normalized Difference Vegetation Index (NDVI) to canal water availability. Finally, for each pixel, net groundwater use for the entire Rechna Doab was calculated as a water balance residual (Eq. 3.23). The field data input for this method consists of routine climatic data, depth of phreatic surface, canal discharges at major offtakes,

and rough information on the soil texture to estimate soil hydraulic properties. The remote sensing input consists of satellite imagery with thermal, visible, and near infrared bands. *The main advantage of this method over conventional techniques is that net groundwater use can be solved from relatively easily available ground data* (Eq. 3.23).

For the period between October 1993 to October 1994,  $82 \text{ mm yr}^{-1}$  of net groundwater use was found in Rechna Doab (see Figure 8.9). The results of the geo-information techniques were compared with other conventional methods, i.e. utilization factor (Eq. 8.2) and specific yield method (Eq. 8.1).

The utilization factor method significantly overestimates (several hundred's percent) groundwater use. This indicates that groundwater withdrawal by tubewells cannot be referred to as net groundwater use. Accounting for net recharge is essential when using these results for groundwater planning.

The specific yield method indicates an average net groundwater use of  $28 \text{ mm yr}^{-1}$ , which is equivalent to an overall fall of phreatic surface of  $215 \text{ mm yr}^{-1}$  if the specific yield,  $S_y = 0.13$ . This method underestimate net groundwater use by 65%. This underestimation is from ignoring groundwater lateral flows. The results from the geo-information techniques and the specific yield method can also be used in conjunction to quantify the lateral flows of groundwater. This concept was applied and found to be in good agreement with the isolines of piezometric heads. During October 1993 to October 1994, an average groundwater inflow of  $53 \text{ mm yr}^{-1}$  was computed for Rechna Doab.

In conclusion, *geo-information techniques for unsaturated zone water balance analysis provide a standardized and comprehensive opportunity of computing current (and past) levels of net groundwater use over large irrigated basins, without dependence on large amounts of field data.* This method is suitable for the re-analysis of historic groundwater use for agriculture in other groundwater-irrigated river basins.



## **SAMENVATTING EN CONCLUSIES**

### *Probleembeschrijving*

De voedsel producerende gebieden van de wereld zijn in toenemende mate afhankelijk van irrigatie m.b.v. grondwater. Het bereiken van een duurzaam grondwatergebruik heeft zich tot een belangrijk onderdeel van de wereld voedselvoorziening verheven. Een ongebroke planning en onbekwaam waterbeheer heeft tot stijgingen en dalingen van het freatisch vlak in semi-aride gebieden zoals Pakistan geleid. Een tekort aan nauwkeurige informatie over het netto grondwatergebruik, dat is het verschil tussen grondwateronttrekking door pompen en netto aanvulling (Vergl. 3.19), is het grote struikelblok voor een effectief beheer en bescherming van waardevolle hulpbronnen zoals water. Netto grondwatergebruik is van nature dynamiek en moeilijk te kwantificeren voor de geïrrigeerde landbouw. Conventionele methodes die worden gebruikt voor het schatten van netto grondwatergebruik in grote gebieden zijn gebaseerd op statistische methoden zoals een utilisatiefactor voor pompen (Vergl. 8.2) en de waterbalans methode van de verzadigde zone (Vergl. 3.20).

De methode van de utilisatiefactor voor pompen (Sectie 8.2) schat de grondwateronttrekking voor irrigatie d.m.v. een inventarisatie van de pompen en de tijdsduur dat de pompen werkzaam zijn, (berekend a.h.v. brandstof/elektriciteitsgebruik of door veld inventarisaties). Deze benadering geeft een totaal overzicht van water dat op grote schaal wordt onttrokken voor irrigatie, maar beschrijft niet het netto grondwatergebruik omdat netto grondwateraanvulling (Vergl. 3.18), dit is het verschil tussen grondwateraanvulling en capillaire opstijging, buiten beschouwing wordt gelaten.

Stijgingen en dalingen van het freatisch oppervlak kunnen worden gekoppeld aan netto grondwatergebruik via de waterbalans van de verzadigde zone. De belangrijkste problemen van deze methode zijn het ontbreken van verbanden tussen (i) laterale grondwaterstroming, (ii) verticale uitwisseling met de onverzadigde zone en (iii) veranderingen in de opslag van bodemvocht. Grondwater simulatiemodellen zijn complex en kunnen (i) oplossen, maar zijn minder geschikt voor het oplossen van (ii).

Dit proefschrift beschrijft de ontwikkeling van een methodologie (Hoofdstuk 3) dat is gebaseerd op het gecombineerd gebruik van remote sensing informatie en GIS technieken voor het schatten van netto grondwatergebruik, zonder daarbij complexe grondwater modellen in te zetten.

### *Studiegebied*

Het onderzoek is uitgevoerd in de Rechna Doab, dat in het hart van het stroomgebied van de Indus ligt (Hoofdstuk 2). Rechna Doab is het sedimentatiegebied tussen de Chenab en Ravi rivieren (Figuur 2.1). Het bruto gebied van deze "doab" is 2.97

miljoen ha en het heeft een maximum lengte van 403 km een maximum breedte van 113 km, inclusief 2.3 miljoen ha bebouwd land. Het klimaat is semi-aride met een jaarlijkse potentiële verdamping (1400 mm/jr) dat de jaarlijkse neerslag ver overtreft (400 mm/jr). Doordat de neerslag gering en ongeregeld is, wordt landbouw alleen maar succesvol bedreven d.m.v. irrigatie. Het kanalen systeem in de Rechna Doab is in 1892 geïntroduceerd door de constructie van het Lower Chenab Canal en is een van de oudste en meest intensief ontwikkelde irrigatiegebieden van de Punjab in Pakistan. Zowel irrigatiewater alsmede grondwater worden nu gezamenlijk, ofschoon in verschillende proporties, over de gehele Rechna Doab gebruikt. Het studiegebied ligt in de rijst-tarwe en suikerriet agro-ecologische zones van de Punjab provincie. Rijst, katoen en veevoer zijn dominant tijdens het zomerseizoen (*kharif*). Tarwe en veevoer zijn de belangrijkste wintergewassen (*rabi*). In sommige gebieden wordt ook suikerriet verbouwd.

### Analyse op veldschaal niveau

Een analyse van de stroming en dynamiek van bodemvocht op veldschaal in het Rechna Doab gebied wordt besproken in Hoofdstuk 4. Twee velden die representatief zijn voor de rijst-tarwe en katoen-tarwe rotatiesystemen zijn geselecteerd voor uitvoerige veldmetingen en zij liggend in gebieden met een ondiep en een diep freatisch vlak. De metingen hebben over de periode juni 2000 t/m mei 2001 plaats gevonden. Het fysisch gebaseerde en numerieke SWAP model (Soil-Water-Atmosphere-Plant) is toegepast om het bodemvochtgehalte en de verticale bodemvocht fluxen in de onverzadigde zone van de twee velden uit te rekenen. SWAP is gekalibreerd en geverifieerd tegen *in situ* metingen van bodemvocht (m.b.v. een *theta probe* die in het frequentie domein opereert) en verdamping (m.b.v. de Bowen-verhouding oppervlakte energie balans techniek). Dit is de eerste keer dat het onverzadigde zone SWAP model is geverifieerd a.h.v. de Bowen- verhouding techniek in Pakistan. De Root Mean Square Error (RMSE) tussen het gemeten en berekende bodemvochtgehalte bleek  $0.02 \text{ cm}^3 \text{ cm}^{-3}$  te zijn voor Faisalabad en  $0.03 \text{ cm}^3 \text{ cm}^{-3}$  voor Pindi Bhattian. De RMSE waarden voor de werkelijke verdamping bleken respectievelijk  $1.07$  en  $0.9 \text{ mm d}^{-1}$  te zijn, hetgeen gelijk is aan een verschil van ongeveer 16% bij een verdamping van  $6 \text{ mm d}^{-1}$ . Het verschil tussen de gemeten en berekende geaccumuleerde verdamping op jaarbasis, was aanzienlijk lager (1.5 tot 3 %).

Het gekalibreerde SWAP model helpt inzicht te verschaffen in de patronen van capillaire opstijging en grondwateraanvulling, alsmede de dagelijkse veranderingen van het bodemvochtprofiel en de bodemvochtvoorraad. De simulatie resultaten onder Pakistaanse condities geven weer dat grondwateraanvulling niet altijd kan worden geschat a.h.v. de waterbalans van de wortelzone; geavanceerde simulatietechnieken zijn nodig om de interactie tussen de verzadigde- en onverzadigde zone te berekenen. De resultaten geven aan dat een aanzienlijke hoeveelheid door pompen onttrokken grondwater weer naar het grondwatersysteem terugstroomt. Dit verschijnsel is duidelijk aanwezig voor condities met een ondiep freatische vlak (2 m diep) en rijst; 50% van de grondwateronttrekkingen stroomt terug naar het freatische

grondwatersysteem. De schatting van de jaarlijkse grondwateraanvulling in het rijst-tarwe systeem is 38.9 cm voor het jaar 2000 – 2001; een reductie van 62% is noodzakelijk om grondwatergebruik op veldniveau duurzaam te maken. Het model rekent voor het katoen-tarwe gebied een jaarlijkse grondwateraanvulling van 23.3 cm uit; duurzaam gebruik van grondwater op veldschaal kan worden bereikt bij een reductie van 36% in de onttrekkingen van grondwater.

### **Analyse op stroomgebied niveau**

Voor de analyse van grondwaterbeheer op stroomgebied niveau, is een *regionalisering methode* ontwikkeld dat extrapolatie van resultaten op veldschaal niveau naar de regionale schaal mogelijk maakt. Deze aanpak bestudeert de mogelijkheden van een op remote sensing gebaseerde regionalisering methode dat de meeste van de waterbalans componenten in de onverzadigde zone schat, o.a. werkelijke verdamping, bodemvochtvoorraad en aanvoer van irrigatiewater.

#### *Werkelijke verdamping*

Werkelijke verdamping is een van de grootste componenten van de waterbalans van geïrrigeerde gebieden onder semi-aride klimaat omstandigheden. Gedurende de afgelopen 20 jaar zijn methodes voor het berekenen van de werkelijke verdamping met behulp van satelliet gegevens ontwikkeld. Hoofdstuk 5 beschrijft de *Surface Energy Balance Algorithm for Land* (SEBAL) methode voor het berekenen van de werkelijke verdamping over uitgestrekte gebieden m.b.v. publiekelijk toegankelijke satelliet gegevens van de National Oceanic and Atmospheric Administration – Advanced Very High Resolution Radiometer (NOAA-AVHRR). De minimum grondgegevens voor SEBAL zijn zonneshijnduur en windsnelheid.

De SEBAL resultaten zijn gevalideerd met (i) het SWAP model, (ii) *in situ* Bowen-verhouding metingen en (iii) een waterbalans residu methode voor een gebied van 2.97 miljoen ha. De nauwkeurigheid van de berekeningen van in de tijd geïntegreerde werkelijke verdamping varieerde tussen 0 tot 10% op veld niveau en 5 % op regionaal niveau. De ruimtelijke- en temporele verdeling van werkelijke verdamping ondersteunt het evalueren van de verdeling in het watergebruik (hetgeen is gerelateerd aan grondwateronttrekkingen voor irrigatie), maar ook voor het beheer, toekennen en verdelen van irrigatiewater over de kanalen. Er is een variatie in werkelijke verdamping van 600 tot 1100 mm yr<sup>-1</sup> over het gehele gebied van de Rechna Doab geconstateerd. Dergelijke informatie kan het plannen van watertoekenning verbeteren.

#### *Bodemvochtvoorraad*

Omdat het moeilijk te kwantificeren is, wordt de bodemvochtvoorraad in hydrologische studies vaak verwaarloosd. Satelliet remote sensing gegevens kunnen nu worden toegepast om het vochtgehalte nabij het landoppervlak (de wortelzone) te berekenen. Een standaard relatie tussen relatief bodemvocht in de wortel zone en de verdampingsfractie is in deze studie gevalideerd m.b.v. *in situ* metingen van

bodemvocht in de wortelzone en verdampingsfractie voor twee locaties in de Rechna Doab. De resultaten geven aan dat toepassing van een standaard curve van relatief bodemvocht en verdampingsfractie (Vergl. 6.4) tot een algemene RMSE van  $0.05 \text{ cm}^3 \text{ cm}^{-3}$  voor katoen, rijst en tarwegebieden in de Rechna Doab leidt.

In dit proefschrift is een nieuwe methode ontwikkeld om de bodemvochtvoorraad in de gehele onverzadigde zone uit het bodemvocht in wortelzone en de diepte van het freatische vlak te berekenen. Ruimtelijke informatie over de diepte van het freatische vlak dient tweemaal per jaar te worden verzameld. De ruimte- en tijdsafhankelijke bodemvocht profielen afkomstig uit het gevalideerde SWAP model voor condities met een ondiep- en diep freatisch vlak, zijn gebruikt om een nieuwe en simpele parameterisatie van bodemvochtverdeling (Figuur 6.4) te ontwikkelen en te verifiëren. De absolute RMSE van de dagelijkse schatting van de bodemvochtvoorraad in de onverzadigde zone bleekt 7 cm te zijn (bij een gemiddelde bodemvochtvoorraad van 110 cm is dit verschil gelijk aan 6%). Er kon geen systematisch verschil in afwijkingen bij een ondiep- en diep freatisch vlak worden geconstateerd.

De methode om de maandelijkse veranderingen in de bodemvochtvoorraad van de onverzadigde zone te berekenen is toegepast voor de gehele Rechna Doab. Puntwaarnemingen van peilbuizen zijn ruimtelijk geïnterpoleerd m.b.v. een geostatistische *kriging* procedure waarmee digitale kaarten van het freatische vlak kunnen worden gemaakt. De conclusie is dat de *ruimtelijke variatie* van de bodemvochtvoorraad van de gehele onverzadigde zone voornamelijk afhangt van de diepte van het freatische vlak, terwijl de *temporele variatie* van de maandelijkse variatie van het bodemvocht in de wortelzone afhangt. Het bodemvocht in de wortelzone is een functie van het toegepaste irrigatie regime. De analyse toont aan (Table 6.3) dat aanzienlijke veranderingen in de bodemvochtvoorraad in de range van  $\pm 10$  cm per maand plaats vinden.

#### *Aanvoer van irrigatiewater*

Voor het begrijpen waar het irrigatiewater naar toe stroomt, is nauwkeurige informatie over de werkelijke verdeling van irrigatiewater binnen een zekere eenheid essentieel. Numerieke technieken voor het schatten van de verdeling van irrigatiewater hebben veel hydraulische gegevens nodig. Deze gegevens zijn niet beschikbaar voor grootschalige irrigatiesystemen. Zes kwantitatieve geomatische modellen met variërende complexiteit en fysische representatie, zijn in deze studie geformuleerd (zie Hoofdstuk 7). Deze modellen maken gebruik van hoge resolutie Landsat-7 beelden en in GIS bestanden opgeslagen posities van de irrigatiekanalen. Deze water distributie modellen vereisen slechts debietmetingen verricht aan het begin van het waterdistributiesysteem (bovenstrooms gedeelte). De modelresultaten zijn vergeleken met debietmetingen van 3 tertiaire waterlopen die in twee verschillende secundaire waterloopssystemen in Rechna Doab (Gajiana en Ghour Dour) gelegen zijn. Deze secundaire waterloopssystemen bestrijken een gebied van respectievelijk 19111 en 8756 ha. De afstand tussen het begin van de geteste secundaire en de tertiaire waterloopssystemen varieert tussen 9 en 23 km. Het model dat de irrigatiewater distributie voor een tertiair waterloopstelsel op basis van de vorm van de geïrrigeerde gebieden uitrekent was met een algehele afwijking van 28% het meeste



nauwkeurig. Een dergelijke afwijking geldt ook voor matig gekalibreerde debietmeetinstrumenten. Kortom, de modelresultaten hoeven niet op voorhand onbekwaam te zijn. De conclusie is dan ook dat remote sensing en geo-informatie technieken kunnen worden gebruikt voor het berekenen van de verdeling van irrigatiewater in grote irrigatiesystemen met gebruik van een minimale hoeveelheid ter plaatse verzamelde invoer gegevens. Echter, het is nodig aanvullende testen met meer uitgebreide datasets uit te voeren.

### *Netto grondwatergebruik*

Hoofdstuk 8 integreert de benadering en de resultaten van de methode voor het berekenen van netto grondwatergebruik die in Hoofdstukken 5 t/m 7 is uiteengezet. Hiervoor is het noodzakelijk kaarten voor het gehele gebied van de Rechna Doab te hebben met daarop de verdeling van de diverse waterbalans componenten zoals (i) werkelijke verdamping, (ii) netto neerslag, (iii) irrigatiewater en (iv) de veranderingen van bodemvocht in de onverzadigde zone. Netto neerslag kaarten zijn berekend uit een lineaire interpolatie van regenmeters die verspreid over het gebied van de Rechna Doab voorkomen. De verdeling van irrigatiewater is geschat m.b.v. geomatisch model 4 (vergl. 7.14) uit Hoofdstuk 7 dat is gebaseerd op het relateren van de *Normalized Difference Vegetation Index* (NDVI) aan de beschikbaarheid van irrigatiewater. Uiteindelijk is het netto grondwatergebruik voor elke pixel in de gehele Rechna Doab uitgerekend als de residu van de waterbalans (Vergl. 3.23). De veldgegevens voor deze methode bestaan uit routinematig verzamelde metingen van klimaat, diepte van het freatische vlak, het debiet door de grotere bovenstroomse kunstwerken en summier informatie over de bodemtextuur om daarmee de bodemhydraulische eigenschappen te schatten. De invoergegevens van de remote sensing methode bestaat uit satellietbeelden met thermische, zichtbare en nabij-infrarode banden. Het belangrijkste voordeel van deze methode boven conventionele methoden is dat netto grondwatergebruik kan worden opgelost d.m.v. relatief gemakkelijk beschikbare grondinformatie (Vergl. 3.23).

Er is een netto grondwatergebruik van  $82 \text{ mm yr}^{-1}$  geconstateerd in de Rechna Doab voor de periode tussen oktober 1993 tot oktober 1994 (zie Figuur 8.9). De resultaten van de nieuwe geo-informatie techniek zijn vergeleken met conventionele methodes zoals de utilisatiefactor (Verg. 8.2) en de grondwaterstand fluctuatie methode (Vergl. 8.1).

De methode van de utilisatiefactor overschat het grondwatergebruik aanzienlijk (verschillende honderden procenten). Dit geeft aan dat grondwateronttrekkingen bij pompen niet als zijnde de netto grondwatergebruik kunnen worden aangemerkt. Het omgaan met netto grondwateraanvulling is essentieel voor het toepassen van de resultaten voor grondwaterplanning.

De grondwaterstand fluctuatie methode geeft een netto grondwatergebruik van  $28 \text{ mm yr}^{-1}$  aan, hetgeen equivalent is aan de algehele daling van het freatische vlak van  $215 \text{ mm yr}^{-1}$ , indien voor de opbrengst coëfficiënt een waarde van  $S_y=0.13$  wordt genomen. De methode onderschat het netto grondwatergebruik met 65%. Deze onderschatting wordt veroorzaakt door het negeren van laterale grondwaterstroming.

De resultaten van de geo-informatie methode en de grondwaterstand fluctuatie methode kunnen tezamen worden gebruikt voor het kwantificeren van de laterale grondwaterstroming. Dit concept is toegepast en er blijkt een goed verband met de contourlijnen van stijghoogte te bestaan. Tussen oktober 1993 en oktober 1994 wordt er voor de gehele Rechna Doab een gemiddelde grondwater instroming van 53 mm yr<sup>-1</sup> berekend.

*De algehele conclusie is dat geo-informatie technieken voor de analyse van de waterbalans van de onverzadigde zone, een standaard en uitgebreide mogelijkheid bieden om huidige en historische niveaus van netto grondwatergebruik van grote geïrrigeerde stroomgebieden, zonder afhankelijkheid van grote hoeveelheden veldmetingen, uit te rekenen. Deze methode is bruikbaar voor een her-analyse van historisch grondwatergebruik voor de landbouw in andere met grondwater geïrrigeerde stroomgebieden.*

## REFERENCES

- Ahmad, M.D. and W.G.M Bastiaanssen, 2002. Remote sensing and GIS based analysis of conjunctive water use in Rechna Doab, Pakistan. Proceedings of the International Workshop on Conjunctive water management for sustainable irrigated agriculture in south Asia April 16-17, 2002 International Water Management Institute (IWMI), Lahore, Pakistan. pp. 119-131.
- Ahmad, M.D., E.G. van Waijjen, M. Kuper, and S. Visser, 1998. *Comparison of different tools to assess the water distribution in secondary canals with ungated outlets*. Research Report 52. International Irrigation Management Institute (IIMI). Pakistan. 68pp.
- Ahmad, M.D., W.G.M. Bastiaanssen and R.A. Feddes, 2002. Sustainable use of groundwater for irrigation: a numerical analysis of the sub-soil water fluxes, *Irrigation and Drainage* 51(3): 227-241.
- Ahmad, S, M.M. Ahmad, M.Yasin, G. Akbar and Z. Khan, 2000. Assessment of shallow groundwater quality: case study of MONA SCARP. *Proceedings of regional groundwater management seminar*, Pakistan Water Partnership (PWP), Islamabad, Pakistan. October 2000.
- Allen, R.G., L.S. Pereira, D. Raes and M. Smith, 1998. *Crop evapotranspiration, guidelines for computing crop water requirements*, FAO Irrigation and Drainage Paper 56, Food and Agriculture Organization of the United Nations (FAO): Rome, Italy, 300 pp.
- Allison, G.B., G.W. Gee and S.W. Tyler, 1994. Vadose-zone techniques for estimating groundwater recharge in arid and semi-arid regions. *Soil Science Society of America Journal* 58: 6-14.
- Arnold, J.G., P.M. Allen and G. Bernhardt, 1993. A comprehensive surface-groundwater flow model, *Journal of Hydrology* 142: 47-69.
- Bastiaanssen, W.G.M., 1995. Regionalization of surface flux densities and moisture indicators in composite terrain, a remote sensing approach under clear skies conditions in Mediterranean climates, Ph.D. thesis, Wageningen Agricultural University, Department of Water Resources, The Netherlands, 271 pp.
- Bastiaanssen, W.G.M., 2000. SEBAL-based sensible and latent heat fluxes in the irrigated Gediz Basin, Turkey, *Journal of Hydrology*, 229:87-100.
- Bastiaanssen, W.G.M., M. Menenti, R.A. Feddes and A.A.M. Holtslag, 1998. A remote sensing Surface Energy Balance Algorithm for Land (SEBAL), part 1: formulation, *Journal of Hydrology*, 212-213: 198-212
- Bastiaanssen, W.G.M., M.D. Ahmad and Z. Tahir, 2002a. Upscaling water productivity in irrigated agriculture using remote sensing and GIS technologies. Forthcoming proceeding of the workshop on *Water Productivity in Agriculture*. International Water Management Institute (IWMI), Colombo. Nov. 15-16, 2001. ([www.iwmi.org](http://www.iwmi.org))

- Bastiaanssen, W.G.M., M.D. Ahmad and Y. Chemin, 2002b. Satellite surveillance of evaporative depletion across the Indus Basin. *Water Resources Research*, the American Geophysical Union (in press).
- Bastiaanssen, W.G.M., R. Sakthivadivel and A. van Dellen, 1999. Spatially delineating actual and relative evapotranspiration from remote sensing to assist spatial modeling of non-point source pollutants, in (Eds.) D.L. Corwin, K. Loague and T.R. Ellsworth, *Assessment of non-point source pollution in the vadose zone*, Geophysical Monograph 108, American Geophysical Union: 179-196.
- Bastiaanssen, W.G.M., R. Singh, S. Kumar, J.K. Schakel and R.K. Jhorar, 1996. *Analysis and recommendations for integrated on-farm water management in Haryana, India: a model approach*. Report 118. DLO Winand Staring Centre for Integrated Land, Soil and Water Research, Wageningen, The Netherlands; 152pp.
- Beekma, J., T.J. Kelleners, Th.M. Boers, M.R. Chaudhry and J.C. Van Dam, 1997. Recharge from irrigated lands. In: I. Simmers (Ed.), *Recharge of Phreatic Aquifers in (Semi-) Arid Areas*. A.A. Balkema, Rotterdam, The Netherlands: 115-127.
- Beekma, J., W. Beekman, Z.I. Raza, J. Akhtar and Th.M. Boers, 1993. *Field determination of soil hydraulic properties of a moderately coarse textured soil in Punjab, Pakistan*. A collaborative study of IWASRI/NRAP and NIAB. Publication No. 117, International Waterlogging and Salinity Research Institute (IWASRI), Lahore, Pakistan.: 33pp
- Belmans, C., J.G. Wesseling and R.A. Feddes, 1983. Simulation of the water balance of a cropped soil. SWATRE. *Journal of Hydrology* 63: 271-286.
- Berkoff, J. and W. Huppert, 1987. Matching crop water requirements in large systems with a variable water supply: experiments in India, ODI-IIMI in full Irrigation Management Network Paper 87/3d, London: Overseas Development Institute.
- Bhutta M.A. and E.J. Vender Velde, 1992. Equity of water distribution along secondary canals in Punjab, Pakistan. *Irrigation and Drainage Systems* 6: 161-177.
- Bindlish, B., W.P. Kustas, A.N. French, G.R. Diak and J.R. Mecikalski, 2001. Influence of near-surface soil moisture on regional heat fluxes: Model results using microwave remote sensing data from SGP97. *IEEE transactions on geoscience and remote sensing*. 39 (8): 1719-1728.
- Bink, N.J. 1996. *The structure of the atmospheric surface layer subject to local advection*, Ph.D. Dissertation, Department of Meteorology, Wageningen University.
- Bolle, H.J. *et al.*, 1993 EFEDA: European field experiments in desertification-threatened area, *Annales Geophysica* 11: 173-189
- Boonstra, J. and M.N. Bhutta, 1995. Groundwater recharge in irrigated agriculture: the theory and practice of inverse modelling. *Journal of Hydrology* 174:357-374.

- Bos, M.G., 1976. *Discharge measurement structures*, ILRI publication no. 20, Alterra, Wageningen, The Netherlands: 464 pp.
- Bos, M.G., S.A. Dayum, W. Bastiaanssen and A. Vidal, 2001. *Remote sensing for water management: The drainage component*. Report on expert consultation meeting organized by representatives of the ICID, IPTRID, ILRI, WaterWatch and the World Bank, Ede-Wageningen May 15-16, 2001. 54pp.
- Braun, H.M.H. and R. Kruijne 1994. Soil conditions. In. H.P. Ritzema (ed.). *Drainage principles and applications*. ILRI Publication 16, Wageningen: 77-110.
- Brooks, R.H., and A.T. Corey, 1964. *Hydraulic properties of porous media*. Hydrology paper 3, Colorado State University, 27 pp.
- Bruin, de, H.A.R. and J.N.M. Stricker, 2000. Evaporation of grass under non-restricted soil moisture conditions, *Hydrological Processes*, 45(3): 391-406
- Brutsaert, W. 1982. Evaporation into the atmosphere, theory, history and applications, Reidel, Dordrecht, The Netherlands 299
- Brutsaert, W. and M. Sugita, 1992. Application of self-preservation in the diurnal evolution of the surface energy balance budget to determine daily evaporation, *Journal of Geophysical Research*, 97(D17): 18377-18382.
- CAN/World Bank (Comisión Nacional del Agua)/World Bank, 1999. *Políticas opcionales para el manejo de la sobreexplotación de acuíferos en México. Estudio sectorial*. Mexico: CAN/World Bank.
- Carlson, T.M., O. Taconet, A. Vidal, R.R. Gillies, A. Olios and K. Humes, 1995. An overview of the workshop on thermal remote sensing held at La Londe les Maures, France, September 20-24 1993, *Agricultural and Forest Meteorology*. 77:141-151
- Carsel, R.F., and R.S. Parrish, 1988. Developing joint probability distributions of soil water characteristics. *Water Resources Research* 24: 755-769.
- Centre for Science and Environment, 1991. *Floods, flood plains and environmental myths*. New Delhi: Centre for Science and Environment, State of India's Environment: A citizens' report no 3.
- Chebouni, A., D.L. Seen, E.G. Njoku, J.P. Lhomme, B. Monteney and Y.H. Kerr, 1997. Estimation of sensible heat flux over sparsely vegetated surfaces, *Journal of Hydrology*, 188-189, 855-868.
- Choudhury, B.J., N.U. Ahmed, S.B. Idos, R.J. Reginato and C.S.T. Daughtry, 1994. Relations between evaporation coefficients and vegetation indices studied by model simulations. *Remote Sensing Environment* 50: 1-17.
- Clarke, R., A.R. Lawrence, and S.S.D. Foster, 1996. *Groundwater—A threatened resources*. UNEP environment Library Series 15.
- Clemmens, A.J. and A.R. Dedrick, 1984. Irrigation water delivery performance. *Irrigation and Drainage Engineering*. 110(1): 1-13.

- Cook, P.G., G.R. Walker and H.D. Barrs, 1990. Mapping the spatial distribution of groundwater recharge. Proceedings of the Murray-Darling 1990 Workshop on Groundwater Research and Management, MILDURA, 13-15 November 1990.
- Cook, P.G., H.D. Barrs and G.R. Walker, 1992. Inferring spatial variation in deep drainage and groundwater recharge from Landsat thematic mapper imagery. Divisional Report 92/5, Division of Water Resources, CSIRO, Australia. 28pp.
- Crago, R.D., 1996. Comparison of the evaporative fraction and the Priestley-Taylor for parameterizing daytime evaporation, *Water Resources Research*, 32(5), 1403-1409.
- Davies, J.A. and C.D. Allen, 1973. Equilibrium, potential and actual evapotranspiration from cropped surfaces in southern Ontario. *Journal of Applied Meteorology* 12: 649-657.
- De Bruin, H.A.R., 1983. A model for the Priestley-Taylor parameter alpha, *Journal of Climate and Applied Meteorology* 22: 572-578.
- De Laat, P.J.M., 1976. A pseudo steady-state solution of water movement in the unsaturated zone of the soil, *Journal of Hydrology*. 30: 19-27.
- De Ridder, N.A. and J. Boonstra, 1994. Analysis of water balances. In H.P. Ritzema (ed.). *Drainage principles and applications*. ILRI Publication 16, Wageningen: pp. 601-633.
- De Rooy, W.C. and A.A.M. Holtslag, 1999. Estimation of surface radiation and energy flux densities from single-level weather data, *Journal of Applied Meteorology*, 38: 526-540.
- De Vries, J.J., 1984. Holocene depletion and active recharge of the Kalahari groundwater—a review and an indicative model. *Journal of Hydrology* 70: 221-232.
- Diak, G.R., W.L. Bland and J. Mecikalski, 1996. A note on first estimates of surface insolation from GOES-8 visible satellite data, *Agricultural and Forest Meteorology* 82: 219-226.
- Döll, P., and S. Siebert, 1999. A digital global map of irrigated area. Center for Environmental Research, University of Kassel, Germany.
- Doorenbos, J. and A.H. Kassam, 1979. *Yield response to water*, Irrigation and Drainage Paper 33, Food and Agricultural Organization of the United Nations, Rome, Italy, 156 pp.
- Downing, R.A. (compiler), 1998. *Groundwater our hidden asset*. Earthwise Series, Geological Survey, Keyworth, Nottingham, UK, 59p.
- Droogers, P., M. Torabi, M. Akbari and E. Pazira, 2001. Field-scale modeling to explore salinity problems in irrigated agriculture. *Irrigation and Drainage* 50: 77-90.
- Dugas, W.A., L.J. Fritschen, L.W. Gay, A.A. Held, A.D. Matthias, D.C. Reicosky, P. Steduto and J.L. Steiner, 1991. Bowen ratio, eddy correlation and portable

- chamber measurements of sensible and latent heat flux over irrigated spring wheat. *Agricultural and Forest Meteorology* 56: 1-20.
- Farah, H.O., 2000. *Estimation of regional evaporation under all sky conditions with satellite and routine weather data*, Ph.D. thesis, Wageningen University, The Netherlands, 170 pp.
- Feddes, R.A., P.J. Kowalik and H. Zaradny, 1978. *Simulation of field water use and crop yield*. Simulation Monographs. Pudc: Wageningen. 189pp.
- Feddes, R.A., P.J.T. van Bakel, P. Kabat, J.H.M. Bronswijk and J. Halbertsma, 1988. Modelling soil water dynamics in the unsaturated zone – state of the art. *Journal of Hydrology*. 100: 69-111.
- Foster, S., J. Chilton, M. Moench, F. Cardy and M. Schiffler, 2000. Groundwater in rural developmeny. Facing the challenges of supply and resource sustainability. World Bank technical report no. 463. World Bank Washington, D.C. USA. 98pp.
- Franks, S.W. and K.J. Beven, 1999. Conditioning a multiple-patch SVAT model using uncertain time-space estimates of latent heat flux as inferred from remotely sensed data, *Water Resources Research*, 35(9): 2751-2761.
- Gee, G.W. and D. Hillel, 1988. Groundwater recharge in arid regions: Review and critique of estimation methods. *Hydrological Processes* 2: 255-266.
- Gieske, A., 1992. *Dynamics of groundwater recharge. A case study in semi-arid Eastern Botswana*, Ph.D. Thesis, Free University Amsterdam. 289pp.
- Glasbey C.A. and G.W. Horgan, 1995. *Image analysis for the biological science*. John Wiley & Sons. England. 218 p.
- Gleick, P.H., 1998. The world's water 1998-1999: The biennial report on fresh water resources. Washington, DC: Island Press.
- GOP 1994, Agriculture Machinery Census, Agriculture Census Organization, Statistics Division, Government of Pakistan (GOP), Gurumangat Road, Gulberg III, Lahore, 1994.
- GOP 1998-99. Agricultural statistics of Pakistan. Ministry of Food, Agriculture and Livestock, Economic Division, Government of Pakistan (GOP), Islamabad.
- Gupta, H.V., S. Soorooshian and P.O. Yapo, 1998. Towards improved calibration of hydrological models: multiple and noncommensurable measures of information, *Water Resources Research*, 34:751-763
- Habib, Z., Z. Tahir and A.R. Khan, 1999. Across the basin analysis of water and land utilization using spatio-temporal information techniques emphasize the need for integrated resource management. In (eds.) A. Musy, M. Fritsch and L.S. Pereira, ICID 2<sup>nd</sup> Inter-Regional Conference on Environment-Water, 1-4 September 1999, Lausanne, Switzerland, 10 pp.
- Haq, A.U., 2000. Self regulation, total control or a gradual and holistic approach? Institutional framework for groundwater management in Punjab, Pakistan.

- Proceedings of regional groundwater management seminar. Pakistan water partnership (PWP), Islamabad, October 2000. pp. 221-229.*
- Healy, R.W. and P.G. Cook, 2002. Using groundwater levels to estimate recharge. *Hydrology Journal* 10:91-109.
- Hendrickx, J.H.M. and G.R. Walker, 1997. Recharge from precipitation. In: I. Simmers (Ed.) *Recharge of Phreatic Aquifers in (Semi-) Arid Areas*. A.A. Balkema, Rotterdam, The Netherlands: 19-111.
- Herschy, R.W., 1995. *Streamflow Measurement*. Second Edition. E & FN Spon. London, UK. 524pp.
- Hiler, E.A. and R.N. Clark, 1971. Stress day index to characterize effects of water stress on crop yields, *Transactions of the American Society of Agricultural Engineering (ASEA)* 14:757-761.
- Hussan, G.Z. and M.N. Bhutta, 1996. A water balance model to estimate groundwater recharge in Rechna Doab, Pakistan. *Irrigation and Drainage Systems* 10: 297-317.
- Jackson, R.D., R.J. Reginato and S.B. Idso, 1977. Wheat canopy temperatures: a practical tool for evaluating water requirements, *Water Resources Research*, 13:651-656.
- Jackson, R.D., S.B. Idso, R.J. Reginato and P.J. Pinter, 1981. Canopy temperature as a crop water stress indicator, *Water Resources Research*, 17:1133-1138.
- Janakarajan, S. 2000. Competition, conflicts and crisis-An example of degraded groundwater regimes and feckless governance in south India. Proceedings of the regional groundwater seminar, Islamabad, October 2000, Pakistan Water Partnership (PWP). pp37-56.
- Jury, W.A., W.R. Gardner and W.H. Gardner, 1991. *Soil Physics*. Fifth edition. John Wiley & Sons, Inc. 328pp.
- Kabat, P., B.J. Broek, van den and R.A. Feddes, 1992. SWACROP: A water management and crop production simulation model. *ICID Bulletin* 92 41(2): 61-84.
- Kalma, J.D and D.L.B. Jupp, 1990. Estimating evaporation from pasture using infrared thermometry: evaluation of a one-layer resistance model, *Agricultural and Forest Meteorology*, 51:223-246
- Kashef, A.I., 1976. Control of salt-water intrusion by recharge wells. *Journal of the Irrigation and Drainage Division, ASCE*, Vol. No. 102, IR4, Proc. Paper 12617, 445-447.
- Kealy, P.S. and S.J. Hook, 1993. Separating temperature and emissivity in thermal infrared multispectral scanner data: implications for recovering land surface temperatures, *IEEE Transactions on Geoscience and Remote Sensing*, 31: 1155-1164



- Khan, A.H., B. Lashari, M.A. Khawaja, A.A. Memon and G.V. Skogerboe, 1998. *Water level fluctuations and discharge variability in Mirpurkhas sub-division, Jamrao canal, Nara circle, Sindh Province, Pakistan*. Research Report No. 75, International Irrigation Management Institute (IWMI), Pakistan. 31p.
- Khan, M.A., 1978. *Hydrological Data, Rechna Doab*, Volume I, Lithology, Mechanical Analysis and Water Quality Data of Testholes/Testwells. Publication Number 25, Project Planning Organization (NZ), Pakistan Water and Power Development Authority (WAPDA), Lahore.
- Kijne, J.W. and M. Kuper, 1995. Salinity and sodicity in Pakistan's Punjab: A threat to sustainability of irrigated agriculture? *International Journal of Water Resources Development* 11:73-86.
- Koorevaar, P., G. Menelik and C. Dirksen, 1983. Elements of soil physics, *Developments in Soil Science* 13, Elsevier, ISBN 0-444-42242-0: 228 pp.
- Kramer, R. and M. Zhu, 1988. Groundwater management in China: Economic and institutional issues. Durham: *Duke University's Center for Resource and Environmental Policy Research*. Duplicated.
- Kroes, J.G., J.G. Wesseling and J.C. van Dam, 2000. Integrated modelling of the soil-water-atmosphere-plant system using the model SWAP 2.0: an overview of theory and an application, *Hydrological Processes*, 14:1993-2002.
- Kuper, M., 1997. *Irrigation management strategies for improved salinity and sodicity control*. Ph.D. Thesis. Water Resources Department. Wageningen University (WU), The Netherlands. 238 pp.
- Kustas, W.P., M.S. Moran, R.D. Jackson, L.W. Gay, L.F.W. Duell, K.E. Kunkel and A.D. Matthias, 1990. Instantaneous and daily values of the surface energy balance over agricultural fields using remote sensing and a reference field in an arid environment, *Remote Sensing of Environment*, 32:125-141.
- Kustas, W.P., E.M. Perry, P.C. Doraiswamy and M.S. Moran, 1994. Using satellite remote sensing to extrapolate evapotranspiration estimates in time and space over a semiarid rangeland basin, *Remote Sensing of Environment*, 49:275-286.
- Latif, M. and S. Sarwar, 1994. Proposal for equitable water allocation for rotational irrigation in Pakistan. *Irrigation and Drainage Systems* 8: 35-48.
- Lerner, D.N., A.S. Issar and I. Simmers, 1990. *Groundwater recharge: A guide to understanding and estimation of natural recharge*, Vol. 8 International Association of Hydrogeologists. 345pp.
- Lunzhang, S., 1994. *Management of groundwater resources in China*. Rome: FAO.
- Malaterre, P.O. and J.P. Baume, 1997. SIC 3.0 A simulation model for canal automation design. Proceedings of the international workshop on *Regulation of irrigation canals: state of the art of research and applications*. Marrakesh, Morocco.

- Maupin, M.A., 1999. *Methods to determine pumped irrigation-water withdrawals from the Snake river between upper Salmon falls and Swan falls dams, Idaho, using electrical power data, 1990-95*. U.S. Geological Survey Water-Resources Investigation Report 99-4175, 20pp.
- Meinzen-Dick R.S. and M.W. Rosegrant, 2001. Overcoming water scarcity and quality constraints: Focus 9. October 2001. International Food Policy Research Institute (IFPRI), USA.
- Meinzer, O.E., 1923. The occurrence of groundwater in the United States with a discussion of principles. USGS Water Supply Pap. 489, 321 pp.
- Menenti, M, S. Azzali and G. d'Urso, 1996. Remote sensing, GIS and hydrological modelling for irrigation management. In *Sustainability of irrigated agriculture*, L.S. Pereira *et al.*, (eds). Kluwer Academic Publishers. The Netherlands. pp. 453-472.
- Menenti, M, T.N.M. Visser, J.A. Morabito and A. Drovandi, 1989. Appraisal of irrigation performance with satellite data and georeferenced information, in (eds.) Rydzewski and Ward, *Irrigation, Theory and Practice*, proc. of the international conference, Univ. of Southampton, 12-15 September 1989: 785-801
- Miller, E.E., and R.D. Miller, 1956. Physical theory for capillary flow phenomena. *Journal of Applied Physics* 27: 324-332.
- Moran, M.S., D.C. Hymer, J. Qi and Y. Kerr, 2002. Comparison of ERS-2 SAR and Landsat TM imagery for monitoring agricultural crop and soil conditions. *Remote Sensing of Environment* 79: 243-252.
- Mualem, Y., 1976. A new model for predicting the hydraulic conductivity of unsaturated porous media. *Water Resources Research* 12: 513-522.
- Mundorff, M. J., P.H. Carrigan Jr., T.D. Steel, and A.D. Randall, 1976. Hydrologic Evaluation of Salinity Control and Reclamation Projects in the Indus Plain, Pakistan-A Summary, US Geological Survey Water-Supply Paper 1608-Q.
- Murray-Rust, H., and D.J. Merrey, 1994. Irrigated agriculture beyond 2000: institutional adaptation and transformation, *IIMI Review* 8(3): 21-28.
- NESPAK-SGI (National Engineering Services Pakistan (Pvt.) Ltd.-Specialist Group, Inc.), 1991. Contribution of private tubewells in the development of water potential. Final report. Islamabad, Pakistan: Planning and Development Division, Ministry of Planning and Development.
- Nicols, W.E. and R.H. Cuenca, 1993. Evaluation of the evaporative fraction for parameterization of the surface energy balance, *Water Resources Research*, 29(11), 3681-3690.
- Owe, M. and A.A. Van De Griend, 1990. Daily surface moisture model for large area semi-arid land application with limited climatic data. *Journal of Hydrology*, 121: 119-132.
- Pelgrum, H. and W.G.M. Bastiaanssen, 1996. An intercomparison of techniques to determine the area-averaged latent heat flux from individual *in situ*

- observations: a remote sensing approach using EFEDA data, *Water Resources Research*, 32(9): 2775-2786.
- Perry, C and M. Hassan, 2000. Control of groundwater use: the limitations of pricing, and a practical alternative. In the proceedings of the regional groundwater management seminar, Pakistan Water Partnership. October 9-11, 2000, Islamabad. pp67-81.
- Postel, S., 1999. *The pillars of sand: Can the irrigation miracle last?* Washington: The Worldwatch Institute.
- Priestley, C.H.B. and R.J. Taylor, 1972. On the assessment of the surface heat flux and evaporation using large scale parameters. *Monthly Weather Review* 100: 81-92.
- Qureshi, A.S., I. Masih and M. Mainuddin, 2001. Groundwater contribution to agriculture, Progress Report 2001. International Water Management Institute (IWMI), Regional Office, Lahore, Pakistan.
- Reeve, R.C., 1957. The measurement of permeability in the laboratory in drainage of agricultural lands. J.N. Lathim, ed., *Agronomy Monograph No. 7*, American Society of Agronomy, Madison, WI, 414-441.
- Refsgaard, J.C., 1997. Parameterization, calibration and validation of distributed hydrological models, *Journal of Hydrology*, 198:69-97
- Rehman, G., H.Z. Munawwar and A. Hussain, 1997. History of irrigated agriculture: A selected appraisal, Salinity management Alternatives for the Rechna Doab, Punjab, Pakistan. Volume-II. Research Report No. R-21.2 International Irrigation Management Institute (IIMI), Lahore, Pakistan. 145pp.
- Remson, I. and S.M., Lang, 1995. A pumping-test method for the determination of specific yield. *Transactions, American Geophysical Union*. 36(2): 321-325.
- Ritzema, 1994. Subsurface flow to drains. In. H.P. Ritzema (ed.). *Drainage principles and applications*. ILRI Publication 16, Wageningen: pp. 263-304.
- Romano, N., B. Brunone and A. Santini, 1998. Numerical analysis of one-dimensional unsaturated flow in layered soils. *Advances in Water Resources* 21: 315-324.
- Sarwar, S, H.M. Nafeez and M.S. Shafique, 1997. *Fluctuations in canal water supplies: A case study*. Research Report No. 27, International Irrigation Management Institute (IIMI), Lahore, Pakistan. 72pp.
- Sarwar, A, W.G.M. Bastiaanssen, J.C. van Dam and M.Th. Boers, 2000. Evaluating drainage design parameters for the fourth drainage project, Pakistan by using SWAP model: Part I – calibration. *Irrigation and Drainage Systems* 14: 257-280.
- Sarwar, A. and W.G.M. Bastiaanssen, 2001. Long-term effects of irrigation water conservation on crop production and environment in semi-arid areas, American Society of Civil Engineering *Irrigation and Drainage Engineering*, 127(6): 331-338.

- Sarwar, A., W.G.M. Bastiaanssen, Th.M. Boers and J.C. van Dam, 2000. Evaluating drainage design parameters for the Fourth Drainage Project, Pakistan by using SWAP model: part 1: calibration, *Irrigation and Drainage Systems*, 14: 315-324.
- Schuurmans, W. and G. Pichel, 1996. Management of water delivery systems (RIBASIM/OMIS). In (ed.) B.J. van den Broek, *Dutch Experience in Irrigation Water Management Modelling*, Winand Staring Centre Report 123, Alterra, Wageningen, The Netherlands: 87-102
- Scott, C.A., W.G.M. Bastiaanssen and M.D. Ahmad, 2002. Mapping Spatio-Temporal Distributions of Soil Moisture Throughout Irrigated Watersheds using Optical and High Resolution Imagery. *ASCE Irrigation and Drainage Engineering* (accepted).
- Seguin, B. and B. Itier, 1983. Using midday surface temperature to estimate daily evaporation from satellite thermal IR data, *International Journal of Remote Sensing*, 4:371-383.
- Sellers, P.J., D.A. Randall, G.J. Collatz, J.A. Berry, C.B. Field, D.A. Dazlich, C. Zhang, G.D. Collelo and I. Bounoua, 1996. A revised land surface parameterization (SIB2) for atmospheric GCMs – part 1 – model formulation, *Journal of Climate*, 9: 676-737
- Sellers, P.J., F.G. Hall, G. Asrar, D.E. Strebbe and R.E. Murphy, 1992. An overview of the First International Satellite Land Surface Climatology Project (ISLSCP) Field Experiment (FIFE), *Journal of Geophysical Research*. 97(D17): 18345-18371.
- Shah, T. and S. Bhattacharya. 1993. Farmer organisations for lift irrigation: Irrigation companies and tubewell co-operatives of Gujarat. *ODI Irrigation Management Network Paper*, 26, June.
- Shah, T., D. Molden, R. Sakthivadivel and D. Seckler, 2000. *The global groundwater situation: Overview of opportunities and challenges*. Colombo, Sri Lanka: International Water Management Institute. 21pp. ([www.iwmi.org](http://www.iwmi.org))
- Shuttleworth, W.J., R.J. Gurney, A.Y. Hsu, and J.P. Ormsby, 1989. FIFE: the variation in energy partitioning at surface flux sites, remote sensing and large scale global processes, Proc. Baltimore symp., Red Book 186, International Association of Hydrological Sciences (IAHS), Oxfordshire, UK: 67-74 .
- Simmers, I. (ed), 1988. *Estimation of natural groundwater recharge*, NATO ASI Series C, Vol. 222 D. (Proc. of the NATO advanced research workshop, Antalya, Turkey, March 1987), Reidel Publishing Company. 510 pp.
- Skogerboe, G.V., M. Aslam, M.A. Khan, K. Mahmood, S. Mahmood and A.H. Khan, 1999 *Inflow-Outflow channel losses and canal lining cost-effectiveness in the Fordwah Eastern Sadiqia (South) irrigation and drainage project*. Research Report No. 85, International Irrigation Management Institute (IIMI), Lahore, Pakistan. 31pp.

- Skogerboe, G.V., Z. Habib, K. Pongput, P.W. Vehmeyer and A.H. Khan, 1998. Canal modernization in the Indus basin irrigation system. In *Modernization of irrigation system operations: proceedings of the 5<sup>th</sup> ITIS network international meeting*, Aurangabad, India 28-30 October 1998. (<http://www.fao.org/docrep/003/x6626e/x6626e08.htm>)
- Smedema, L., 2000. Irrigation-induced River Salinization: Five Major irrigated basins in the Arid Zone. International Water Management Institute, Colombo. 87pp.
- Smedema, L.K., and D.W. Rycroft, 1983. *Land drainage: planning and design of agricultural drainage systems*. Batsford Academic and Educational Ltd. London. 376p.
- Smets, S.M.P., M. Kuper, J.C. Van Dam and R.A. Feddes, 1997, Salinization and crop transpiration of irrigated fields in Pakistan's Punjab. *Agricultural Water Management* 35: 43-60.
- SMO 1996, Unpublished published data. SCARP Monitoring Organization (SMO), of Water and Power Development Authority (WAPDA) Lahore, Pakistan.
- Sobrino, J.A., C. Coll and V. Caselles, 1991. Atmospheric correction for land surface temperature using NOAA-11 AVHRR channels 4 and 5, *Remote Sensing of Environment*, 38:19-34.
- Soer, G.J.R., 1980. Estimation of regional evapotranspiration and soil moisture conditions using remotely sensed crop surface temperatures, *Remote Sensing of Environment*, 9:27-45.
- Sophocleous, M. (ed), 1998. Perspectives on sustainable development of water resources in Kansas: Kansas Geological Survey Bulletin. 239 pp.
- Stewart, J.B., 1988. Modelling surface conductance of pine forest, *Agricultural and Forest Meteorology*, 43: 19-35.
- Stewart, J.B., W.P. Kustas, K.S. Humes, W.D. Nichols, M.S. Moran and H.A.R. de Bruin, 1994. Sensible heat flux-radiometric surface temperature relationship fro 8 semi-arid areas, *Journal of Applied Meteorology* 33:1110-1117.
- Sugita, M. and W. Brutsaert, 1990. Regional surface fluxes from remotely sensed skin temperature and lower boundary layer measurements, *Water Resources Research*, 26(12), 2937-2944.
- Tahir, Z. and Z. Habib, 2000. *Land and water productivity: Trends across Punjab canal commands*. Working Paper No. 14, Pakistan country series number 3, International Water Management Institute (IWMI) 35p. ([www.iwmi.org](http://www.iwmi.org)).
- Townley, L.R., 1998. Shallow groundwater systems. In. P. Dillon and I. Simmers (ed.). *Shallow groundwater systems*. A.A. Balkema Publishers, Rotodam, The Netherlands.: pp. 3-12.
- Traeen, M.A.K., K. Mahmood, A. Iqbal, M. Khan and M. Kuper, 1996. *Water Distribution at the Secondary Level in the Chistian Sub-Division*. Research Report No. 5, International Irrigation Management Institute (IIMI), Lahore, Pakistan. 179 pp.

- Troufleau, D., J.P. Lhomme, B. Montenev and A. Vidal, 1997. Sensible heat flux and radiometric surface temperature over sparse Sahelian vegetation, I. An experimental analysis of the  $kB^{-1}$  parameter, *Journal of Hydrology*, 188-189, 815-838.
- Valiente, J.A., M. Nunez, E. Lopez-Baeza and J.F. Moreno, 1995. Narrow-band to broad-band conversion of Meteosat-visible channel and broad-band albedo using AVHRR-1 and 2 channels, *International Journal of Remote Sensing*, 16(6): 1147-1166.
- Van Dam, J.C. and R. A. Feddes, 1996. Modelling of water flow and solute transport for irrigation and drainage. In: L.S. Pereira *et al.*, (Eds.), *Sustainability of Irrigated Agriculture*, Kluwer Academic Publishers, Dordrecht, The Netherlands: 211-231.
- Van Dam, J.C. and R.A. Feddes, 2000. Numerical simulation, evaporation and shallow groundwater levels with Richards equation. *Journal of Hydrology* 233: 72-85.
- Van Dam, J.C., J. Hygen, J.G. Wesseling, R.A. Feddes, P. Kabat, P.E.V. van Walsum, P. Groenendijk and C.A. van Diepen, 1997. Simulation of water flow, solute transport and plant growth in the Soil-Water-Atmosphere-Plant Environment Theory of SWAP version 2.0. Report 71. Department of Water Resources, Wageningen Agricultural University, Technical Doc. 45 DLO Winand Staring Center, Wageningen. Agricultural University. 167pp.
- Van De Griend, A.A. and M. Owe, 1993. On the relationship between thermal emissivity and the Normalized Difference Vegetation Index for natural surfaces, *International Journal of Remote Sensing*, 14(6), 1119-1131.
- Van Dijk, P.M., M.W. Lubczynski, J.L. Farr and G. Gabaake, 1996. Application of RS, GIS and groundwater modelling techniques in recharge evaluation at Palla Road, Botswana. *SIRDC Conference on the Application of Remotely Sensed Data and GIS in the Environmental and Natural Resources Assessment in Africa*. Harare, Zimbabwe March 15-22, 1996.
- Van Genuchten, M. Th., 1980. A closed form equation for predicting the hydraulic conductivity of unsaturated soils. *Soil Science Society of America Journal* 44:892-898.
- Van Genuchten, M.Th., 1987. *A numerical model for water and solute movement in and below the root zone*. Research Report, US Salinity Laboratory: Riverside, CA.
- Van Waijjen E.G., W.W.H. Hart, M. Kuper and R. Brouwer, 1997. Using a hydrodynamic flow model to plan maintenance activities and improve water distribution: Application to the Fordwah distributary in Punjab, Pakistan. *Irrigation and Drainage Systems* 11(4): 367-386.
- Vander Velde, E.J. and J.W. Kijne, 1992. Salinity and irrigation operation in Punjab, Pakistan. Workshop on *India-IIMI collaborative research in irrigation management*, February 12-13, 1992, New Dehli, India.

- Visser S.J., M. Kuper, M.A. Khan and R. Brouwer, 1997. Canal water distribution at the secondary level in the Punjab, Pakistan. *ICID Journal* 1998, 47(1): 1-17.
- Wang J., W.G.M. Bastiaanssen, Y. Ma and H. Pelgrum, 1998. Aggregation of land surface parameters in the oasis-desert systems of Northwest China, *Hydrological Processes* 12:2133-2147.
- Wang, J., Y. Ma., M. Menenti, W.G.M. Bastiaanssen and Y. Mitsuta, 1995. The scaling up of processes in the heterogeneous landscape of HEIFE in full with the aid of satellite remote sensing, *Journal of Meteorology of Japan*, 73(6): 1235-1244.
- WAPDA, 1981. Soil Salinity Survey Irrigated areas of Indus Basin 41 Million Acres Pakistan Water and Power Development Authority (WAPDA), Survey and Research Organization, Planning Division, Lahore, Pakistan.
- WAPDA, 2001. Indus basin irrigation system historic rivers and canals discharge data (1999-00). Pakistan Water and Power Development Authority, Lahore. WAPDA.
- Wester, P., B.M. Pimentel and C.A. Scott, 1999. *Institutional response to groundwater depletion: The aquifer management councils in the state of guanajuato, Mexico*. Paper presented at the international symposium on integrated water management in agriculture, Gómez Palacio, Mexico June 16-18, 1999.
- Wolters, W. and M.N. Bhutta, 1997. Need for integrated irrigation and drainage management, example of Pakistan. Proceedings of the ILRI symposium, *Towards Integrated Irrigation and Drainage Management*, Wageningen, The Netherlands.
- Wösten, J.H.M. and M.Th. van Genuchten, 1988. Using texture and other soil properties to predict the unsaturated soil hydraulic properties. *Soil Science Society of America Journal* 52: 1762-1770.
- Yates, S.R., M.Th. van Genuchten, A.W. Warrick and F.J. Leij, 1992. Analysis of measured, predicted and estimated hydraulic conductivity using the RETC computer program. *Soil Science Society of America Journal* 56: 347-354.
- Zhang, Y.C., W.B. Rossow and A.A. Lacis, 1995. Calculation of surface and top of atmosphere radiative fluxes from physical quantities based on ISCCP in full data sets: 1. Method and sensitivity to input data uncertainties, *Journal of Geophysical Research*, 100 (D1): 1149-1165.





## ITC DISSERTATION LIST

1. **Akinyede**, 1990, Highway cost modelling and route selection using a geotechnical information system
2. **Pan He Ping**, 1990, 90-9003757-8, Spatial structure theory in machine vision and applications to structural and textural analysis of remotely sensed images
3. **Bocco Verdinelli, G.**, 1990, Gully erosion analysis using remote sensing and geographic information systems: a case study in Central Mexico
4. **Sharif, M**, 1991, Composite sampling optimization for DTM in the context of GIS
5. **Drummond, J.**, 1991, Determining and processing quality parameters in geographic information systems
6. **Groten, S.**, 1991, Satellite monitoring of agro-ecosystems in the Sahel
7. **Sharifi, A.**, 1991, 90-6164-074-1, Development of an appropriate resource information system to support agricultural management at farm enterprise level
8. **Zee, D. van der**, 1991, 90-6164-075-X, Recreation studied from above: Air photo interpretation as input into land evaluation for recreation
9. **Mannaerts, C.**, 1991, 90-6164-085-7, Assessment of the transferability of laboratory rainfall-runoff and rainfall - soil loss relationships to field and catchment scales: a study in the Cape Verde Islands
10. **Ze Shen Wang**, 1991: 90-393-0333-9, An expert system for cartographic symbol design
11. **Zhou Yunxian**, 1991, 90-6164-081-4, Application of Radon transforms to the processing of airborne geophysical data
12. **Zuviria, M. de**, 1992, 90-6164-077-6, Mapping agro-topoclimates by integrating topographic, meteorological and land ecological data in a geographic information system: a case study of the Lom Sak area, North Central Thailand
13. **Westen, C. van**, 1993, 90-6164-078-4, Application of Geographic Information Systems to landslide hazard zonation
14. **Shi Wenzhong**, 1994, 90-6164-099-7, Modelling positional and thematic uncertainties in integration of remote sensing and geographic information systems
15. **Javelosa, R.**, 1994, 90-6164-086-5, Active Quaternary environments in the Philippine mobile belt
16. **Lo King-Chang**, 1994, 90-9006526-1, High Quality Automatic DEM, Digital Elevation Model Generation from Multiple Imagery
17. **Wokabi, S.**, 1994, 90-6164-102-0, Quantified land evaluation for maize yield gap analysis at three sites on the eastern slope of Mt. Kenya
18. **Rodriguez, O.**, 1995, Land Use conflicts and planning strategies in urban fringes: a case study of Western Caracas, Venezuela
19. **Meer, F. van der**, 1995, 90-5485-385-9, Imaging spectrometry & the Ronda peridotites
20. **Kufoniyi, O.**, 1995, 90-6164-105-5, Spatial coincidence: automated database updating and data consistency in vector GIS

21. **Zambezi, P.**, 1995, Geochemistry of the Nkombwa Hill carbonatite complex of Isoka District, north-east Zambia, with special emphasis on economic minerals
22. **Woldai, T.**, 1995, The application of remote sensing to the study of the geology and structure of the Carboniferous in the Calañas area, pyrite belt, SW Spain
23. **Verweij, P.**, 1995, 90-6164-109-8, Spatial and temporal modelling of vegetation patterns: burning and grazing in the Paramo of Los Nevados National Park, Colombia
24. **Pohl, C.**, 1996, 90-6164-121-7, Geometric Aspects of Multisensor Image Fusion for Topographic Map Updating in the Humid Tropics
25. **Jiang Bin**, 1996, 90-6266-128-9, Fuzzy overlay analysis and visualization in GIS
26. **Metternicht, G.**, 1996, 90-6164-118-7, Detecting and monitoring land degradation features and processes in the Cochabamba Valleys, Bolivia. A synergistic approach
27. **Hoanh Chu Thai**, 1996, 90-6164-120-9, Development of a Computerized Aid to Integrated Land Use Planning (CAILUP) at regional level in irrigated areas: a case study for the Quan Lo Phung Hiep region in the Mekong Delta, Vietnam
28. **Roshannejad, A.**, 1996, 90-9009284-6, The management of spatio-temporal data in a national geographic information system
29. **Terlien, M.**, 1996, 90-6164-115-2, Modelling Spatial and Temporal Variations in Rainfall-Triggered Landslides: the integration of hydrologic models, slope stability models and GIS for the hazard zonation of rainfall-triggered landslides with examples from Manizales, Colombia
30. **Mahavir, J.**, 1996, 90-6164-117-9, Modelling settlement patterns for metropolitan regions: inputs from remote sensing
31. **Al-Amir, S.**, 1996, 90-6164-116-0, Modern spatial planning practice as supported by the multi-applicable tools of remote sensing and GIS: the Syrian case
32. **Pilouk, M.**, 1996, 90-6164-122-5, Integrated modelling for 3D GIS
33. **Duan Zengshan**, 1996, 90-6164-123-3, Optimization modelling of a river-aquifer system with technical interventions: a case study for the Huangshui river and the coastal aquifer, Shandong, China
34. **Man, W.H. de**, 1996, 90-9009-775-9, Surveys: informatie als norm: een verkenning van de institutionalisering van dorp - surveys in Thailand en op de Filippijnen
35. **Vekerdy, Z.**, 1996, 90-6164-119-5, GIS-based hydrological modelling of alluvial regions: using the example of the Kisaföld, Hungary
36. **Pereira, Luisa**, 1996, 90-407-1385-5, A Robust and Adaptive Matching Procedure for Automatic Modelling of Terrain Relief
37. **Fandino Lozano, M.**, 1996, 90-6164-129-2, A Framework of Ecological Evaluation oriented at the Establishment and Management of Protected Areas: a case study of the Santuario de Iguaque, Colombia
38. **Toxopeus, B.**, 1996, 90-6164-126-8, ISM: an Interactive Spatial and temporal Modelling system as a tool in ecosystem management: with two case studies: Cibodas biosphere reserve, West Java Indonesia: Amboseli biosphere reserve, Kajiado district, Central Southern Kenya

39. **Wang Yiman**, 1997, 90-6164-131-4, Satellite SAR imagery for topographic mapping of tidal flat areas in the Dutch Wadden Sea
40. **Asun Saldana-Lopez**, 1997, 90-6164-133-0, Complexity of soils and Soilscape patterns on the southern slopes of the Ayllon Range, central Spain: a GIS assisted modelling approach
41. **Ceccarelli, T.**, 1997, 90-6164-135-7, Towards a planning support system for communal areas in the Zambezi valley, Zimbabwe; a multi-criteria evaluation linking farm household analysis, land evaluation and geographic information systems
42. **Peng Wanning**, 1997, 90-6164-134-9, Automated generalization in GIS
43. **Lawas, C.**, 1997, 90-6164-137-3, The Resource Users' Knowledge, the neglected input in Land resource management: the case of the Kankanaey farmers in Benguet, Philippines
44. **Bijker, W.**, 1997, 90-6164-139-X, Radar for rain forest: A monitoring system for land cover Change in the Colombian Amazon
45. **Farshad, A.**, 1997, 90-6164-142-X, Analysis of integrated land and water management practices within different agricultural systems under semi-arid conditions of Iran and evaluation of their sustainability
46. **Orlic, B.**, 1997, 90-6164-140-3, Predicting subsurface conditions for geotechnical modelling
47. **Bishr, Y.**, 1997, 90-6164-141-1, Semantic Aspects of Interoperable GIS
48. **Zhang Xiangmin**, 1998, 90-6164-144-6, Coal fires in Northwest China: detection, monitoring and prediction using remote sensing data
49. **Gens, R.**, 1998, 90-6164-155-1, Quality assessment of SAR interferometric data
50. **Turkstra, J.**, 1998, 90-6164-147-0, Urban development and geographical information: spatial and temporal patterns of urban development and land values using integrated geo-data, Villaviciencia, Colombia
51. **Cassells, C.**, 1998, Thermal modelling of underground coal fires in northern China
52. **Naseri, M.**, 1998, 90-6164-195-0, Characterization of Salt-affected Soils for Modelling Sustainable Land Management in Semi-arid Environment: a case study in the Gorgan Region, Northeast, Iran
53. **Gorte B.G.H.**, 1998, 90-6164-157-8, Probabilistic Segmentation of Remotely Sensed Images
54. **Tenalem Ayenew**, 1998, 90-6164-158-6, The hydrological system of the lake district basin, central main Ethiopian rift
55. **Wang Donggen**, 1998, 90-6864-551-7, Conjoint approaches to developing activity-based models
56. **Bastidas de Calderon, M.**, 1998, 90-6164-193-4, Environmental fragility and vulnerability of Amazonian landscapes and ecosystems in the middle Orinoco river basin, Venezuela
57. **Moameni, A.**, 1999, Soil quality changes under long-term wheat cultivation in the Marvdasht plain, South-Central Iran
58. **Groenigen, J.W. van**, 1999, 90-6164-156-X, Constrained optimisation of spatial sampling: a geostatistical approach
59. **Cheng Tao**, 1999, 90-6164-164-0, A process-oriented data model for fuzzy spatial objects

60. **Wolski, Piotr**, 1999, 90-6164-165-9, Application of reservoir modelling to hydrotopes identified by remote sensing
61. **Acharya, B.**, 1999, 90-6164-168-3, Forest biodiversity assessment: A spatial analysis of tree species diversity in Nepal
62. **Akbar Abkar, Ali**, 1999, 90-6164-169-1, Likelihood-based segmentation and classification of remotely sensed images
63. **Yanuariadi, T.**, 1999, 90-5808-082-X, Sustainable Land Allocation: GIS-based decision support for industrial forest plantation development in Indonesia
64. **Abu Bakr, Mohamed**, 1999, 90-6164-170-5, An Integrated Agro-Economic and Agro-Ecological Framework for Land Use Planning and Policy Analysis
65. **Eleveld, M.**, 1999, 90-6461-166-7, Exploring coastal morphodynamics of Ameland (The Netherlands) with remote sensing monitoring techniques and dynamic modelling in GIS
66. **Yang Hong**, 1999, 90-6164-172-1, Imaging Spectrometry for Hydrocarbon Microseepage
67. **Mainam, Félix**, 1999, 90-6164-179-9, Modelling soil erodibility in the semiarid zone of Cameroon
68. **Bakr, Mahmoud**, 2000, 90-6164-176-4, A Stochastic Inverse-Management Approach to Groundwater Quality
69. **Zlatanova, Z.**, 2000, 90-6164-178-0, 3D GIS for Urban Development
70. **Ottichilo, Wilber K.**, 2000, 90-5808-197-4, Wildlife Dynamics: An Analysis of Change in the Masai Mara Ecosystem
71. **Kaymakci, Nuri**, 2000, 90-6164-181-0, Tectono-stratigraphical Evolution of the Cankori Basin (Central Anatolia, Turkey)
72. **Gonzalez, Rhodora**, 2000, 90-5808-246-6, Platforms and Terraces: Bridging participation and GIS in joint-learning for watershed management with the Ifugaos of the Philippines
73. **Schetselaar, Ernst**, 2000, 90-6164-180-2, Integrated analyses of granite-gneiss terrain from field and multisource remotely sensed data. A case study from the Canadian Shield
74. **Mesgari, Saadi**, 2000, 90-3651-511-4, Topological Cell-Tuple Structure for Three-Dimensional Spatial Data
75. **Bie, Cees A.J.M. de**, 2000, 90-5808-253-9, Comparative Performance Analysis of Agro-Ecosystems
76. **Khaemba, Wilson M.**, 2000, 90-5808-280-6, Spatial Statistics for Natural Resource Management
77. **Shrestha, Dhruva**, 2000, 90-6164-189-6, Aspects of erosion and sedimentation in the Nepalese Himalaya: highland-lowland relations
78. **Asadi Haroni, Hooshang**, 2000, 90-6164-185-3, The Zarshuran Gold Deposit Model Applied in a Mineral Exploration GIS in Iran
79. **Raza, Ale**, 2001, 90-3651-540-8, Object-oriented Temporal GIS for Urban Applications
80. **Farah, Hussein**, 2001, 90-5808-331-4, Estimation of regional evaporation under different weather conditions from satellite and meteorological data. A case study in the Naivasha Basin, Kenya
81. **Zheng, Ding**, 2001, 90-6164-190-X, A Neural - Fuzzy Approach to Linguistic Knowledge Acquisition and Assessment in Spatial Decision Making

82. **Sahu, B.K.**, 2001, Aeromagnetics of continental areas flanking the Indian Ocean; with implications for geological correlation and Gondwana reassembly
83. **Alfestawi, Y.**, 2001, 90-6164-198-5, The structural, paleogeographical and hydrocarbon systems analysis of the Ghadamis and Murzuq Basins, West Libya, with emphasis on their relation to the intervening Al Qarqaf Arch
84. **Liu, Xuehua**, 2001, 90-5808-496-5, Mapping and Modelling the Habitat of Giant Pandas in Foping Nature Reserve, China
85. **Oindo, Boniface Oluoch**, 2001, 90-5808-495-7, Spatial Patterns of Species Diversity in Kenya
86. **Carranza, Emmanuel John**, 2002, 90-6164-203-5, Geologically-constrained Mineral Potential Mapping
87. **Rugege, Denis**, 2002, 90-5808-584-8, Regional Analysis of Maize-Based Land Use Systems for Early Warning Applications
88. **Liu, Yaolin**, 2002, 90-5808-648-8, Categorical Database Generalization in GIS
89. **Ogao, Patrick**, 2002, 90-6164-206-X, Exploratory Visualization of Temporal Geospatial Data using Animation
90. **Abadi, Abdulbaset M.**, 2002, 90-6164-205-1, Tectonics of the Sirt Basin – Inferences from tectonic subsidence analysis, stress inversion and gravity modelling
91. **Geneletti, Davide**, 2002, 90-5383-831-7, Ecological Evaluation for Environmental Impact Assessment



## **CURRICULUM VITAE**

Mobin-ud-Din Ahmad was born on 2 February 1970 in Faisalabad, Pakistan. After secondary school, he joined the University of Agriculture, Faisalabad, Pakistan, from where he obtained the degree of B.Sc. Agricultural Engineering in December 1991. He was awarded a King's Scholarship from Thailand for his Master of Engineering studies at the Asian Institute of Technology (AIT), Bangkok, in the field of Irrigation Engineering and Management. After completing the Master of Engineering degree in November 1994, he joined the International Water Management Institute (IWMI) in Pakistan.

At IWMI he became member of a group of researchers working on remote sensing (RS) and geographic information system (GIS) applications for water resources management. Most of his research work was conducted in Pakistan, where he worked on methodologies for irrigation and salinity mapping, land use classifications (cropping pattern and intensity), actual evapotranspiration estimations and water use performance using satellite imagery from tertiary to main system level. He has worked in international research teams and has extensive experience with the use of different GIS and image processing software and modelling of transient water flow in open channels and soils. In February 1999, he started his Ph.D. studies at the International Institute for Geo-information Science and Earth Observation (ITC), The Netherlands, as a sandwich programme between ITC and IWMI, while registering at Wageningen University in the Netherlands through the Department of Water Resources.

Presently, Mobin-ud-Din Ahmad is working as a Water Resources Engineer (GIS/RS) at IWMI's Regional Office for Pakistan, Central Asia and the Middle East.

The research reported in this thesis was supported by the International Institute for Geo-information Science and Earth Observation (ITC) and International Water Management Institute (IWMI) through a 'sandwich' PhD fellowship.

Mobin-ud-Din Ahmad  
International Water Management Institute (IWMI)  
12 km Multan Road, Chowk Thokar Niaz Baig,  
Lahore-53700, Pakistan  
Tel: +92 (0)42 5410050-53  
Fax: +92 (0)42 5410054  
  
Email: [a.mobin@cgiar.org](mailto:a.mobin@cgiar.org)  
[mdahmad@yahoo.com](mailto:mdahmad@yahoo.com)